

PDF hosted at the Radboud Repository of the Radboud University Nijmegen

The following full text is a publisher's version.

For additional information about this publication click this link.

<http://hdl.handle.net/2066/146246>

Please be advised that this information was generated on 2018-07-07 and may be subject to change.

4633

Ultrafast dynamics of hot carriers
in GaAs (hetero)structures

Peter Christianen

**Ultrafast dynamics of hot carriers
in GaAs (hetero)structures**

Peter Christianen

Christianen, Petrus Christianus Maria

Ultrafast dynamics of hot carriers in GaAs
(hetero)structures / Petrus Christianus Maria

Christianen. - [S.l. : s.n.]. - Ill.

Proefschrift Nijmegen. - Met lit. opg. - Met samenvatting
in het Nederlands.

ISBN 90-9006185-1

Trefw.: halfgeleiders / fotoluminescentie.

Ultrafast dynamics of hot carriers in GaAs (hetero)structures

een wetenschappelijke proeve op het gebied van
de Natuurwetenschappen

Proefschrift

ter verkrijging van de graad van doctor aan
de Katholieke Universiteit Nijmegen,
volgens besluit van het College van Decanen
in het openbaar te verdedigen op
vrijdag 2 juli 1993,
des namiddags te 1.00 uur precies

door

Petrus Christianus Maria Christianen

geboren op 6 juli 1966
te Hoeven

Promotor: Prof. Dr. H. van Kempen

Co-promotor: Dr. H.J.A. Bluysen

Het werk beschreven in dit proefschrift maakt deel uit van het onderzoeksprogramma van de Stichting voor Fundamenteel Onderzoek der Materie (FOM) en is mede mogelijk gemaakt door financiële steun van de Nederlandse Organisatie voor Wetenschappelijk Onderzoek (NWO).

Dit boekje beschrijft de resultaten van 4 jaar promotie onderzoek uitgevoerd op de afdeling Experimentele Vaste Stoffysica 2 (EVSF2) o.l.v. Herman van Kempen. Op deze plaats wil ik iedereen bedanken die mij op enigerlei wijze heeft geholpen gedurende deze periode. Met het risico dat ik sommigen vergeet, wil ik toch enkele mensen met name bedanken, zonder wie dit boekje er zonder meer anders had uitgezien.

Allereerst wil ik alle EVSF2-medewerkers van de afgelopen jaren bedanken voor de prettige sfeer en plezierige samenwerking, en in het bijzonder de technici Jan Gerritsen, Jan Hermesen en Kees Beers voor het oplossen van allerlei probleempjes, al of niet van technische aard, en Riki Gommers voor het regelen van alle administratieve zaken. De initiator van het korte puls fotoluminescentie onderzoek in Nijmegen, Dr. H. Bluysen, wil ik bedanken voor zijn immer kritische, maar altijd hartelijke begeleiding. Mijn voorgangers Henk Reinen en Tos Berendschot hebben me wegwijds gemaakt in de fysica van de ladingsdragersdynamica en me de fijne kneepjes van het vak geleerd; hiervoor ben ik ze nog steeds erg dankbaar. Adriaan van 't Hof dank ik voor het uitvoeren van diverse kleine en grote projecten, die absoluut noodzakelijk zijn geweest voor het welslagen van mijn experimenten, wat meestal gepaard ging met een aanzienlijke uitbreiding van mijn vocabulaire. Met Marrie van de Mooren was het prima vertoeven op één kamer, mede dankzij zijn altijd relativerende opmerkingen aangaande de belangrijke dingen des levens. Guido Knippels dank ik voor het uitvoeren van de metingen aan het verticaal transport aan superroosters en Erik de Bekker voor de zeer prettige wijze waarop we hebben samengewerkt tijdens zijn afstudeerperiode. Theo Rasing ben ik zeer erkentelijk voor zijn interesse in mijn werk en voor de geboden gelegenheid om met de gepulste Ti:saffier laser te werken. Maar ik dank vooral Albert van Etteger voor het realiseren van vele optische opstellingen, het 'uitlenen' van ontelbare (optische) componenten en alle verleende hulp.

De samenwerking met de halfgeleidergroep van Prof. J. Wolter aan de T.U. Eindhoven is voor mij zeer waardevol geweest. Niet alleen groeiden Maarten Leys en Willem van der Vleuten uitstekende samples op bestelling, en zorgde Peter Nouwens indien nodig voor de contactering, ook voor theoretische ondersteuning kon ik in Eindhoven terecht; Pieter van Hall wil ik bij deze bedanken voor zijn enthousiaste en stimulerende medewerking, die ik als uitermate aangenaam heb ervaren.

De medewerkers van het Magnetenlab o.l.v. Jos Perenboom, te weten Klaas van Hulst, Hung van Luong, Jos Rook, Harry Balster, Lijnis Nelemans, Peter van der Linden en Olek Wittlin dank ik voor het verzorgen van de nodige Tesla's en de aanwezige infrastructuur. Further, I would like to thank John Singleton for being the initiator of many co-operations with foreign colleagues, which resulted eg. in the nice collaboration with Martyn Chamberlain and Mark Stanaway from Nottingham University. Jan Kees Maan en Annalisa Fasolino dank ik voor hun kritische aanwijzingen aangaande het manuscript en Paul Hageman van EVSF3 voor het groeien van een bulk GaAs sample.

Tenslotte bedank ik al mijn (sport)vrienden, kennissen en huisgenoten, en zeker ook mijn ouders en mijn zus, die meer dan eens onvrijwillig deelgenoot zijn geweest van mijn frustraties. Maar zonder meer mijn grootste dank, die nauwelijks in woorden is uit te drukken, gaat uit naar Astrid, voor al haar Liefde, steun en relativerende humor.

Contents

1 Introduction	1
References	4
2 Experimental arrangements and techniques	5
2.1 Introduction	6
2.2 Semiconductor materials	6
2.2.1 GaAs	6
2.2.2 GaAs/(Ga,Al)As heterostructures	7
2.2.3 Application of a magnetic field	8
2.2.4 Metal-semiconductor interface	9
2.3 Ultrafast dynamics of photo-excited carriers	10
2.3.1 Carrier-carrier scattering	11
2.3.2 Intervalley scattering	11
2.3.3 Phonon cooling	12
2.3.4 Recombination and luminescence	13
2.4 Experimental arrangements	13
2.4.1 The picosecond laser system	14
2.4.2 The femtosecond laser system	14
2.5 Time-resolved photoluminescence techniques	14
2.5.1 Picosecond up-conversion technique	14
2.5.2 Subpicosecond photoluminescence Correlation Technique	16
References	18
3 Lineshape analysis of picosecond time-resolved high excitation photolumi- nescence spectra	21
3.1 Introduction	22
3.2 Experimental details and results	23
3.3 Lineshape analysis	27
3.3.1 Single-particle model with k-conservation	28
3.3.2 Single-particle model neglecting k-conservation	29
3.3.3 Many-particle lineshape model	30
3.4 Discussion of the lineshape analysis results	32
3.4.1 Overall lineshape	32
3.4.2 Carrier density and effective temperature	34
3.4.3 Band-gap renormalization	35
3.4.4 Radiative recombination coefficient	36

3.4.5	High-energy tail shoulders	37
3.5	Conclusions	38
	References	39
4	Cooling reduction due to a rapid density decay of hot carriers in GaAs	41
4.1	Introduction	42
4.2	Experimental details and results	43
4.3	Analysis of the photoluminescence spectra	44
4.4	Stimulated recombination	48
4.5	Model calculation	50
4.6	Discussion	53
4.6.1	Results model calculation	53
4.6.2	Recombination heating	53
4.6.3	Radiative recombination coefficient	56
4.7	Conclusions	59
	References	60
5	Ultrafast carrier dynamics at a metal-semiconductor interface	63
5.1	Introduction	64
5.2	Sample composition	65
5.3	Experimental details and results	66
5.4	The Monte Carlo simulations	71
5.5	Theoretical results and discussion	72
5.5.1	Results of the Monte-Carlo simulations	72
5.5.2	Calculations including a contact regeneration time	76
5.6	Conclusions	81
	References	82
6	Energy Relaxation of hot 2D carriers in high magnetic fields due to optical and acoustic phonons	85
6.1	Introduction	86
6.2	Experimental details	86
6.3	Experimental results and model calculation	87
6.4	Discussion	91
6.5	Conclusions	91
	References	92
7	Vertical transport in a GaAs/(Ga,Al)As superlattice containing an enlarged quantum well in high in-plane magnetic fields	93
7.1	Introduction	94
7.2	Experimental details	94
7.3	Results	95
7.4	Discussion	99
7.5	Conclusions	101

References	101
Summary	105
Samenvatting	109
List of publications	113
Curriculum Vitae	115

Chapter 1

Introduction

During the last decades the fundamental understanding of the physical properties of semiconductors and their technological applications has improved drastically. This applies not in the last place to direct band-gap semiconductors like GaAs, which have the direct possibility for optical and opto-electronic applications, such as semiconductor lasers, optical detectors and switches. This has led to an overwhelming scientific interest in the physics of compound semiconductors (III-V, II-VI) with a direct band-gap, which was further enhanced by the development to full maturity of sophisticated crystal growth techniques such as Metal Organic Vapour Phase Epitaxy (MOVPE), Molecular Beam Epitaxy (MBE) and later on the combination of both techniques in CBE (Chemical Beam Epitaxy) or MOMBE (Metal Organic Molecular Beam Epitaxy). Nowadays it is relatively easy to grow very pure semiconductor crystals. In addition these elaborate growth methods offer fascinating prospects to do quantum mechanical engineering, as proposed first by Esaki and Tsu¹, by depositing atomic layer upon atomic layer of distinct semiconductors, with different band-gap energies or doping levels, in a well defined way. A wide variety of devices or carrier systems has been invented and produced. This includes carrier confinement in thin sheets of material, so-called quantum wells and heterojunctions, bandstructure engineering of artificial (super)lattices with a macroscopic periodicity as compared to the atomic periodicity and the realization of huge carrier mobilities following the concept of modulation doping. These semiconductor layered structures exhibit many new basic physical phenomena like the Integral² and Fractional Quantum Hall effect^{3, 4}. These developments have stimulated a large technological and research effort, resulting in the fabrication and investigation of eg. high mobility transistors⁵, quantum well lasers^{6, 7} and switches and modulators based on excitonic nonlinearities⁸.

Knowledge of the fundamental physics of hot carriers in semiconductors is of major importance for the understanding of carrier behaviour in the presence of high electric fields, i.e. device performance. Consequently hot carrier physics has become an important research topic, which was initially restricted to transport measurements. Later on hot carriers were created by laser photo-excitation⁹ and optical techniques were applied to study the relevant energy relaxation and scattering processes. The advent of laser systems capable of generating light pulses with a duration in the pico- or femtosecond time-domain, initiated a new period of intense research of hot carriers in direct band-gap semiconductors, since the important energy and momentum exchange between carriers and phonons and between carriers mutually, could be monitored in real time. Moreover, the strive towards faster semiconductor devices, such as optical switches, received new impulses.

This thesis deals with the ultrafast dynamics of hot carriers in GaAs (hetero)structures,

under various experimental conditions, such as the application of high electric or magnetic fields or intense photo-excitation. Basically a magnetic field is applied in order to gain insight in the implications of a changing density of states function on the scattering mechanisms. The combination of both an electric field and laser excitation is of significance for opto-electronic devices, governed by ultrafast high-field non linear carrier transport. Variation of the laser intensity changes essentially the carrier density, which offers the possibility to go from low to high densities, entering the regime where many-particle interactions become important. Different photoluminescence techniques are used to probe the carrier distributions after pulsed laser excitation. The time-evolution of the photoluminescence signal recorded on a picosecond timescale reveals the interesting fundamental physics of the hot carrier dynamics. This thesis is organised as follows.

Chapter 2 will give a brief introduction of the GaAs (hetero)structures used with specific emphasis to the carrier scattering mechanisms important in the performed experiments on a (sub)picosecond timescale. The ultrafast carrier dynamics is governed predominantly by carrier-carrier and carrier-phonon interactions, whereas the electron-hole recombination supplies us with a powerful tool to study these mechanisms. The time-resolved photoluminescence techniques will be discussed, starting off from the introduction of the picosecond Ti:sapphire laser and the femtosecond Colliding Pulse Mode ring dye laser, followed by the two detection methods used, i.e. the photoluminescence up-conversion and the photoluminescence correlation techniques.

The lineshape of photoluminescence spectra contains valuable information about the carrier distributions in their respective bands. In particular the carrier density and the effective temperature of the hot carriers are extracted from the photoluminescence lineshape. The picosecond time-evolution of both density and temperature monitors the ultrafast carrier dynamics. However, the actual values for carrier density and temperature, as obtained from the recorded lineshape, depends on the particular model used for electron-hole recombination, as will be shown in chapter 3. Moreover, it is not obvious how to calculate the photoluminescence lineshape in the case of high densities and low temperatures of the carriers, when many-particle interactions may play an important role. In chapter 3 a lineshape study of picosecond time-resolved photoluminescence spectra will be presented, with specific interest to high excitation conditions, where the experimentally obtained photoluminescence spectra exhibit anomalous high-energy side intensity shoulders, unexplained by single-particle lineshape analysis models.

In general the carrier lifetime due to spontaneous recombination in high quality GaAs is much longer than the times involved in the energy relaxation process. Consequently the decay of the carrier density is usually neglected in the theoretical analysis of the carrier cooling. Chapter 4 however presents time-resolved photoluminescence experiments on bulk GaAs in which, under high excitation conditions, a very rapid carrier density decay rate is observed, simultaneously with a significant reduction in the hot carrier cooling rate. These results are discussed in terms of an energy relaxation model, including the usual carrier phonon interactions, featuring the occurrence of stimulated recombination in order to explain the ultrafast carrier density decay. The cooling rate reduction is directly related to the rapid decay of the density due to recombination heating¹⁰, which stresses the importance

of the determination of both the time-dependent density and temperature in a picosecond cooling experiment, as opposed to the determination of merely the temperature. Furthermore, knowledge of the influence of a short carrier lifetime on the energy loss rates of hot carriers is important for the performance of direct band-gap semiconductor lasers¹¹.

Chapter 5 deals with the problem of real space charge transfer of carriers photo-injected in the high electric field at a metal-semiconductor interface. By using a subpicosecond photoluminescence correlation technique the ultrafast separation of photo-excited electrons and holes is monitored in real time. The experiments are analyzed with help of a Monte-Carlo simulation, which appears to be a very powerful method in order to describe carrier behaviour in semiconductors. The ultrafast response of the injected carriers strongly depends on the modelling of the contacts of the device, and ultimately is not only critically dependent on the device RC-time, but also on the excited carrier density. This investigation visualizes some fundamental restrictions to the performance of fast opto-electronic devices and the results are applicable directly to e.g. the operation of fast optical switches¹².

Application of a high magnetic field forces carriers to move in cyclotron orbits perpendicular to the field direction. The energy states are quantized in Landau levels, which results in an effective dimensionality reduction. As a result it becomes possible to study carrier systems with a quasi-zero dimensional density of states by the application of a magnetic field to a quantum well structure. The fundamental implications for the carrier-phonon interactions has been studied extensively with the use of both continuous wave as well as time-resolved photoluminescence spectroscopy¹³⁻¹⁶. Although the time-resolved experiments have provided valuable information on the carrier-phonon coupling in these systems, a quantitative description of the results is difficult due to the variation in time of all the relevant parameters. Chapter 6 presents cooling experiments of hot carriers in a quantum well structure under application of magnetic fields up to 17 T, using continuous wave photoluminescence, which provide a better quantitative understanding of previous reported time-resolved data. Whether a particular phonon scattering mechanism, LO- or acoustic phonon scattering, dominates the carrier cooling is found to rely heavily on the Landau level occupation, i.e. the carrier density and temperature. Consequently the excitation conditions determine whether the cooling rate enhances (acoustic phonons) or diminishes (LO phonons) with magnetic field.

Finally, chapter 7 describes a photoluminescence study on the vertical transport of carriers in a GaAs/(Ga,Al)As superlattice, with in-plane fields of up to 25 T at temperatures in the range 4-80 K. Vertical transport at 4 K, determined by exciton transport, is shown to be less efficient than free carrier-like transport at higher temperatures (47 and 80 K). Application of a high in-plane magnetic field becomes of specific fundamental interest when the magnetic length approaches the artificial (super)periodicity¹⁷, which determines the miniband structure, resulting in a significant reduction of the vertical transport, as is shown in the presented results.

References

- [1] L. Esaki and R. Tsu, *IBM Res. Note RC-2418* (1969); L. Esaki, *IEEE J. Quantum Electronics QE-22*, 1611 (1986).
- [2] K. v. Klitzing, G. Dorda and M. Pepper, *Phys. Rev. Lett.* **45**, 494 (1980).
- [3] D.C. Tsui and A.C. Gossard, *Appl. Phys. Lett.* **38**, 550 (1981).
- [4] D.C. Tsui, H.C. Störmer and A.C. Gossard, *Phys. Rev. Lett.* **48**, 1559 (1982).
- [5] H. Sakaki, *IEEE J. Quantum Electron.* **QE22**, 1845 (1986).
- [6] L.C. Chin and A. Yariv, *J. of Luminescence* **30**, 551 (1985).
- [7] T.T.J.M. Berendschot, H.A.J.M. Reinen, H.J.A. Bluyssen, C. Harder and H.P. Meier, *Appl. Phys. Lett.* **54**, 1827 (1989).
- [8] D.S. Chemla, *J. of Luminescence* **30**, 502 (1985).
- [9] J. Shah, *Solid-State Electron.* **21**, 43 (1978).
- [10] D. Bimberg and J. Mycielski, *J. Phys. C: Solid State Phys.* **19**, 2363 (1986).
- [11] V.I. Tolstikhin, *Sov. Techn. Phys. Lett.* **18**, 50 (1992).
- [12] P.J. van Hall and V. Brücker, *Proc. of the 8th Vilnius Symposium on Ultrafast Phenomena in Semiconductors* (Vilnius, Lithuania, 1992).
- [13] J.F. Ryan, R.A. Taylor, A.J. Turberfield and J.M. Worlock, *Surf. Sci.* **170**, 511 (1986).
- [14] R.W.J. Hollering, *Phd. thesis*, University of Nijmegen (1986).
- [15] T.T.J.M. Berendschot, *Phd. thesis*, University of Nijmegen (1989).
- [16] H.A.J.M. Reinen, *Phd. thesis*, University of Nijmegen (1990).
- [17] J.C. Maan, *Festkörperprobleme (Advances in Solid State Physics)* **27**, edited by P. Grosse, (Vieweg, Braunschweig, 1987) p 137-167.

Chapter 2

Experimental arrangements and techniques

Abstract

The semiconductor materials used are briefly described, with specific emphasis to relevant scattering mechanisms, such as carrier-carrier, carrier-phonon and intervalley scattering. The experimental photoluminescence techniques used are discussed, in particular the picosecond up-conversion and the femtosecond correlation techniques.

2.1 Introduction

Optical spectroscopy provides a powerful tool to study the behaviour of hot carriers in semiconductors, resulting in the employment of various techniques in the past. In the experiments described in this thesis photoluminescence techniques have been used. Photoluminescence, i.e. radiative recombination of electrons and holes, contains information about the distributions of the electrons and holes in their respective bands. In addition, since the availability of laser systems which can generate ultrashort laser pulses, hot carrier research has been extended to the ultrafast dynamics of carriers and phonons in the presence of external magnetic and electric fields or intense optical excitation^{1, 2}. Nowadays pure semiconductor material can be produced relatively easily, in which the spontaneous radiative carrier lifetimes are much longer than the ultrafast carrier dynamics. This makes photoluminescence spectroscopy a very convenient carrier distribution probe, even on short timescales. Further, since it has been shown that the optical matrix element, which determines the strength of the recombination, is not affected by a magnetic field³, photoluminescence is ideally suited to monitor the behaviour of carrier systems in magnetic fields. All these features of photoluminescence have been exploited in this thesis to study ultrafast carrier dynamics and recombination in GaAs and GaAs/(Ga,Al)As compounds.

In this chapter the semiconductor structures on which the experiments have been performed, will be introduced briefly (section 2.2), together with carrier scattering mechanisms of importance on a short timescale (section 2.3). Subsequently the laser systems used to perform the time-resolved photoluminescence measurements will be described (2.4) and finally the luminescence techniques, i.e. up-conversion and photoluminescence correlation, will be discussed (2.5).

2.2 Semiconductor materials

2.2.1 GaAs

Many important properties of carriers in GaAs are related directly to its bandstructure, which is partially shown in figure 2.1. In contrast to the more conventional semiconductors Ge and Si, GaAs has a direct energy-gap at $\mathbf{k}=0$ (the centre of the Brillouin zone), formed by the Γ_6 and Γ_8 extrema of the conduction and valence bands respectively, which makes this material of particular interest for optical applications. At $\mathbf{k}=0$ the heavy- and light-hole bands are degenerate, while the spin-orbit split-off band Γ_7 is positioned about 0.35 eV below the Γ_8 -maximum. At energies close to the direct band-gap the dispersion relation between energy and wavevector is described adequately by parabolic bands:

$$E_{e,h}(\mathbf{k}) = \frac{\hbar^2}{2m_{e,h}} \mathbf{k}^2 \quad (2.1)$$

where $E_{e,h}$ is the energy above the band-edge and $m_{e,h}$ is the effective mass for the electrons and holes, which differs substantially from the free electron mass m_0 .

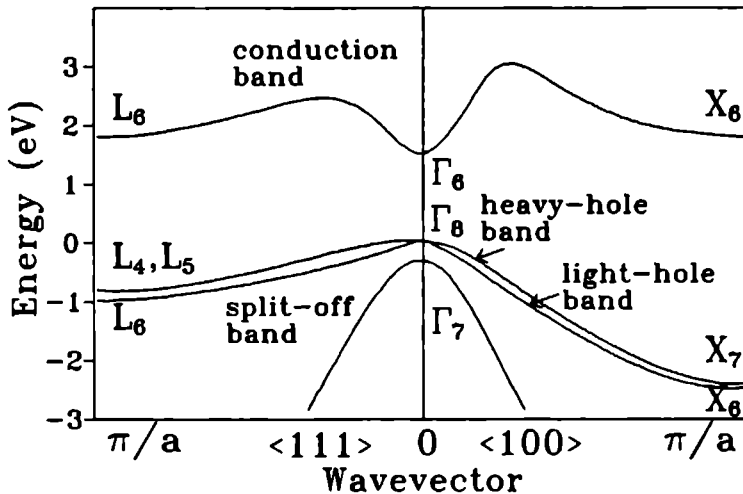


Figure 2.1 Part of the bandstructure of GaAs, with the direct band-gap at the center of the Brillouin zone, formed by the Γ_6, Γ_8 extrema of the conduction and valence bands. X_6 and L_6 correspond to the minima of the conduction band at the edge of the Brillouin zone.

The band-gap energy of GaAs depends strongly on the lattice temperature, and varies from 1.43 eV at 300 K to 1.52 eV at 4.2 K⁴.

Another important feature of the bandstructure of GaAs is formed by the presence of two other minima in the conduction band at the edge of the Brillouin zone. The L- and X-minima are situated in the $\langle 111 \rangle$ and $\langle 100 \rangle$ (and equivalent) directions at energies of about 0.29 eV and 0.43 eV respectively above the Γ -minimum. Electrons can scatter from the Γ -valley to the L- and X-satellite valleys by emission or absorption of zone-edge phonons.

2.2.2 GaAs/(Ga,Al)As heterostructures

After the development of sophisticated growth techniques, such as Metal Organic Vapour Phase Epitaxy (MOVPE) and Molecular Beam Epitaxy (MBE) it became possible to deposit monolayers of semiconductor materials with different band-gap energies on top of each other in a well defined way. In particular heterostructure systems consisting of alternating GaAs and (Ga,Al)As layers have attracted considerable research interest, due to the fact that the different lattices match almost perfectly, so that only little strain is introduced. In addition, the band-gap of (Ga,Al)As can be controlled by the aluminum content. When a very thin layer of smaller band-gap material (GaAs) is sandwiched between wider band-gap material ((Ga,Al)As), the motion of the carriers perpendicular to the layer structure is quantized. Figure 2.2 shows schematically the real space band-scheme of the resulting quantum well. A discrete spectrum of energy levels (subbands) is created for the carriers in the well, given by

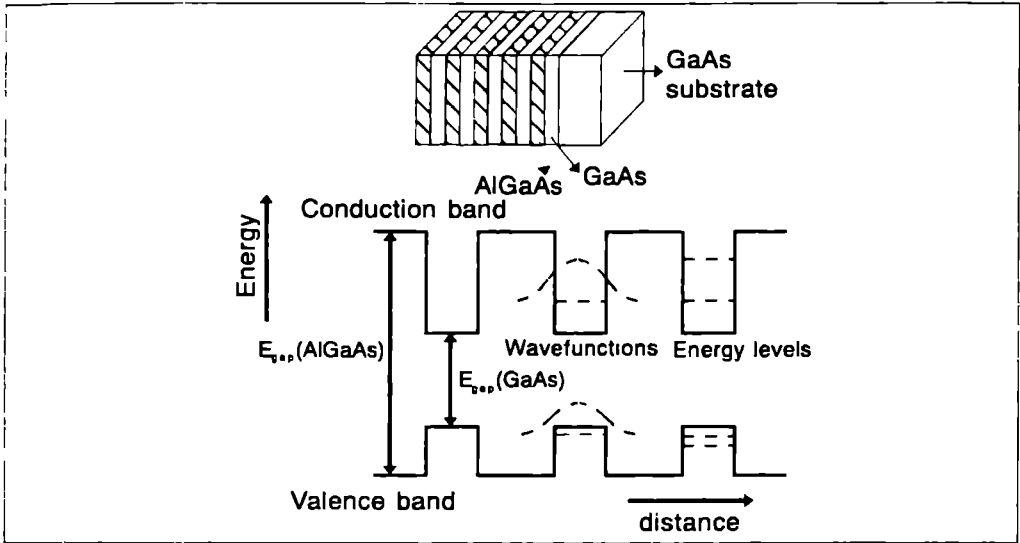


Figure 2.2: Schematic representation of a GaAs/(Ga,Al)As quantum well structure, with the envelope wavefunctions and the subband energy levels.

the bound state energies of a finite square well. The values of the subband energies depend on the quantum well width, the effective carrier masses and the barrier height. Furthermore nonparabolicity^{5, 6} and wavefunction extension in the (Ga,Al)As barriers have to be taken into account. The number of subbands increases with increasing well width. The quantum confinement gives rise to a quasi-two dimensional behaviour of the carriers, for which the density of states is given by:

$$g(E) = \sum_i \frac{m}{\pi \hbar^2} \theta(E - E_i) \quad (2.2)$$

where the summation i runs over the different subbands and $\theta(E)$ is the Heaviside step function and E_i is the subband energy.

When the width of the barrier layers is decreasing, the overlap of the wavefunctions of the carriers in adjacent wells becomes larger. In the case penetration of the wavefunctions in the barriers is smaller than the periodicity of a large sequence of alternating wells and barriers, a new superlattice is formed, with a new bandstructure of minibands which are separated by minigaps^{7, 8}. The so-called vertical transport through these minibands, parallel to the growth direction, has become an important research topic and is discussed in more detail in chapter 7.

2.2.3 Application of a magnetic field

A magnetic field B applied perpendicular to the plane of a quantum well structure fully quantizes the carriers due to the formation of Landau Levels. The resulting energy levels are

given by:

$$E = E_i + (N + \frac{1}{2})\hbar\omega_c \quad N = 0, 1, 2, \dots \quad (2.3)$$

with E_i is the subband energy and $\omega_c = \frac{eB}{m}$ is the cyclotron frequency.

Consequently the density of states is quasi-zero dimensional, i.e. no states exist in between the Landau Levels, which has stimulated considerable research effort in order to understand the fundamental consequences of dimensionality reduction⁹⁻¹². In real systems the discrete energy levels are broadened due to the occurrence of several scattering processes. A number of broadened density of states functions have been proposed, such as elliptic, lorentzian or gaussian broadened energy states. The actual consequences for the lineshape of magneto-photoluminescence spectra have been investigated extensively by Berendschot^{11, 13}, who found empirically that a gaussian shaped density of states function describes conveniently experimental photoluminescence spectra. As a result for each subband the density of states can be written as:

$$g(E) = \frac{1}{\pi l^2} \left(\frac{\pi}{2}\right)^{-\frac{1}{2}} \sum_{N=0}^{\infty} \frac{1}{\Gamma_N} \exp\left\{-\frac{2[E - (N + \frac{1}{2})\hbar\omega_c]^2}{\Gamma_N^2}\right\} \quad (2.4)$$

where $l = \sqrt{\frac{\hbar}{eB}}$ is the magnetic length, N runs over the Gaussian broadened Landau levels with linewidths Γ_N . The degeneracy of a Landau Level is given by $\frac{eB}{\hbar}$.

2.2.4 Metal-semiconductor interface

When a metal is brought into contact with a semiconductor a barrier is formed at the interface, analogous to a one-sided abrupt pn-junction¹⁴. Consider a n-type semiconductor, with a work function less than that of the metal. In contact the Fermi-levels are forced to coincide at both sides of the interface, which results in the formation of a Schottky barrier of height ϕ_b and a band-bending region as is shown schematically in figure 2.3, without (a) and with (b) an applied bias voltage V . Consequently an electric field is formed by a negative charge at the metal surface, balanced by a positive space charge in the semiconductor. The charge at the metal surface consists of extra conduction electrons in a thin sheet with a thickness of about the Thomas-Fermi screening distance ($\sim 0.5 \text{ \AA}$). In the n-type semiconductor electrons recede from the interface, leaving uncompensated donor ions, which provide for the balancing positive charge. Since the donor concentration N_D in the semiconductor is many orders of magnitude less than the concentration of electrons in the metal, the region depleted of electrons extends to a layer of appreciable thickness W , in which the semiconductor bands are bent upwards (figure 2.3). The width of the depletion region depends on the applied bias voltage V , the donor concentration N_D , the temperature T and the specific metal and semiconductor used, and can be calculated by solving the Poisson equation¹⁴. In the depletion region approximation¹⁵, which assumes that the space charge due to the ionised donors amounts to eN_D for $0 < x < W$ ($x=0$ at the interface) and is zero for $x > W$, the depletion region thickness is given by:

$$W = \sqrt{\frac{2e\epsilon\epsilon_0}{eN_D} (V_{bi} - V - \frac{k_b T}{e})} \quad (2.5)$$

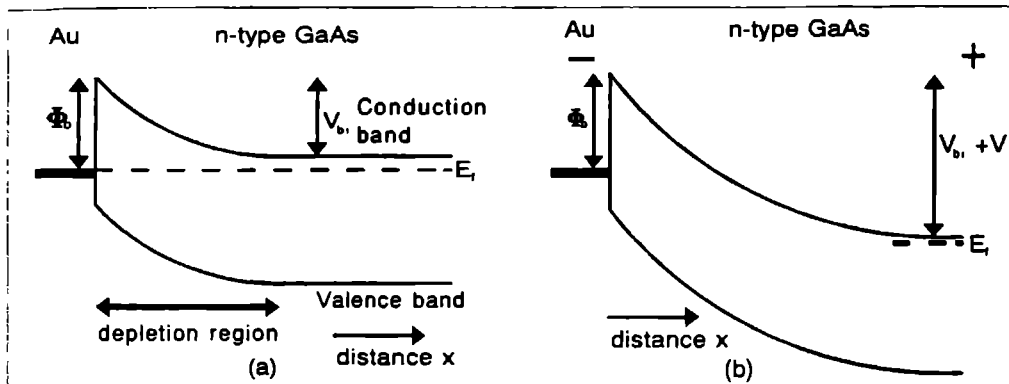


Figure 2.3: Schematic representation of the band-bending region at a metal-semiconductor (Au-n-GaAs) interface without (a) and with (b) an applied bias voltage V .

where ϵ is the dielectric constant of the semiconductor and V_{bi} is indicated in figure 2.3. The constant space charge within the depletion region gives rise to a linearly decreasing electric field \mathcal{E} , maximal at the interface ($x=0$) and zero at $x=W$, which is given by:

$$|\mathcal{E}(x)| = \sqrt{\frac{2eN_D}{\epsilon\epsilon_0}(V_{bi} - V - \frac{k_b T}{e}) - \frac{eN_D}{\epsilon\epsilon_0}x} \quad (2.6)$$

This results in parabolic decreasing bands (figure 2.3). As a consequence both the width of the depletion region and the electric field strength at the interface increase with increasing reverse bias, i.e. negative V (figure 2.3 (b)).

It should be noted that the actual formation of a Schottky barrier is strongly modified by surface states, interfacial (oxide) layers and the Schottky-effect¹⁴⁻¹⁶. The actual schematic description however is sufficient to envision what happens in the case of photo-excitation of electrons and holes. Due to their opposite charges they will be separated in space, resulting in a photo-current, which will be described in detail in chapter 5.

2.3 Ultrafast dynamics of photo-excited carriers

If a semiconductor is illuminated with ultrashort laser pulses with a photon energy exceeding the band-gap energy, electrons and holes are created in respectively conduction and valence bands. The rate of energy input into the carrier system is determined by the difference between laser photon energy and energy gap E_{gap} , and the electron-hole pair generation rate. The subsequent carrier dynamics and energy relaxation is determined by a number of processes, such as: 1) carrier-carrier scattering, 2) intervalley scattering or inter-band phonon scattering, 3) phonon cooling or intra-band phonon scattering, and 4) (non)radiative carrier recombination. In the following these processes are described briefly, with special attention to their role in the ultrafast carrier relaxation.

2.3.1 Carrier-carrier scattering

Since the wavevector of the laser photons can be neglected with respect to the wavevectors of the carriers, the carriers are created by vertical optical transitions ($\Delta k = 0$) into non-equilibrium distributions. The intercarrier interactions (electron-electron, electron-hole and hole-hole) mainly provide for the redistribution of momentum and energy among the carriers on a very short timescale. This ultrafast intercarrier scattering has been subject of many time-resolved investigations focusing onto the development of the initial somewhat broadened mono-energetic distribution towards a thermalized carrier gas. Only very short after intense pulsed laser excitation a non-equilibrium carrier distribution has been observed^{17, 18}, which reveals intercarrier scattering times as short as 200 fs or smaller. On a picosecond timescale the carrier distributions can be regarded as thermalized, characterized by Fermi-Dirac distributions which are determined by an effective carrier temperature and quasi-Fermi levels, i.e. a carrier density. It should be emphasized that in most cases the effective temperature still is much higher than the lattice temperature, so that often is spoken of hot carriers. Moreover, the carrier-carrier scattering rates strongly depend on the carrier density. In favourable circumstances, i.e. low carrier densities, the electron and hole distributions may be thermalized among themselves, but still have different temperatures on a picosecond timescale²⁰. For higher photo-excited carrier densities usually the temperature of the electron and hole distributions are equal on a picosecond timescale²⁰⁻²².

2.3.2 Intervalley scattering

When electrons are photo-created in the Γ -valley in GaAs with an excess energy larger than the energy of the L- and X-satellite valleys in the $\langle 111 \rangle$ and $\langle 100 \rangle$ (and equivalent) \mathbf{k} -directions respectively (figure 2.1), they can scatter to these valleys. This intervalley scattering process involves a large change in momentum, which is of the order of magnitude of the first Brillouin zone radius. This momentum may be taken up by a zone-edge phonon. Due to the relatively large effective mass in the satellite valleys ($\sim 0.5m_0$) the density of states is relatively high. In addition, due to the presence of several equivalent valleys in the different \mathbf{k} -directions, the L- and X-minima have a 4-fold and 6-fold degeneracy respectively. Both the large effective mass and the degeneracy of the satellite valleys make intervalley scattering very efficient. A variety of optical techniques has been used to measure these intervalley scattering rates, such as time-resolved raman scattering²³, hot photoluminescence²⁴⁻²⁷ and femtosecond pump-probe transmission measurements^{28, 29}. The importance of intervalley scattering after short laser pulse excitation has been illustrated elegantly by measuring the rise time of the near band-gap photoluminescence intensity for excitation energies above and below the energy of the satellite valleys^{30, 31}. The initial rise time appeared much shorter in the case electrons are created below the energy of the subsidiary valleys as compared to electron excitation with sufficient energy for intervalley transfer. In the latter case the electrons scatter rapidly to the satellite valleys, where they do not contribute to the photoluminescence signal. Subsequently the electrons return to the Γ -valley within approximately 10 ps, leading to a delay in the photoluminescence rise time^{30, 31}.

It is clear that also the electron transport in high electric fields is affected by intervalley

scattering. Electrons are heated very effectively by an electric field and gain an excess energy sufficient for scattering to the L-valley at a field of about 3 kV/cm³². In the satellite valleys the electrons are much heavier, leading to a reduced mobility as compared to electrons in the Γ -valley. These considerations lead roughly to two distinct field regions for the electron drift velocity, that is the electron mobility. At low fields the electron mobility is high, and at high fields when all the electrons are supposed to be transferred to the satellite valleys, the mobility is much lower. In the intermediate region the drift-velocity versus field curve shows a distinct optimum¹⁴, which can result in velocity overshoot effects in GaAs photoconductors, which have been observed experimentally by using a time-resolved photoconductivity technique³³⁻³⁵. The implications of intervalley scattering on the ultrafast high field carrier dynamics in GaAs will be discussed in more detail in chapter 5.

2.3.3 Phonon cooling

The excess energy of the hot carrier distribution after photo-excitation is transferred to the lattice by carrier-phonon interactions. These carrier-phonon interactions have been the subject of many (time-resolved) investigations². In polar semiconductors like GaAs, the carriers interact with phonons by basically two different mechanisms, polar and non-polar interactions. Moreover, since the GaAs unit cell contains more than one atom, apart from acoustic phonons, also optical phonons must be taken into account:

1. Non-polar scattering arises from the oscillation of atoms around their equilibrium positions. The resulting scattering of carriers is adequately described by the theorem of the deformation potential, for both optical and acoustic waves¹⁹.
2. Polar phonon interactions arise in a semiconductor crystal which consists of dissimilar atoms where the bonds are partly ionic and the unit cell does not contain a center of symmetry. The oscillation of the ions induces a polarization of the lattice, leading to the so-called piezo-acoustic (piezo-electric) and polar optical scattering processes.

The relative importance of the distinct phonon scattering mechanisms in GaAs has been calculated by Pugno *et al.*³⁶ using simple expressions. It appears that most of the hot carrier cooling experiments have been performed in the range where optical phonon scattering, in particular due to longitudinal optical (LO) phonons, dominates the energy relaxation process, that is for carrier temperatures above about 50 K³⁶. Below this temperature the carriers interact predominantly with acoustic phonons.

One of the most striking experimental results concerning the picosecond optical phonon cooling of carriers, is formed by the drastic reduction of the measured cooling rates with increasing carrier densities. Initially this was suggested to originate from the screening of the polar phonon interaction. Later on it turned out that the significant cooling reduction is the result of a built-up of a non-equilibrium distribution of optical phonons². In the initial stage of the energy relaxation process a large number of optical phonons are emitted, which must decay into large wavevector acoustic phonons, determined by energy and momentum conservation. This decay time appeared to be larger than the optical phonon emission time, resulting in the development of a non-equilibrium phonon distribution, much larger than the

equilibrium phonon population at the bath temperature. Consequently also re-absorption of so-called hot phonons must be considered, which tend to reduce the net carrier cooling rate whenever the carrier temperature exceeds the threshold for phonon emission. This reduction of the carrier cooling rate can be as high as 20 times for high carrier densities.

The dispersion relation for acoustic phonons is given by $\hbar\omega_{\mathbf{q}} = \hbar c_s \mathbf{q}$, where c_s is the sound velocity in the material. As a result acoustic phonons can interact efficiently with the bath outside the excitation area, so that no acoustic phonon heating is expected.

2.3.4 Recombination and luminescence

Photo-excited electrons and holes can recombine via nonradiative or radiative recombination processes, where in the latter case luminescence radiation is emitted. The radiative transitions may occur at or near the band-edges due to a variety of mechanisms, possibly related to crystal imperfections or impurities. However, for sufficiently pure semiconductor material the radiative recombination is governed merely by free carriers or by excitons. An electron and hole can be bound to each other by the Coulomb interaction to form an exciton with a binding energy R_H^* , analogous to the hydrogen atom. The value of the binding energy is given by the excitonic Rydberg $(m_r/m_0)\epsilon^2$ times the Rydberg energy of hydrogen (13.6 eV), where m_r is the reduced mass of the exciton and ϵ is the dielectric constant, which yields for bulk GaAs a value of R_H^* of about 4 meV. In case of high carrier densities however the Coulomb interaction is screened and the band-gap energy is reduced due to many-particle interactions^{37, 38}, leading to the disappearance of distinct exciton states. Since in this study the density of the photo-excited carriers is rather high, we only consider band-to-band recombination.

When time-resolved photoluminescence spectra are used to probe the ultrafast carrier relaxation, the spectral lineshape must be analyzed in order to obtain the time-evolution of both the density and the effective temperature of the carriers. In general the resulting parameters depend on the particular model used for the band-to-band recombination process. Therefore, several models for the photoluminescence lineshape have been used, which will be described in chapter 3.

Common carrier lifetimes due to spontaneous recombination in good quality GaAs are much longer than the processes involved in the energy relaxation, which makes the photoluminescence technique extremely useful in measuring the time-evolution of the distributions of the carriers without affecting the cooling rate itself. However, in case the recombination time becomes comparable to the times involved in the cooling process, the recombination has to be included in the analysis. The effect of such a short carrier lifetime on the carrier cooling will be discussed extensively in chapter 4.

2.4 Experimental arrangements

In order to improve our insight in the different ultrafast processes described in the previous section, we have exploited different photoluminescence techniques, using laser systems with a light output ranging from continuous wave to picosecond and femtosecond pulses. Continuous wave or time-integrated photoluminescence experiments use really straightforward laser systems and set-ups, which will not be discussed further.

2.4.1 The picosecond laser system

For the experiments on a picosecond timescale described in chapters 3 and 4 we made use of the following, commercial available, laser system. A continuous wave Argon ion laser (Spectra Physics, Model 2040E) is used as a pump source for a pulsed Ti:sapphire laser (Spectra Physics, Tsunami) which is actively mode-locked with an opto-acoustic modulator. The laser output is a train of stable pulses with a duration of 1.3 ps, deduced by means of an autocorrelation technique. The average power amounts to 2 W with a repetition rate of 84 MHz. The wavelength can be tuned easily from 720 nm to 850 nm.

2.4.2 The femtosecond laser system

For the subpicosecond photoluminescence correlation measurements described in chapter 5 we made use of a home-built Colliding Pulse Mode (CPM) ring dye laser, which has been described in detail by Berendschot¹¹, so only a brief description will be given here. The design of the CPM laser resembles the concept of Valdmanis and Fork⁴⁰. The laser generates stable output pulses with a typical pulse width of 60 fs, a repetition rate of 100 MHz and an average power of 20 mW per beam, centred at a wavelength of about 620 nm. In the CPM laser the concept of passive mode-locking is applied, which means that next to a saturable amplifier dye (Rhodamine 6G) also a saturable absorber dye (3,3'-diethyloxadicarbocyanine-iodide, DODCI) has been inserted in the ring cavity. The amplifier dye is pumped by a continuous wave Argon ion laser (Spectra Physics, Model 171) operating at a wavelength of 514 nm. In order to obtain the shortest possible pulses a sequence of four quartz prisms⁴¹ has been inserted to correct for pulse broadening due to group-velocity dispersion and self-phase modulation¹¹.

2.5 Time-resolved photoluminescence techniques

Since the availability of laser systems which are able to generate ultrashort laser pulses, a large number of experimental techniques have been developed by which measurements can be performed with a time-resolution only limited by the pulse width. In this section two experimental techniques will be described which have been used to perform photoluminescence measurements with (sub)picosecond time-resolution, i.e. the up-conversion technique and the photoluminescence correlation technique.

2.5.1 Picosecond up-conversion technique

The up-conversion technique makes use of frequency-mixing of luminescence light with a short laser pulse in a non linear crystal, generating sum-frequency radiation⁴². The mixing only occurs for that part of the photoluminescence signal which coincides with the laser pulse, which makes pulse width limited time-resolution possible, provided certain conditions are satisfied.

The experimental picosecond up-conversion set-up is displayed schematically in figure 2.4, and is very similar to the set-ups described by Hollering³⁹ and Reinen¹². The light beam generated by a pulsed Ti:sapphire laser system is split in two by a beam splitter. One part is

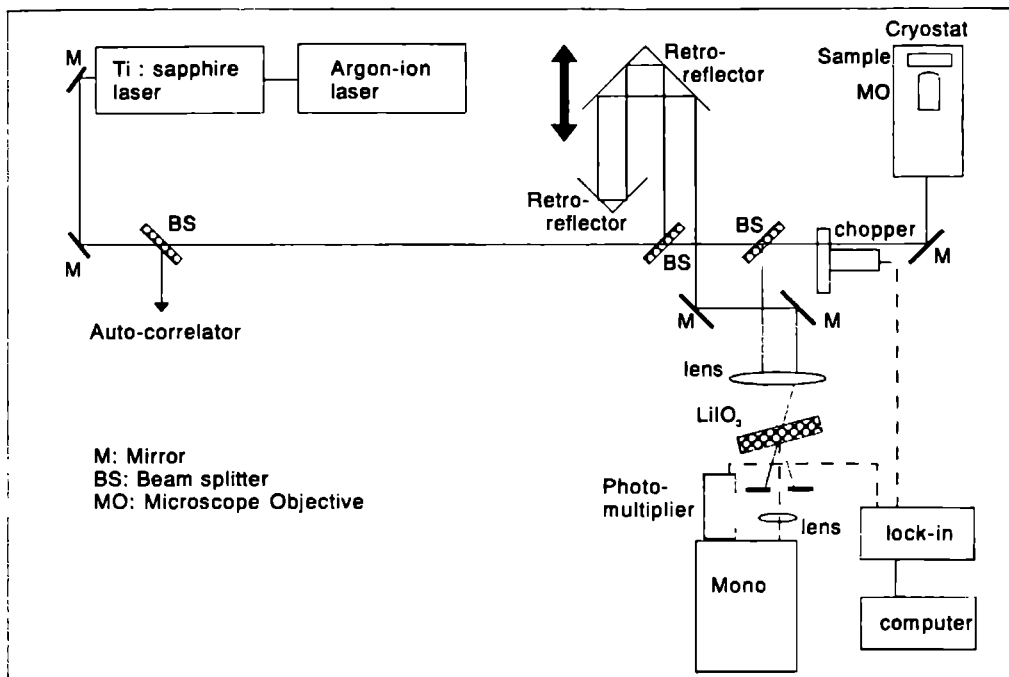


Figure 2.4: Schematic representation of the experimental set-up for the time-resolved photoluminescence up-conversion measurements.

mechanically chopped and subsequently focused by a microscope objective onto the sample surface. The other part is guided through a delay-line, consisting of two retro-reflectors, one of which can be translated by steps of $1 \mu\text{m}$ using a stepping control motor, in order to lengthen the optical path of the laser beam. The luminescence radiation emitted by the sample is guided by a beam splitter into a light-gate, consisting of a non linear LiIO_3 crystal, where it is up-converted by the laser light returning from the delay line. The up-converted radiation is focused into a 1 m grating monochromator (Monospek) and is detected by a EMI 9789/82 QB photomultiplier tube, with the use of a lock-in amplifier.

Sum-frequency generation between the laser pulses (ω_1) and the luminescence (ω_2) is obtained at a frequency $\omega_1 + \omega_2$, whenever both signals overlap in time. The intensity of the sum-frequency radiation is proportional to the product of intensities of the luminescence and the laser light. Since the intensities of subsequent laser pulses is the same and their duration is short as compared to the duration of the luminescence, the intensity of the up-converted signal is a measure for the luminescence intensity. By tuning the length of the delay line, the time-evolution of the luminescence signal at frequency ω_2 is monitored. In addition by scanning the monochromator over $\omega_1 + \omega_2$ at a fixed length of the delay line a full luminescence spectrum is recorded, emitted at a certain time after laser excitation. However, apart from energy conservation ($\omega_3 = \omega_1 + \omega_2$) frequency-mixing also requires

phase-matching⁴³, i.e. $\mathbf{k}_3 = \mathbf{k}_1 + \mathbf{k}_2$, where \mathbf{k}_1 , \mathbf{k}_2 and \mathbf{k}_3 correspond to the wavevectors of the laser pulse, luminescence signal and sum-frequency signal respectively. In LiIO_3 the phase-matching condition can be obtained by adjusting the angle between the crystal optical axes and the wavevectors of the light. This implies that in measuring the spectral distribution of the luminescence radiation the angle of the non linear crystal has to be adjusted for each wavelength. Therefore the non linear crystal is mounted on a stepping control motor, capable of making steps of 0.01 degrees, which is tuned synchronously with the monochromator. The approximately linear relation of the crystal angle as a function of the luminescence wavelength is determined experimentally for each laser wavelength used. This calibration procedure is described extensively by Hollering³⁹ and Reinen¹², for different laser wavelengths.

The thickness of the non linear crystal affects both the up-conversion efficiency and the ultimate time-resolution⁴⁴. The efficiency is proportional to the square of the crystal thickness. However, the thickness of the crystal is restricted by the spectral bandwidth and the group-velocity mismatch between the fundamental and generated pulses, which are inversely and linear proportional to the crystal thickness respectively⁴⁴. For substantially different laser wavelengths or pulse widths different crystals are needed. The actual LiIO_3 crystal thickness amounts to 3 mm, while it was cut at an angle of 40 degrees with respect to the optic axes, leading to a time-resolution of a few picoseconds and optimal up-conversion efficiency for the laser wavelengths used (~ 730 nm) in combination with luminescence emitted by GaAs (~ 800 nm).

It should be noted that the frequency-mixing technique also can be used to monitor the shape of the laser pulses or measure their duration, by means of the autocorrelation of the pulses³⁹.

2.5.2 Subpicosecond photoluminescence Correlation Technique

In the photoluminescence correlation technique the time-resolution is achieved by the introduction of a certain time delay δt between two equal pulses incident on the sample, and the measurement of the photoluminescence intensity as a function of δt . The technique makes use of the bimolecular nature of the recombination process, i.e. the luminescence intensity is proportional to the product of the electron and hole populations. We follow the approach as proposed by Rosen *et al.*⁴⁵, in which a background-free photoluminescence correlation signal is measured, as opposed to the method of Von der Linde *et al.*⁴⁶. The experimental set-up is shown schematically in figure 2.5. The beam of laser pulses generated by a CPM laser is split into two equal parts by a beam splitter (BS). One part is mechanically chopped at frequency ω_1 and reflected by a retro-reflector, which can be translated in steps of $0.1 \mu\text{m}$ by using a stepping control motor. The other part is chopped at frequency ω_2 . Both beams are collinearly focused onto the sample surface by a microscope objective. In order to avoid coherence effects when the two pulses overlap in time⁴⁶, the polarization of one beam is rotated over 90 degrees using a $\lambda/2$ -wave plate. The luminescence radiation emitted by the sample is guided through a 1 m grating monochromator (Monospek) and detected by a cooled GaAs photomultiplier. The luminescence signal detected by the photomultiplier is integrated by a lock-in amplifier, tuned at frequency $\omega_1 - \omega_2$, which gives the correlation between the carrier distributions photo-injected by the two laser pulses, i.e. the detected signal necessarily results

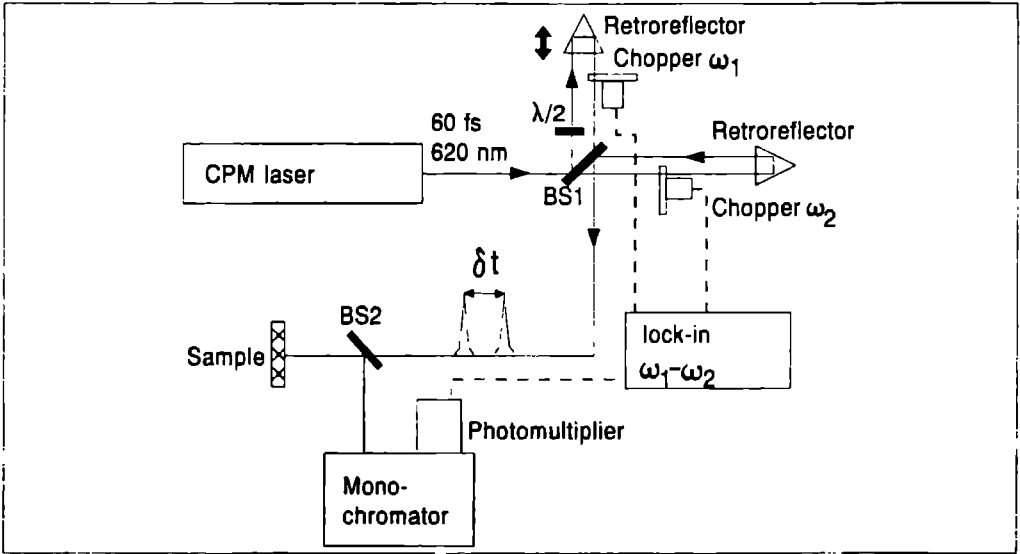


Figure 2.5: Schematic representation of the experimental set-up for the time-resolved photoluminescence correlation measurements.

from both laser pulses. When the time delay between the laser pulses is too large the carrier distributions generated by the first pulse are gone (e.g. by recombination or other processes) when the second pulse arrives. The correlated photoluminescence intensity measured as a function of the time delay in between the pulses therefore contains information about the dynamical behaviour of the photo-excited carriers.

In the case of an experimental set-up as is shown in figure 2.5 the total time-integrated photoluminescence intensity at a certain energy $\hbar\omega$ for a time delay δt between the pulses can be written as:

$$\int I(t, \hbar\omega, \delta t) dt \propto \int [n_1(E_e, t) \cos(\omega_1 t) + n_2(E_e, t) \cos(\omega_2 t)] \times [p_1(E_h, t) \cos(\omega_1 t) + p_2(E_h, t) \cos(\omega_2 t)] dt \quad (2.7)$$

where

$n_1(t), n_2(t), p_1(t), p_2(t)$ are the photo-excited electron (n) and hole (p) occupations at energies E_e and E_h respectively, from the laser pulses 1 and 2.

$E_e + E_h = \hbar\omega - E_{\text{gap}}$ with E_{gap} the band-gap energy.

$n_2(t) = n_1(t + \delta t)$ and $p_2(t) = p_1(t + \delta t)$ when the photo-excited electron and hole distributions due to the two laser pulses are assumed to be equal, and only shifted in time.

The terms $\cos(\omega_1 t)$ and $\cos(\omega_2 t)$ which represent the chopper action, are slowly varying as compared to the typical carrier relaxation times and can be put before the integral. As a

result the signal at frequency $\omega_1 - \omega_2$ is proportional to

$$I(\hbar\omega, \delta t) = \int I(t, \hbar\omega, \delta t) dt \propto \int [n(E_e, t) p(E_h, t + \delta t) + n(E_e, t + \delta t) p(E_h, t)] dt \quad (2.8)$$

Thus the measured time-integrated signal is the cross-correlation of the electron concentration excited by one beam and the hole concentration excited by the other. Moreover, measurement of the correlated photoluminescence signal at different photon energies $\hbar\omega$ can supply us with information about the energetic distributions of the carriers. However, all the information is hidden in a non-transparent correlation function, which may make the interpretation of an experiment difficult. In addition, in case the carrier dynamics consists of two subsequent processes, this method may combine them into one time constant, due to the time-integrated form of the ultimate correlation function measured.

On the other hand, the photoluminescence correlation technique can be realised very simply, due to its simple set-up, and possesses a time-resolution only limited by the laser pulse width. The signal-to-noise ratio is often very good since the luminescence radiation is detected directly, whereas in eg. the up-conversion technique a non linear crystal is required to accomplish the time-resolution needed. This may result in a low efficiency, especially for short laser pulses, when very thin non linear crystals have to be used.

References

- [1] *Semiconductors Probed by Ultrafast Laser Spectroscopy*, edited by R.R. Alfano (Academic Press, New York, 1984).
- [2] J. Shah, *J. Phys. (Paris)* **42**, C-7 445 (1981); J. Shah, *IEEE J. Quantum. Electron.* **QE-22**, 1728 (1986); S.A. Lyon, *J. of Lumin.* **35**, 121 (1986); J. Shah, *Solid State Electron.* **32**, 1051 (1989).
- [3] F. Belezny and G. Pataki, *Phys. Stat. Sol.* **8**, 805 (1965).
- [4] C.R. Pidgeon, *Phys. Rev.* **154**, 737 (1967).
- [5] D.C. Rogers, J. Singleton, R.J. Nicholas, C.T. Foxon and K. Woodbridge, *Phys. Rev.* **B34**, 4002 (1986).
- [6] U. Ekenberg, *Proc. 19th Int. Conf. on the Physics of Semiconductors* (Warsaw, Poland, 1988) p. 287; U. Ekenberg, *Phys. Rev.* **B36**, 6152 (1987).
- [7] L. Esaki and R. Tsu, *IBM Res. Note* **RC-2418** (1969); L. Esaki, *IEEE J. Quantum Electronics* **QE-22**, 1611 (1986).
- [8] J.C. Maan *Festkörperprobleme (Advances in Solid State Physics)* **27**, edited by P. Grosse, (Vieweg, Braunschweig, 1987) p 137-167.
- [9] R.W.J. Hollering, T.T.J.M. Berendschot, H.J.A. Bluyssen, H.A.J.M. Reinen, P. Wyder and F. Roozeboom, *Phys. Rev.* **B38**, 13323 (1988).
- [10] J.F. Ryan, R.A. Taylor, A.J. Turberfield and J.M. Worlock, *Surf. Sci.* **170**, 511 (1986).
- [11] T.T.J.M. Berendschot, *Phd. thesis*, University of Nijmegen (1989).

- [12] H.A.J.M. Reinen, *Phd. thesis*, University of Nijmegen (1990).
- [13] T.T.J.M. Berendschot, H.A.J.M. Reinen and H.J.A. Bluysen, *Solid State Commun.* **63**, 873 (1987).
- [14] S.M. Sze, *Physics of Semiconductor Devices*, 2nd edition, (Wiley & Sons, New York, 1981).
- [15] E.H. Rhoderick and R.H. Williams, *Metal-Semiconductor Contacts*, 2nd edition, (Clarendon Press, Oxford, 1988).
- [16] *Metal-Semiconductor Schottky barrier junctions and their applications*, edited by B.L. Sharma, (Plenum Press, New York, 1984).
- [17] J.L. Oudar, D. Hulin, A. Migus, A. Antonetti and F. Alexandre, *Phys. Rev. Lett.* **55**, 2074 (1985).
- [18] W.H. Knox, C. Hirlimann, D.A.B. Miller, J. Shah, D.S. Chemla and C.V. Shank, *Phys. Rev. Lett.* **56**, 1191 (1986); W.H. Knox, D.S. Chemla, G. Livescu, J.E. Cunningham and J.E. Henry, *Phys. Rev. Lett.* **61**, 1290 (1988).
- [19] J. Bardeen and W. Shockley, *Phys. Rev.* **80**, 72 (1950).
- [20] W.W. Rühle, J. Collet, M. Pugnet and K. Leo, *Condensed Systems of Low Dimensionality*, edited by J.L. Beeby *et al.* (Plenum Press, New York, 1991).
- [21] M. Asche and O.G. Sarbei, *Phys. Stat. Sol. (b)* **141**, 487 (1987).
- [22] W. Pötz, *Phys. Rev.* **B36**, 5016 (1987).
- [23] C.L. Collins and P.Y. Yu, *Phys. Rev.* **B30**, 4501 (1984).
- [24] B.P. Zakharchenya, V.I. Zemskii, and D.N. Mirlin, *Sov. Phys. JETP* **43**, 569 (1976).
- [25] D.N. Mirlin, I. Ja. Karlik, L.P. Nikitin, I.I. Reshina and V.F. Sapega, *Solid State Commun.* **37**, 757 (1981).
- [26] G. Fasol and H.P. Hughes, *Phys. Rev.* **B33**, 2953 (1986).
- [27] R.G. Ulbrich, J.A. Kash and J.C. Tsang, *Phys. Rev. Lett.* **62**, 949 (1989).
- [28] P.C. Becker, H.L. Fragnito, C.H. Brito Cruz, J. Shah, R.L. Fork, J.E. Cunningham, J.E. Henry and C.V. Shank, *Appl. Phys. Lett.* **53**, 2089 (1988).
- [29] C.L. Tang, I.A. Walmsley and F.W. Wise, *Appl. Phys. Lett.* **52**, 850 (1988).
- [30] J. Shah, B. Deveaud, T.C. Damen, W.T. Tsang, A.C. Gossard and P. Lugli, *Phys. Rev. Lett.* **59**, 2222 (1987).
- [31] D.Y. Oberli, J. Shah and T.C. Damen, *Phys. Rev.* **B40**, 1323 (1989).
- [32] K. Seeger, *Semiconductor Physics*, 3rd edition, (Springer-Verlag, Berlin, 1985).
- [33] R.B. Hammond, *Physica* **134B**, 475 (1985).
- [34] A. Evan Iverson, G.M. Wysin, D.L. Smith, and A. Redondo, *Appl. Phys. Lett.* **52**, 2148 (1988).

- [35] K. Meyer, M. Pessot, G. Mourou, R. Grondin and S. Chamoun, *Appl. Phys. Lett.* **53**, 2254 (1988).
- [36] M. Pugnet, J. Collet and A. Cornet, *Solid State Commun.* **38**, 531 (1981).
- [37] P. Vashishta and R.K. Kalia, *Phys. Rev.* **B25**, 6492 (1982).
- [38] R. Zimmermann, *Phys. Stat. Sol. (b)* **146**, 371 (1988).
- [39] R.W.J. Hollering, *Phd. thesis*, University of Nijmegen (1986).
- [40] J.A. Valdmanis and R.L. Fork, *IEEE J. of Quantum Electron.* **QE-22**, 112 (1986).
- [41] R.L. Fork, O.E. Martinez and J.P. Gordon, *Opt. Lett.* **9**, 150 (1984).
- [42] H. Mahr and M.D. Hirsch, *Opt. Commun.* **13**, 96 (1975).
- [43] D.A. Kleinmann, *Laser Handbook, Vol. 2*, edited by T.E. Arechi (Schulz-Dubois, 1972).
- [44] J. Shah, *IEEE J. of Quantum Electron.* **QE-24**, 276 (1988).
- [45] D. Rosen, A.G. Doukas, Y. Budanski, A. Katz, and R.R. Alfano, *Appl. Phys. Lett.* **39**, 935 (1981); D. Rosen, A.G. Doukas, A. Katz, Y. Budanski, and R.R. Alfano in *Semiconductors Probed by Ultrafast Laser Spectroscopy*, edited by R.R. Alfano (Academic Press, New York, 1984).
- [46] D. von der Linde, J. Kuhl and E. Rosengart, *J. of Luminescence* **24/25**, 675 (1981).

Chapter 3

Lineshape analysis of picosecond time-resolved high excitation photoluminescence spectra

Abstract

Picosecond time-resolved photoluminescence spectra of nearly resonantly excited carriers in bulk GaAs have been measured. The spectra show anomalous shoulders at their high-energy tails, especially pronounced at high densities and low temperatures of the electron-hole plasma. The positions of the shoulders with respect to the main peak seem to be correlated with the plasma density. In order to understand this feature several lineshape analysis methods have been used, including an elaborate many-particle model which incorporates plasmon-assisted optical transitions, and simple single-particle models with and without \mathbf{k} -conservation. It has been found that neither of the models used can describe precisely the lineshapes of the measured high excitation spectra. However, from the best lineshape fits reliable values for the carrier density and temperature could be extracted. The many-body model and the simple model without \mathbf{k} -conservation give very similar results, whereas the simple model including \mathbf{k} -conservation results in higher temperatures, leading to deviating carrier cooling curves.

3.1 Introduction

Lineshape analysis of photoluminescence and gain spectra has been used frequently in the past to gain insight in the physical processes of carriers in semiconductors such as energy relaxation¹, electron-hole recombination and band-gap renormalization²⁻⁴. For this analysis single-particle models, with and without \mathbf{k} -conservation, as well as many-particle models have been used.

Following the early work of Göbel *et al.*⁵ in GaAs, a number of optical studies has been reported, where in the lineshape analysis \mathbf{k} -conservation was assumed to break down^{6, 7}. This approach led to reasonable lineshapes of GaAs gain spectra, in contrast to the \mathbf{k} -conservation model⁵. Therefore it was believed that the \mathbf{k} -conservation model can only be used when many-body interactions are taken into account. Due to inter-particle interactions photons with an energy smaller than the band-gap energy can be emitted, leading to the appearance of a low-energy tail in photoluminescence spectra. Moreover, reduction of the exchange-correlation energy with the electron-hole plasma density causes a significant band-gap shrinkage, resulting in a spectral shift of the photoluminescence. Both the low-energy tail and the band-gap renormalization demonstrate the importance of many-body effects on optical spectra for degenerate carrier distributions. Although also in the single-particle model without \mathbf{k} -conservation no specific many-particle interactions are taken into account, some broadening of the single-carrier states is simulated by the contribution to the photoluminescence intensity of transitions between states with different wavevectors.

During the last decades several models have been reported, following the early proposal of Landsberg⁸, to describe the spectral low-energy tail with help of transitions between lifetime broadened carrier states. Haug *et al.*⁹ derived a general expression for the collision broadening, including damped plasmon-assisted transitions, which influence the photoluminescence and gain spectra in addition to a screened Coulomb interaction between the electron-hole pairs. This model, featuring Lorentzian broadened carrier states, predicts appropriate lineshapes of gain spectra of GaAs⁹. The exact collision broadening model of Haug *et al.* has been used to extract electron-hole plasma parameters from photoluminescence spectra of CdTe¹⁰ and GaAs¹¹. It has been found that the resulting effective temperature is always lower than the temperature deduced from an exponential fit to the high-energy tail of a spectrum, due to the particular wavevector dependence of the collision broadening, elucidating part of the remaining discrepancy between the calculated energy relaxation rate and the experimentally observed cooling curves. Furthermore the band-gap reduction with increasing carrier density has been found to be close to well-accepted theoretical predictions¹⁰. The collision broadening values of Haug have been inserted in other expressions for the photoluminescence lineshape to give a nice description of the experimental spectra of (Ga,Al)As. In addition appropriate band-gap renormalization values have been obtained, although a lower energy cut-off had to be invoked to avoid tailing of states deep into the gap, due to the peculiar asymptotic behaviour of the Lorentzian collision broadening^{2, 3}. Selloni *et al.*³ performed an exhaustive comparison between several lineshape models, including many-particle interactions, and found nearly equal densities and temperatures for all models and minor differences in the band-gap renormalization.

In this chapter we present picosecond time-resolved photoluminescence spectra of nearly resonantly excited carriers in GaAs for different laser excitation intensities. From the spectra reliable values for the carrier density and the effective temperature were extracted by using two single-particle recombination models, with and without k -conservation, and the many-particle model introduced by Haug *et al.*⁹. Comparison of the results shows that both the many-body model and the simple model neglecting k -conservation give similar values for the effective temperature and density of the carriers, whereas the simple model including k -conservation results in higher temperature values. Determination of merely the temperature from an exponential fit to the high-energy tail can yield even higher values. For practical purposes it appears that the most convenient way to determine temperature and density is by using the single-particle model without k -selection.

Further, the high excitation spectra show anomalous shoulders at their high-energy tail of which the energy position with respect to the main peak seems to be correlated with the electron-hole plasma density. The spectral lineshape of the shoulders can be described well by a single-particle lineshape neglecting k -conservation. However, these shoulders can, even by the many-particle model including plasmon-assisted optical transitions, not be explained.

The chapter is organised as follows. Section 3.2 deals with the introduction of the samples used and the presentation of the picosecond time-resolved photoluminescence up-conversion measurements. In section 3.3 the three different photoluminescence lineshape models will be discussed. Section 3.4 describes the results of the different lineshape analysis models, and section 3.5 reviews the main conclusions.

3.2 Experimental details and results

The time- and energy-resolved photoluminescence experiments were performed on two different samples. Sample Aix456, grown by MOVPE at the university of Nijmegen, consists of an undoped $0.25\ \mu\text{m}$ -thick GaAs layer which is sandwiched between (Ga,Al)As layers of $0.1\ \mu\text{m}$ ($[\text{Al}]=0.65$) and $4\ \mu\text{m}$ ($[\text{Al}]=0.55$) thickness. The uppermost (Ga,Al)As layer ($0.1\ \mu\text{m}$) is capped by a GaAs layer of $100\ \text{\AA}$. Sample W285, grown at the university of technology in Eindhoven by MBE, contains a $0.25\ \mu\text{m}$ -thick GaAs layer sandwiched between two (Ga,Al)As layers ($[\text{Al}]=0.35$) of $0.1\ \mu\text{m}$ and $0.2\ \mu\text{m}$ thickness, and a top capping GaAs layer of $170\ \text{\AA}$ -thickness. In both samples the (Ga,Al)As layers are transparent for the incident laser light and prevent carrier diffusion in the growth direction. The thickness of the GaAs layer is smaller than the absorption length of about $0.5\ \mu\text{m}$ at the used laser wavelengths. As a result a more or less homogeneous carrier distribution was photo-injected. In sample W285 a superlattice buffer layer ($50 \times 42\ \text{\AA}$ GaAs/ $60\ \text{\AA}$ AlAs) has been inserted between the deepest (Ga,Al)As-layer and the semi-insulating GaAs substrate in order to prevent carrier excitation in the substrate, which could result in a disturbing photoluminescence background intensity at the GaAs wavelength.

Carrier distributions were excited directly in the undoped GaAs layers by picosecond laser pulses, generated by a mode-locked Ti:sapphire laser, optically pumped by a continuous wave Argon ion laser. The laser beam was mechanically chopped to allow for lock-in detection and

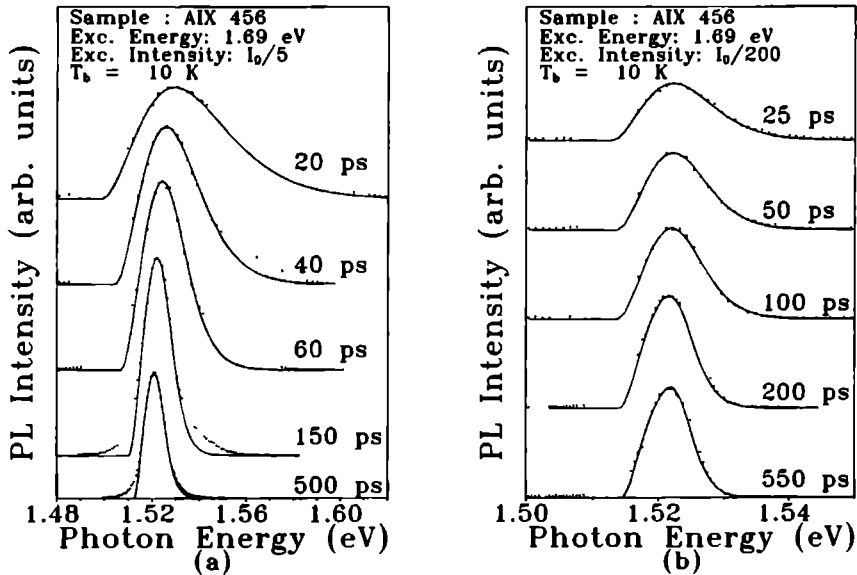


Figure 3.1: Measured (dotted curves) and calculated (solid curves) photoluminescence (PL) spectra at different times after excitation for excitation levels $I_0/5$ (a) and $I_0/200$ (b) for sample Aix456.

was focused to a $20\ \mu\text{m}$ -diameter spot onto the sample surface by a microscope objective. The photoluminescence radiation from the GaAs-layer was collected in a backscattering geometry using the same microscope objective. Energy-resolved photoluminescence spectra with picosecond time-resolution were recorded with help of the up-conversion technique using a non linear LiIO_3 crystal as a lightgate. The up-converted photoluminescence light was guided through a 1 m monochromator (Monospek) and detected with an EMI 9789/82 QB photomultiplier tube and a lock-in amplifier. The sample was kept at a bath temperature of 10 K (see chapter 2 for more details).

Time-resolved photoluminescence spectra were measured for a number of excitation intensities ranging from $I_0/200$ to I_0 ($I_0 = 1.5\ \text{kW}/\text{cm}^2$) and three different laser photon energies (1.65 eV, 1.69 eV and 1.72 eV). Typical photoluminescence spectra recorded after excitation of sample Aix456 with laser energy 1.69 eV, are displayed by the dotted curves in figure 3.1 at different times after excitation and two excitation levels: $I_0/5$ (a) and $I_0/200$ (b). The spectra for one laser intensity are all shown on the same vertical scale but arbitrarily vertically shifted for clarity. Excitation with laser energy 1.65 eV did not specifically alter the spectra. The solid lines in figure 3.1 represent photoluminescence lineshape calculations using an expression of a single-particle model for band-to-band recombination neglecting k -conservation, which will be discussed in detail in section 3.3.2. Generally four parameters are adjusted to obtain a good match between calculated and measured photoluminescence spec-

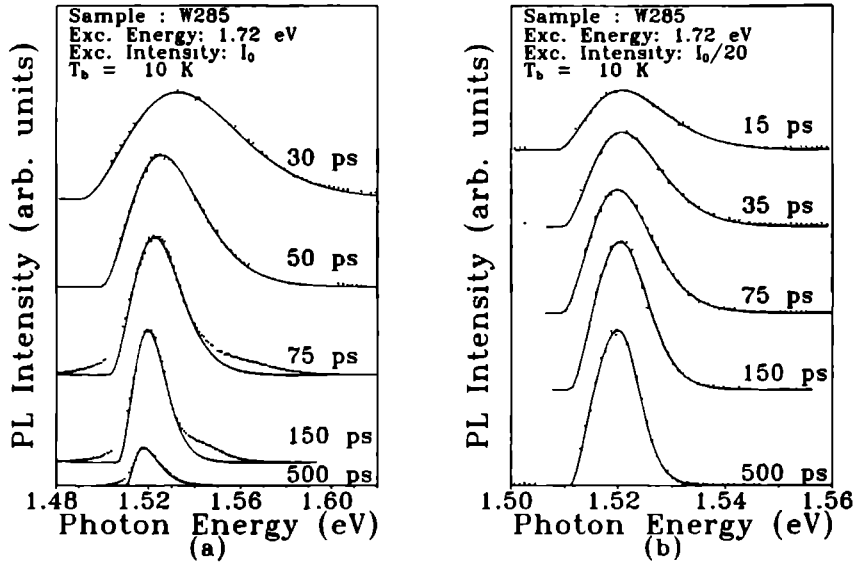


Figure 3.2: Measured (dotted curves) and calculated (solid curves) photoluminescence (PL) spectra at different times after excitation for excitation levels I_0 (a) and $I_0/20$ (b) for sample W285.

tra. The low-energy onset of the intensity is determined by the band-gap energy E_{gap} . The spectral high-energy slope reflects the effective temperature T_{eff} of the carrier distributions, which are assumed to be thermalized. Obviously the increasing high-energy slope with time in figure 3.1 is related to the picosecond carrier cooling. The spectral width corresponds to the band-filling, i.e. the carrier density $n_{e,h}$. Finally the calculated spectra are multiplied by a proportionality factor to scale the lineshape vertically to the data. This proportionality factor corresponds to the coefficient in front of the photoluminescence intensity, which contains for instance the optical matrix element, and is related to the usual radiative recombination coefficient B_r .

The spectra at low excitation intensity (figure 3.1 (b)) are relatively well described by the calculated ones, apart from their low-energy tails. This part of the spectrum corresponds to photons emitted with an energy smaller than the band-gap energy and cannot be explained by the actual single-particle lineshape. This low-energy tail can be explained with help of lifetime broadening of the single-carrier states due to inter-particle collisions, i.e. many body interactions⁸. For example an electron at the band-edge can instantaneously lose energy due to a collision and recombine under emission of a below-band-gap photon. The higher the lifetime broadening parameter Γ at the band-edge, the deeper the tailing of the photoluminescence intensity into the energy gap. In addition the same interactions between the particles cause the band-gap to renormalize, resulting in a band-gap reduction with increasing carrier density. So the simple single-particle recombination model, which does not

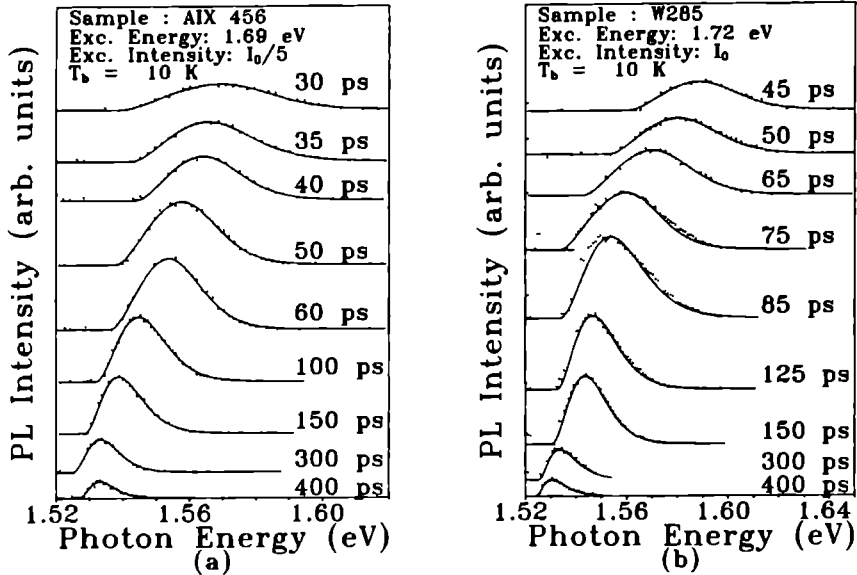


Figure 3.3: Time-evolution of the high-energy intensity shoulders (dotted curves), obtained by subtracting the fitted single-particle lineshapes from the experimental spectra, for sample AIX456 (a) and W285 (b). The solid curves correspond to single-particle lineshapes neglecting k -conservation.

include many-body interactions, cannot describe the low-energy tail and is only expected to follow nicely the spectral high-energy part as it does.

However, in the case of the high excitation level (figure 3.1 (a)) also a pronounced intensity shoulder is observed at the high-energy side of the spectra. Both the energetic position and the intensity of the shoulder evolve in time after excitation, indicating its physical nature. It is interesting to note that the shoulders are specifically pronounced at high excitation density in combination with low effective temperatures. In this regime lifetime broadening effects can be expected to show up in photoluminescence spectra, when the carrier effective temperature T_{eff} approaches the collision broadening parameter Γ ($k_b T_{eff} \sim \Gamma$)¹², i.e. when the high-energy slope is close to the low-energy slope. The actual low effective carrier temperatures ($T_{eff} < 150$ K), even under these high excitation conditions, are the direct result of the nearly resonant carrier photo-excitation (electron excess energies are smaller than 5 times the LO-phonon energy).

The intensity shoulders at the spectral high-energy side do not depend on the particular sample involved. The dotted curves in figure 3.2 show typical photoluminescence spectra obtained after excitation of sample W285 with laser energy 1.72 eV. The experimental spectra at low excitation intensity are, apart from their low-energy tail, well described by the solid curves, calculated by the no k -conservation single-particle recombination model (figure

3.2(b)). However, for the high excitation data clearly resolved intensity shoulders are visible, similar to the ones observed from sample Aix456.

Due to the excellent signal-to-noise ratio of the high excitation spectra it is possible to gain insight in the actual time-evolution of the high-energy side intensity shoulder by subtracting the calculated single-particle lineshapes from the measured spectra. The time-evolution of typical remaining spectra is displayed in figure 3.3 for both samples. It is striking that also these spectra can be described well by a single-particle lineshape neglecting \mathbf{k} -selection, as is shown by the solid curves. Although this subtraction method is rather arbitrary, the time-evolution of the high-energy slope (effective temperature) and spectral width (carrier density) of the shoulders roughly follow the similar features of the main photoluminescence peak. This suggests that the shoulder may be a replica of the main peak. Further the position of the shoulder clearly shifts in time to lower energy, simultaneously with the decreasing spectral width, i.e. carrier density.

3.3 Lineshape analysis

The experimentally determined time-resolved photoluminescence spectra are analyzed with the help of three different lineshape models, in an attempt to find in the first place a good description of the high-energy intensity shoulders. Moreover, resulting values for crucial parameters as temperature, density and renormalized band-gap obtained by the lineshape analyses will be compared mutually.

For the lineshape analysis we have used the single-particle models with and without \mathbf{k} -conservation and the collision broadening model as introduced by Haug *et al.*⁹. The latter model serves as a representative for the many-body lineshape models discussed in the literature, which all give approximately equal values for the carrier density and temperature^{3, 12} and only minor differences for the band-gap renormalization³.

All models start from a general single-particle expression for the band-to-band recombination rate τ per unit volume at a certain photon energy $\hbar\omega$:

$$\tau(\hbar\omega) = K' \int \int d\mathbf{k}_e d\mathbf{k}_h f_e(\mathbf{k}_e) f_h(\mathbf{k}_h) \delta(\hbar\omega - E_{\text{gap}} - E_e - E_h) \delta(\mathbf{k}_e - \mathbf{k}_h) \quad (3.1)$$

- The coefficient K' contains the optical matrix element, which is assumed to be independent of energy.
- Both the conduction and valence bands are assumed to be parabolic, characterised by effective masses m_e and m_h respectively. Therefore the energies E_e and E_h (measured with respect to the respective band extrema) of electrons and holes with wavevectors \mathbf{k}_e and \mathbf{k}_h respectively, can be written as:

$$E_{e,h}(\mathbf{k}_{e,h}) = \frac{\hbar^2 \mathbf{k}_{e,h}^2}{2m_{e,h}} \quad (3.2)$$

Incorporation of a nonparabolic conduction band for electrons¹³, reveals negligible changes in the photoluminescence lineshape and resulting parameters. The heavy-

and light-hole valence bands are replaced by a single band with an effective mass of $0.5m_0$, where m_0 is the free electron mass.

- The carriers are distributed among the wavevector (energy) states according to Fermi-Dirac distribution functions $f_{e,h}(E_{e,h}(k_{e,h}))$:

$$f_{e,h}(E_{e,h}(k_{e,h})) = \frac{1}{\exp((E_{e,h}(k_{e,h}) - E_{F_{e,h}})/k_b T_{e,h}) + 1} \quad (3.3)$$

which depends on the quasi Fermi-levels $E_{F_{e,h}}$ and the effective carrier temperatures $T_{e,h}$, also collectively determining the carrier density $n_{e,h}$:

$$n_{e,h} = \int f_e(E - E_{F_e})g_e(E)dE = \int f_h(E - E_{F_h})g_h(E)dE \quad (3.4)$$

Herein $g_{e,h}(E)$ represent the density of states functions of electrons and holes. Since the presented experimental photoluminescence spectra have only picosecond time-resolution and the thermalization processes are expected to occur on a much faster timescale^{1, 14, 15}, the assumption that the carrier distributions obey Fermi-Dirac statistics is justified. Moreover, in view of the actual excitation intensities, which result in carrier densities larger than 10^{16} cm^{-3} (see section 3.4), the electron and hole temperatures $T_{e,h}$ can be regarded as equal : $T_e = T_h = T_{\text{eff}}$ for times larger than 20 ps after excitation¹¹.

- The second δ -function on the right hand side of equation (3.1) expresses the conservation of wavevector in the recombination process, since the photon wavevector can be neglected with respect to the carrier wavevectors.
- The photon energy $\hbar\omega$ is determined by the electron and hole energies $E_{e,h}$ added to the band-gap energy E_{gap} . In all the models the band-gap energy is an adjustable parameter, assuming a band-gap renormalization governed by rigid band shifts.

3.3.1 Single-particle model with k-conservation

The first lineshape model is a simple single-particle model, incorporating preservation of the \mathbf{k} -selection rule, but without any broadening of the carrier states. The formula follows directly from equation (3.1). After applying the \mathbf{k} -selection δ -function this equation passes into:

$$r(\hbar\omega) = K \int dk k^2 f_e(k) f_h(k) \delta(\hbar\omega - E_{\text{gap}} - \frac{\hbar^2 k^2}{2\mu}) \quad (3.5)$$

where μ is the reduced excitonic mass ($1/\mu = 1/m_e + 1/m_h$).

Application of the energy conservation δ -function, yields:

$$r(\hbar\omega) = K \sqrt{\frac{2\mu}{\hbar^2}(\hbar\omega - E_{\text{gap}})} f_e\left(\frac{\mu}{m_e}(\hbar\omega - E_{\text{gap}})\right) f_h\left(\frac{\mu}{m_h}(\hbar\omega - E_{\text{gap}})\right) \quad (3.6)$$

The high-energy tail ($\hbar\omega > E_{\text{gap}}$, $\hbar\omega > E_{F_e} + E_{F_h}$) can be approximated by a single exponential, which depends only on the effective temperature:

$$r(\hbar\omega) \propto \exp\left[\frac{-\hbar\omega}{k_b T_{\text{eff}}}\right] \quad (3.7)$$

This expression has been widely used to extract values for the effective temperatures from experimental photoluminescence spectra without performing a complete lineshape analysis¹.

The coefficient K incorporates the optical matrix element M and can be written as¹⁶:

$$K = \frac{4\pi e^2 E_{\text{gap}}}{\pi \epsilon_0 m_0^2 \hbar^2 c^3} |M|^2 \quad (3.8)$$

where n is the refractive index of GaAs.

K is related to the usual radiative recombination coefficient B_r according to the definition of the latter¹⁶:

$$B_r n_{e,h}^2 \equiv \int d(\hbar\omega) r(\hbar\omega) \quad (3.9)$$

which leads to:

$$B_r n_{e,h}^2 = K \int d(\hbar\omega) \sqrt{\frac{2\mu}{\hbar^2} (\hbar\omega - E_{\text{gap}})} f_e\left(\frac{\mu}{m_e} (\hbar\omega - E_{\text{gap}})\right) f_h\left(\frac{\mu}{m_h} (\hbar\omega - E_{\text{gap}})\right) \quad (3.10)$$

This formula leads for a non-degenerate carrier distribution to the well-known $T_{\text{eff}}^{-3/2}$ -dependence for the radiative recombination coefficient^{17, 18}.

3.3.2 Single-particle model neglecting k-conservation

The single-particle model neglecting the \mathbf{k} -selection rule is closely related to the one assuming \mathbf{k} -conservation. Omitting the δ -function which implies \mathbf{k} -conservation in equation (3.1) and replacing the \mathbf{k} -integrals by energy-integrals yields:

$$r(\hbar\omega) = C \int_0^{\hbar\omega - E_{\text{gap}}} dE g_e(E) g_h(\hbar\omega - E - E_{\text{gap}}) f_e(E) f_h(\hbar\omega - E - E_{\text{gap}}) \quad (3.11)$$

It should be noted that the coefficient C is not equal to K in equation (3.6). As a matter of fact, insertion of equation (3.11) into equation (3.9) and separate integration over the conduction and valence bands (which is a reasonable approximation since no selection rule is applied) yields a coefficient C which is close to B_r ¹⁶.

In this approach without \mathbf{k} -conservation all transitions between occupied electron and hole states separated by energy $\hbar\omega$ contribute to the photoluminescence intensity, irrespective of their actual \mathbf{k} -values, as is illustrated in figure 3.4. Consider a photon with energy $\hbar\omega$ which within the \mathbf{k} -conservation model can be generated by only one vertical transition (with wavevector $k = \sqrt{\frac{2\mu}{\hbar^2} (\hbar\omega - E_{\text{gap}})}$), indicated by the solid arrow. In the no \mathbf{k} -selection picture however this photon can be generated by all electrons occupying states in the conduction band, which are separated by energy $\hbar\omega$ with occupied hole states in the valence band (schematically represented by the dashed arrows). In the case of $\hbar\omega = E_{\text{gap}}$ in both models only one transition can be responsible, which implies a zero effective broadening at the band-edge. Hence, in both models no radiation with an energy smaller than the band-gap energy can be emitted. With increasing $\hbar\omega$ however an increasing number of carrier states are contributing to the no \mathbf{k} -conserving photoluminescence signal. Consequently a phenomenological effective broadening is present, without any theoretical justification, which

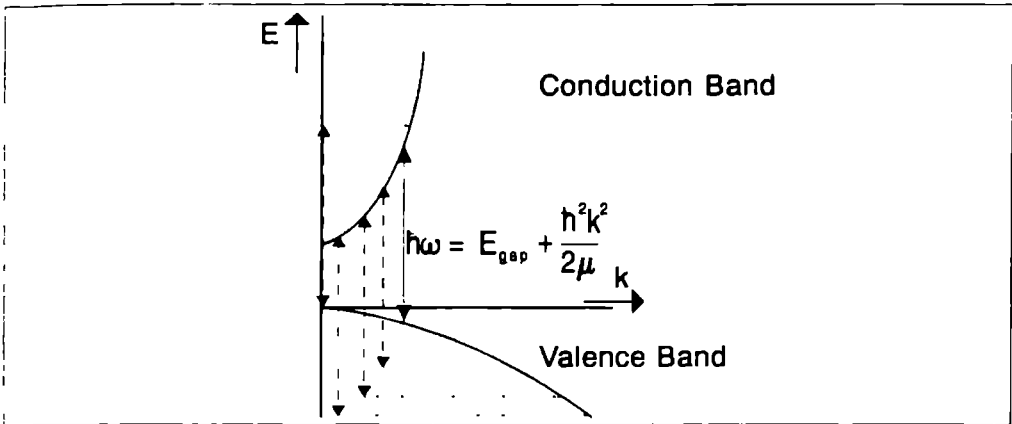


Figure 3.4: Schematic representation of the recombination model without k -selection (dashed arrows) as compared with the model including k -selection (solid arrow).

increases from zero at the band-edge to finite values at higher photon energies. This effective broadening will tend to enlarge the photoluminescence intensity at higher energies resulting in a reduced high-energy slope. In order to obtain the same slope as compared to the k -conservation model this may result in lower values for the effective temperature.

Evidently the picture of the no k -conservation recombination model does not implicitly rely on a solid theoretical background, but is only used frequently due to its simplicity and its successful description of experimental photoluminescence^{6, 7, 19} and gain^{5, 6} spectra.

3.3.3 Many-particle lineshape model

Both the low-energy tail of experimental photoluminescence spectra and the band-gap shrinkage for high carrier densities, reveal the significance of inter-carrier interactions, i.e. many-body effects, in highly excited semiconductors. In order to explain the low-energy tail Landsberg proposed a lifetime broadening of the single-carrier states⁸. The hole left in the distribution of electrons after the recombination event may be filled up by other electrons scattering to the empty state, making the latter state lifetime broadened. In this picture the broadening parameter at zero temperature will go to zero at the Fermi-level, because the empty state which approaches the Fermi-level from below can be filled up only by a decreasing number of electrons. As a result Landsberg proposed a linear decreasing broadening which is maximal at the band-edge, creating a significant low-energy tail, and zero at the Fermi-level. More recently Haug *et al.*⁹ calculated the collision broadening and its effect on optical spectra, for more general applications, i.e. finite temperatures. The recombination process is taken to be k -conserving, like in expression (3.5). The carriers states are lifetime broadened, which in fact means that the energy-conservation δ -function is replaced by a Lorentzian, which

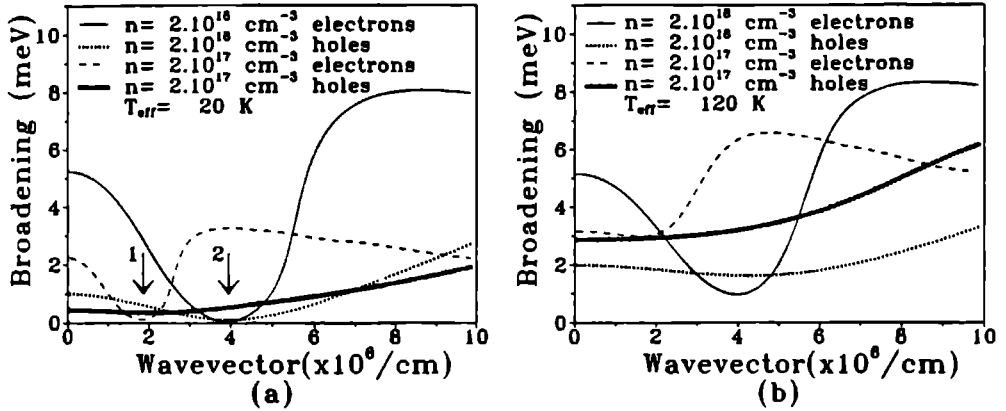


Figure 3.5: Collision broadening of electron and holes, as a function of wavevector, for two carrier densities and temperatures, calculated following Haug et al.⁹. The arrows 1 and 2 indicate the Fermi-wavevectors for low and high density respectively.

contains the $|\mathbf{k}|$ -dependent broadening parameter $\Gamma(k, \hbar\omega)$ ^{9, 10}:

$$\tau(\hbar\omega) = A \int dk k^2 f_e(k) f_h(k) \frac{\Gamma(k, \hbar\omega)}{[\hbar\omega - E_{\text{gap}} - \frac{\hbar^2}{2\mu} k^2]^2 + \Gamma^2(k, \hbar\omega)} \quad (3.12)$$

The total collision broadening parameter is composed out of the collision broadening for electrons and holes : $\Gamma(k, \hbar\omega) = \Gamma(k, E_e) + \Gamma(k, E_h)$. The broadening is induced by direct and indirect plasmon-assisted optical transitions, which are calculated using the dielectric constant in the plasma-pole approximation, i.e. also a lifetime broadening of the plasmon states due to inter-valence band absorption is included.

The same plasma pole approximation can also be used to calculate the density dependence of the exchange-correlation energy of a dense electron-hole plasma²⁰, leading to numerical values for the band-gap renormalization ΔE_{gap} very close to those originating from more sophisticated calculations at zero temperature, approximately given by^{21, 22}:

$$\frac{\Delta E_{\text{gap}}}{R_H^*} = -4.64 (n_{e,h} a_B^*)^{\frac{3}{4}} \quad (3.13)$$

where R_H^* is the excitonic Rydberg energy and a_B the excitonic Bohr radius.

Figure 3.5 displays a few examples of the k -dependent collision broadening parameter for electrons and holes for two values of both the carrier density and effective temperature. For low temperatures and high densities the collision broadening indeed starts off from a relatively high value at the band-edge and goes to zero at the Fermi-wavevector, as first proposed by Landsberg. Actually the broadening parameter goes to zero quadratically since at low temperature the empty state approaching the Fermi-level from below can be filled only

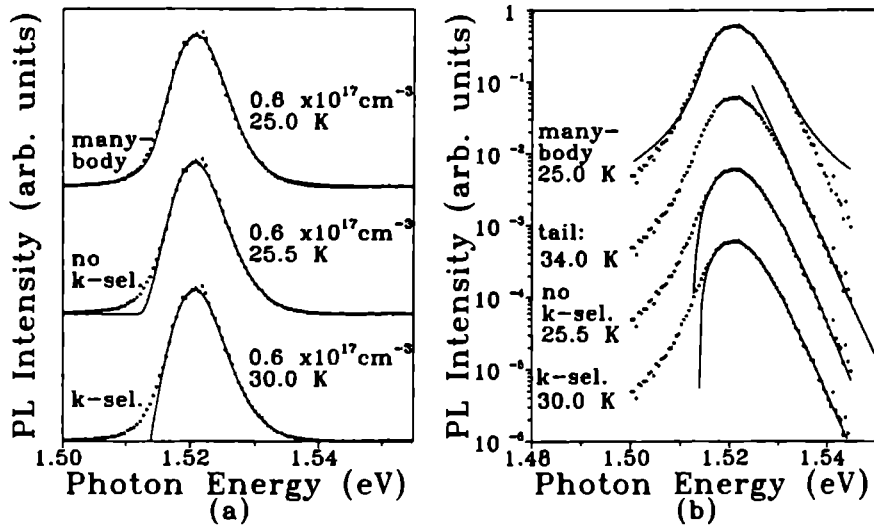


Figure 3.6 *Calculated (solid curves) photoluminescence (PL) lineshapes for the different recombination models used, as compared with a low excitation experimental spectrum (dotted curves), on linear (a) and semi-logarithmic (b) scale. The results for the different models are vertically shifted for clarity.*

by a quadratically decreasing number of electrons. Subsequently the broadening parameter increases again beyond the Fermi-level since the inverted reasoning holds for an electron occupying a state above the Fermi-level and can only decay in the empty states above it. Apparently for higher temperatures the broadening parameter at the Fermi-level increases. The effect of the broadening is the largest for electrons in the case of high densities and low temperatures, i.e. degenerate distributions. It should be noted that whereas in the proposal of Landsberg only the low-energy tail (below the Fermi-level) is affected by the broadening, the actual approach also affects the high-energy tail, i.e. the effective carrier temperature. As a matter of fact, due to the increasing broadening parameter beyond the Fermi-level, the temperature should be taken lower to obtain the same high-energy slope as compared with the single-particle k -selection model. Surprisingly the same qualitative argument was found earlier for the simple single-particle approach without conservation of k , due to its increasing effective broadening with photon energy (section 3.3.2).

3.4 Discussion of the lineshape analysis results

3.4.1 Overall lineshape

Calculated photoluminescence lineshapes due to the different described recombination models are depicted in figure 3.6 both on linear (a) and semi-logarithmic (b) scale, for one typical low

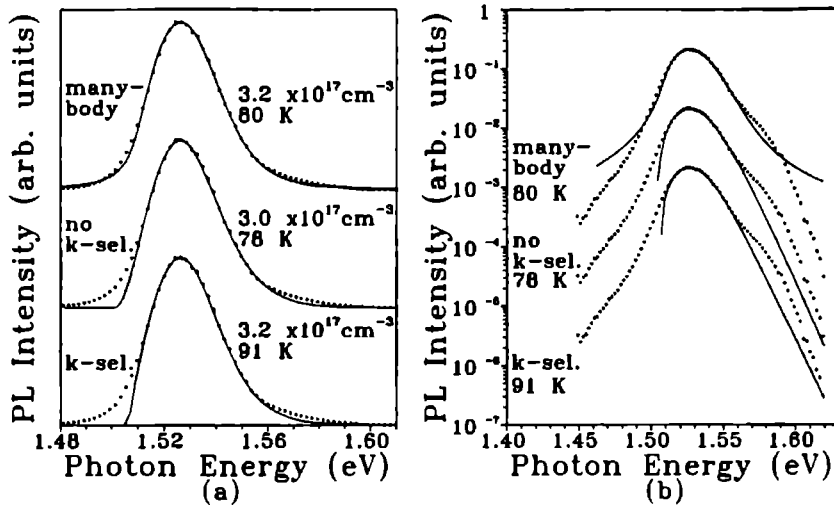


Figure 3.7: Calculated (solid curves) photoluminescence (PL) lineshapes for the different recombination models used, as compared with a high excitation experimental spectrum (dotted curves), on linear (a) and semi-logarithmic (b) scale. The results for the different models are vertically shifted for clarity.

excitation photoluminescence measurement without a high-energy intensity shoulder. The results for the different models are arbitrarily vertically shifted for clarity. All lineshape models used describe the experimental data reasonably well. As expected only the many-particle model lineshape exhibits a low-energy tail, which slightly overestimates the observed intensity below the band-gap. It is striking that the many-body lineshape also overestimates the intensity at the high-energy side at signal intensities roughly two decades below the peak, which is the direct result of the increasing broadening parameter Γ beyond the Fermi-wavevector (figure 3.5).

Figure 3.7 shows the calculated lineshapes of a high excitation spectrum, in which an intensity shoulder is visible at its high-energy side. Once more the low-energy tail intensity is overestimated by the many-particle model, which is due to the peculiar asymptotic behaviour of the Lorentzian broadening. Introduction of a low-energy cut-off elucidates this problem², without affecting the resulting values for the band-gap renormalization. Clearly the high-energy intensity shoulder is not described properly by the many-body model. An enhanced photoluminescence intensity is generated at high photon energies, as compared to the single-particle models, but the high-energy asymptotic behaviour observed in the measurements is not nicely reproduced. Apparently the many-particle model overestimates the intensity below two decades from the peak at both spectral sides, which suggests the calculated broadening parameter to be too large.

With regard to the overall lineshape both single-particle models are very similar.

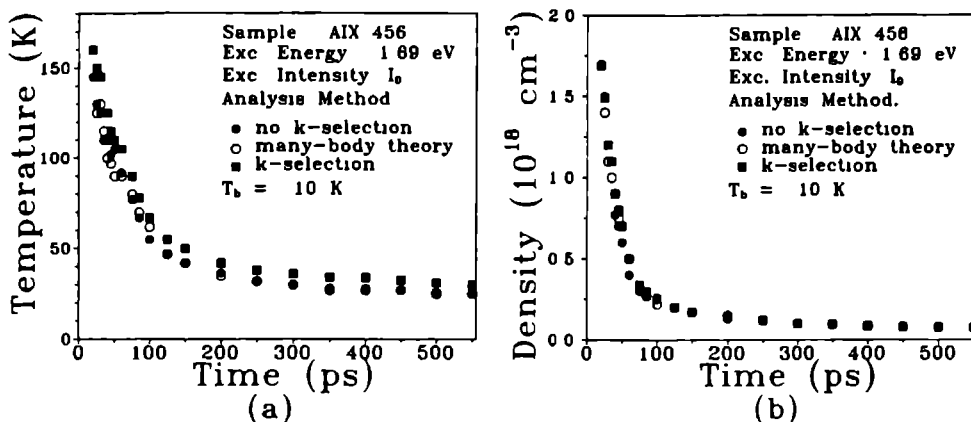


Figure 3 8 Time-evolution of the effective temperature (a) and carrier density (b), as obtained from the different recombination models used, after high excitation of sample AIX456

This means that for bulk GaAs the neglect of k -conservation does not affect the overall photoluminescence lineshape, in contrast to gain spectra⁵

3.4.2 Carrier density and effective temperature

Time-evolutions of the carrier density and the effective temperature as a result of the lineshape analysis by the three different models are displayed in figure 3 8 for the highest excitation intensity. The values for the carrier densities and effective temperatures were determined with a relative uncertainty within 10% and 5% respectively. The values for the carrier density are very similar for each of the used models, and show a rapid decay of the carrier density within the first 100 ps. The origin of this fast carrier density decay and its consequences for the picosecond carrier cooling will be discussed in detail in chapter 4.

Values of the effective temperature from the simple single-particle model without k -selection are comparable with values from the elaborate many-particle lineshape model. However, the temperature deduced from the k -conservation single-particle model appears to be always slightly higher. The lower temperature resulting from the first two models can be traced back directly to the increasing (effective) broadening with increasing photon energy. This leads to an enhanced photoluminescence intensity at higher energies, which implies that the temperature must be taken lower to obtain the same high-energy slope as compared to the simple k -selection model. In fact the phenomenological effective broadening in case of no k -selection fortuitously results in the same effective temperature with respect to the many-body model.

Only in the case of low excitation powers also an exponential fit to the high-energy tail could be performed (see also figure 3 6(b)). Typical results are depicted in figure 3 9. Once more the simple k -conservation model is found to generate slightly higher temperatures with

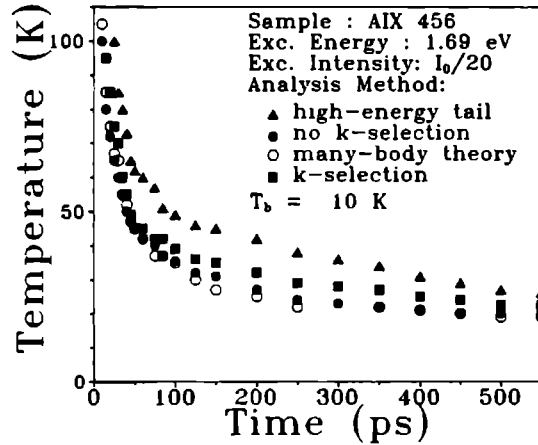


Figure 3.9: *Time-evolution of the effective temperature as obtained from four different methods, after low excitation of sample AIX456.*

respect to the other two models. It should be noted that in case of low excitation only a tight three decades photoluminescence intensity could be measured. Consequently the exponential fit also results in a higher temperature than the k-conservation model, which expresses the fact that the use of equation (3.7) in the present case is not allowed, i.e. the proper asymptotic behaviour is not yet reached at 2 decades below the peak. However, the measurement of more intensity decades does not elucidate the problem entirely, since the final asymptotic behaviour is equal to that of the simple k-conservation model, which also results in higher temperature values, leading to wrong carrier cooling curves.

3.4.3 Band-gap renormalization

Values for the band-gap renormalization, as obtained by the different lineshape models, are presented in figure 3.10. The dashed curve corresponds to the calculation of the band-gap shrinkage as a function of the carrier density, according to equation (3.13). The renormalization is measured in Rydberg energy as a function of the usual inter-particle distance r_s . Figure 3.10 expresses the importance of incorporating many-particle interactions in the recombination model, in order to predict reliable values for the band-gap renormalization, as a function of the carrier concentration. The single-particle models overestimate systematically the band-gap reduction, especially for high densities (small r_s). The reason is obvious, since both simple models do not generate photoluminescence intensity within the band-gap. In order to describe as best as possible the rising wing of the photoluminescence intensity, which lies partially within the band-gap, the spectrum must be shifted to lower energies, resulting in a lower value of the band-gap. It should be noted that also the band-gap shrinkage obtained by the many-particle model is slightly larger than the values according to equation (3.13), but the general agreement is reasonable.

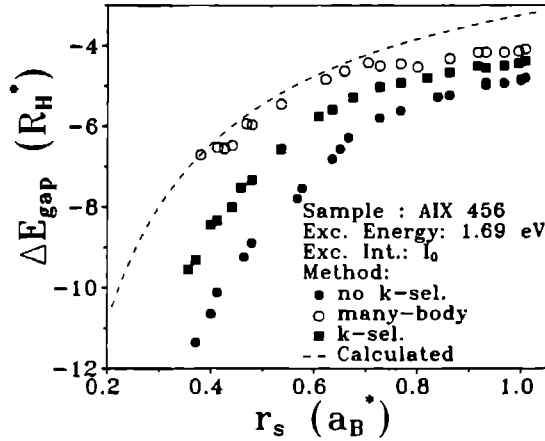


Figure 3.10: The band-gap renormalization ΔE_{gap} in Rydberg energy as a function of the inter-particle distance r_s , given by $\frac{4}{3}\pi r_s^3 = 1/n_{e,h}$, as obtained by the different lineshape models. The dashed curve represents the theoretically expected values according to equation (3.13)

3.4.4 Radiative recombination coefficient

In the analysis procedures the calculated lineshapes are multiplied by a proportionality factor to match them vertically to the experimental traces (expressions (3.6), (3.11) and (3.12)). The obtained values for the proportionality factors K , C , and A for respectively the simple models with and without k -conservation and the many-particle analysis, are shown in figure 3.11 as a function of time after excitation. Note that also the carrier density and effective temperature are strongly time-dependent (figure 3.8). The obtained values for the proportionality factor are merely relative values, since no absolute photoluminescence intensities were measured. The determination of the photoluminescence decay time due to spontaneous recombination is a well-known technique to do a absolute measurement of the recombination coefficient. The dashed curve in the figure corresponds to the relative value of B_r according to equation (3.9).

For times larger than 150 ps both A and K are found to be constant. Usually this factor in front of the photoluminescence intensity is assumed to be constant, which leads for non-degenerate carrier distributions to a $T_{\text{eff}}^{-3/2}$ -dependence of B_r , according to equation (3.10)^{17, 18}. From the measurements however, a non-constant K is found ($t \leq 150$ ps) in the region where the density starts at a high value and subsequently drastically decreases (figure 3.8 (b)), leading to B_r values indicated by the dashed curve in figure 3.11. Indeed these values of B_r are very close to the obtained values for C , already recognized by Lasher *et al.*¹⁶.

The present results show that the B_r determination may depend critically on the experimental conditions, which would explain why the experimentally determined values for B_r

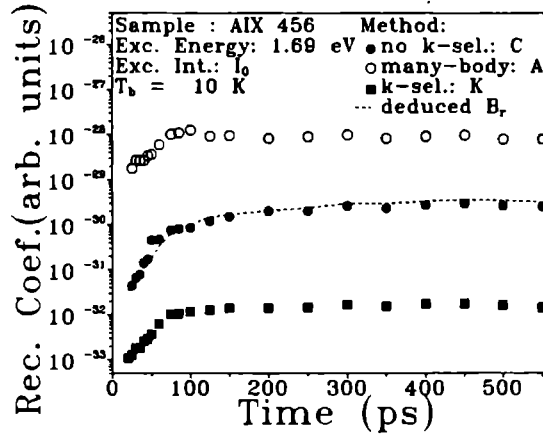


Figure 3.11: The proportionality factor as a function of time after excitation, as obtained from the different lineshape models. The corresponding time-evolution of the carrier density and temperature is given in figure 3.8. The dashed curve represents the obtained time-dependent B_r following from the measured K (squares), according to equation (3.10).

cover several decades $(0.2-50) \times 10^{-9} \text{ cm}^3\text{s}^{-1}$ (see eg. Table (4.1)), which cannot be explained by just the temperature dependence. Possibly the results of figure 3.11 confirm the statement that a constant B_r ceases to be meaningful for degenerate systems²³. However, further research is needed concerning this point, in order to investigate whether the diminished relative photoluminescence intensity at high degeneracy levels is the direct result of a reduced B_r , or just due to the onset of a competition between the radiative recombination process and other (nonradiative) processes at high densities.

3.4.5 High-energy tail shoulders

The high-energy tail shoulders clearly visible in the high excitation photoluminescence spectra of both samples are not reproduced by the many-particle model, suggesting that this feature can not be described by many-body effects only. It should be mentioned that the shoulder cannot be explained either by the insertion of a second (light-hole valence) band, since the energy separation between the shoulder and the main peak is too large. From the lineshape analysis the time-dependent peak position ΔE_s of the shoulder, with respect to the main peak, can be deduced simultaneously with the time-evolution of the carrier density. The results are depicted in figure 3.12 for both samples. The shoulder peak position seems to be correlated with the obtained electron-hole plasma density. This density dependence of ΔE_s and the nice description of the shoulder lineshape with the simple no \mathbf{k} -conservation model, indicate that the possibility of the shoulder being a plasmon-effect can not be ruled out. However, Selloni *et al.*³ discussed several many-body recombination models each incorporat-

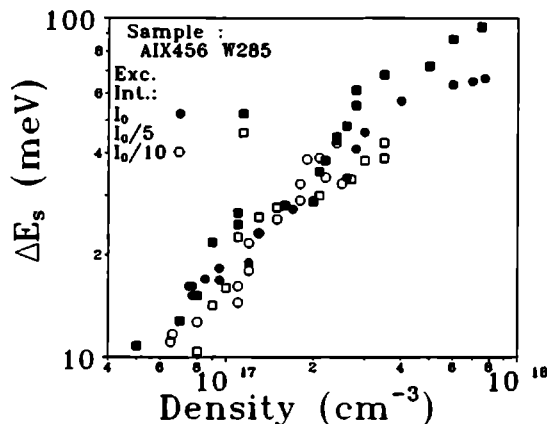


Figure 3.12: *The peak position of the high-energy tail shoulder ΔE_s , with respect to the main peak as a function of the carrier concentration for both samples and several laser excitation intensities.*

ing differently plasmon effects, but neither of them are reported to generate a high-energy side plasmon replica.

Another many-particle effect arises from the screened Coulomb interaction between electron and holes, leading to an enhanced photoluminescence intensity at the Fermi-level (Fermi-edge singularity)⁹ which is observed experimentally in modulation-doped quantum-well systems²⁴. However, the presently observed intensity shoulders are positioned in the high-energy tail rather than at the Fermi-level. Moreover, for the actual experimental parameter values the enhancement factor at the Fermi-level is expected to be of no importance⁹. Clearly, further investigation is needed to improve the insight in the specific cause for the high-energy intensity shoulders.

3.5 Conclusions

In summary, high excitation picosecond time-resolved photoluminescence spectra have been reported, which exhibit clear high-energy intensity shoulders, unexplained by single-particle recombination models. The feature has been observed to be specifically pronounced in the case of degenerate carrier distributions, i.e. high carrier densities and low temperatures. Moreover, the energetic position seems to be correlated with the electron-hole plasma density. These results suggest the intensity shoulder to be caused by many-particle interactions. However, the shoulder is not described properly by an elaborate many-particle recombination model, incorporating plasmon-assisted optical transitions. Consequently further investigation will be needed to explain the physical behaviour of the high-energy shoulder.

The carrier density and effective temperature obtained by using a single-particle no \mathbf{k} -conservation model appeared to be equal to the values deduced from the many-particle model.

The effective temperature resulting from the \mathbf{k} -conservation simple model have been found to be rather high, in particular when merely the high-energy tail is used. Both simple lineshape models have been found to overestimate the band-gap renormalization with increasing carrier concentration, whereas the values from the many-particle model reasonably agree with theory. Finally, a reduced radiative recombination coefficient has been found in case of high carrier densities, which makes the concept of a constant recombination coefficient in lifetime measurements for degenerate distributions questionable.

References

- [1] J. Shah, *J. Phys. (Paris)* **42**, C-7 445 (1981); J. Shah, *IEEE J. Quantum. Electron.* **QE-22**, 1728 (1986); S.A. Lyon, *J. of Lumin.* **35**, 121 (1986); J. Shah, *Solid-State Electron.* **32**, 1051 (1989).
- [2] M. Capizzi, S. Modesti, A. Frova, J.L. Staehli, M. Guzzi and R.A. Logan, *Phys. Rev.* **B29**, 2028 (1984).
- [3] A. Selloni, S. Modesti and M. Capizzi, *Phys. Rev.* **B30**, 821 (1984).
- [4] G. Tränkle, H. Leier, A. Forchel, H. Haug, C. Ell and G. Weimann, *Phys. Rev. Lett.* **58**, 419 (1987).
- [5] E. Göbel, *Appl. Phys. Lett.* **24**, 492 (1974).
- [6] S. Tanaka, H. Kobayashi and S. Shinoya, *J. Phys. Soc. Jpn.* **49**, 1051 (1980).
- [7] R.W.J. Hollering, T.T.J.M. Berendschot, H.J.A. Bluyssen, H.A.J.M. Reinen, P. Wyder and F. Roozenboom, *Phys. Rev.* **B38**, 13323 (1988).
- [8] P.T. Landsberg, *Phys. Stat. Sol.* **15**, 623 (1966).
- [9] H. Haug and D.B. Tran Thoai, *Phys. Stat. Sol. (b)* **98**, 581 (1980).
- [10] J.H. Collet, W.W. Rühle, M. Pugno, K. Leo and A. Million, *Phys. Rev.* **B40**, 12296 (1989).
- [11] W.W. Rühle, J. Collet, M. Pugno and K. Leo, *Condensed Systems of Low Dimensionality*, edited by J.L. Beeby *et al.* (Plenum Press, New York, 1991).
- [12] E.J.A de Bekker, *doctoral thesis*, University of Nijmegen (1992).
- [13] S. Chaudhuri and K.K. Bajaj, *Phys. Rev.* **B29**, 1803 (1984).
- [14] D.J. Erskine, A.J. Taylor and C.L. Tang, *Appl. Phys. Lett.* **45**, 54 (1984); A.J. Taylor, D.J. Erskine and C.L. Tang, *J. Opt. Soc. Am.* **B2**, 663 (1985).
- [15] W.H. Knox, C. Hirlimann, D.A.B. Miller, J. Shah, D.S. Chemla and C.V. Shank, *Phys. Rev. Lett* **56**, 1191 (1986); W.H. Knox, D.S. Chemla, G. Livescu, J.E. Cunningham and J.E. Henry, *Phys. Rev. Lett.* **61**, 1290 (1988).
- [16] G. Lasher and F. Stern, *Phys. Rev.* **133**, A553 (1964).
- [17] Y.P. Varshni, *Phys. Stat. Sol.* **19**, 459 (1967).

- [18] G.W. 't Hooft and C. van Opdorp, *Appl. Phys. Lett.* **42**, 813 (1983); G.W. 't Hooft, M.R. Leys and H.J. Thalen-v.d. Mheen, *Superlattices and Microstructures* **1**, 307 (1985).
- [19] P.C.M. Christianen, H.A.J.M. Reinen, H.J.A. Bluysen and M.R. Leys, *Proc. 20th Int. Conf. on the Physics of Semiconductors (Thessaloniki, Greece)*, edited by E.M. Anastassakis and J.D. Joannopoulos (World Scientific, 1990) page 2526.
- [20] F. Thuselt, *Physics Letters* **94A**, 93 (1983).
- [21] P. Vashishta and R.K. Kalia, *Phys. Rev.* **B25**, 6492 (1982).
- [22] R. Zimmermann, *Phys. Stat. Sol. (b)* **146**, 371 (1988).
- [23] P.T. Landsberg, *Proc. Phys. Soc. (London)* **70B**, 282 (1957).
- [24] M.S. Skolnick, J.M. Rorison, K.J. Nash, D.J. Mowbray, P.R. Tapster, S.J. Bass and A.D. Pitt, *Phys. Rev. Lett.* **58**, 2130 (1987).

Chapter 4

Cooling reduction due to a rapid density decay of hot carriers in GaAs

Abstract

The combined effect of a short carrier lifetime and of phonon emission on the cooling rate of nearly resonantly excited carriers in bulk GaAs has been investigated using picosecond time-resolved photoluminescence. It has been found that intense photo-excitation of carriers results in very short carrier density decay times of about 20 ps, as opposed to common carrier lifetimes of about 1 ns observed for low excitation levels. Furthermore a considerable reduction of the cooling rate has been found. The rapid density decay and the significant cooling reduction can be well described by an energy relaxation model, only when stimulated recombination is taken into account in addition to the usual carrier-phonon interactions. Within this model the short carrier lifetime affects the carrier cooling in two opposite ways; (1) the rapidly decreasing carrier density reduces the cooling through recombination heating, and (2) the extra loss of energy of the recombining carriers enhances the cooling. Mechanism (1) dominates and leads to an overall reduction of the cooling rate. The applicability of the used model for stimulated recombination for the actual measurements will be discussed in terms of the absolute value of the radiative recombination coefficient and of possible competing mechanisms, such as plasma expansion.

4.1 Introduction

The cooling of a hot electron-hole plasma via emission of phonons has been studied extensively in recent years, both by steady state and time-resolved experimental techniques¹. Initially the influence of the recombination rate, i.e. the finite carrier lifetime, has been neglected in the theoretical analysis of the experimental cooling curves. However, when the carrier lifetime becomes comparable to the time during which the photo-excited carriers relax to the band extrema through phonon emission, the energy relaxation rate due to recombination can no longer be neglected. This is exactly the regime we want to investigate in this chapter. In fact our measurements show that intense nearly resonant excitation reduces the lifetime of carriers in bulk GaAs, from nanoseconds to about 20 ps, comparable to the typical energy relaxation times.

In order to clarify the relation between the carrier lifetime and the cooling rate we examine a simplified picture: consider a highly excited semiconductor where recombination occurs without changing the mean energy of the carrier system. If no other energy relaxation processes are allowed, a rapid density reduction is necessarily associated to a raise in the effective temperature to keep the mean energy constant. Bimberg *et al.*² have shown that for a Fermi-Dirac distribution of hot carriers in GaAs, when the recombination time is decreased this so-called recombination heating causes higher carrier temperatures. The rate of temperature change has been found to be inversely proportional to the lifetime of the carriers². Especially in the case of direct-gap semiconductors, with their relatively short carrier lifetimes, this recombination heating plays an important role in the ultrafast carrier cooling. Indeed, this was confirmed experimentally by Leo *et al.*³ who found an enhanced cooling rate in annealed GaAs due to an increased carrier lifetime. Furthermore Rühle *et al.*⁴ showed that additional heating processes can occur in samples where nonradiative recombination is important. Carrier lifetimes comparable to the typical relaxation times have also been observed in GaAs quantum wells. Shum *et al.*⁵ observed a carrier density decay time as short as 10 ps in undoped GaAs quantum wells together with a non-equilibrium-phonon-stimulated phonon replica. The observed cooling reduction however was discussed merely in terms of phonon heating, and no recombination heating was incorporated.

The previous discussion implies that the carrier cooling must be reanalysed in the case of highly excited GaAs whenever the carrier lifetime is drastically reduced due to the occurrence of stimulated recombination. This lifetime reduction due to stimulated recombination has been studied by several groups. By use of quasi steady-state transmission Dapkus *et al.*⁶ found a decrease of the carrier lifetime from 1 ns to 200 ps with increasing carrier density in a bulk $n^+/n/n^+$ GaAs sample due to stimulated recombination. A similar reduction of the carrier lifetime with increasing density resulting from stimulated recombination, has been observed by Göbel *et al.*⁷ who measured luminescence decay times as short as 70 ps in a GaAs/(Ga,Al)As quantum well structure, confirmed recently by Cingolani *et al.*⁸. Very short carrier lifetimes due to stimulated recombination has been found in a similar structure by Dubard *et al.*⁹ using a time-resolved absorption technique. Comparable lifetimes has been found by Reinen *et al.*¹⁰ in a GaAs/(Ga,Al)As quantum well system and by Christianen *et al.*¹¹ in bulk GaAs using a time-resolved photoluminescence technique. Recently Rühle *et al.*¹² reported a relatively rapid carrier density decay (time constant 110 ps) in bulk GaAs,

not unambiguously related however to stimulated recombination.

In this chapter we report a study of the effect of ultrashort carrier lifetimes on the cooling behaviour of hot carriers in nearly resonantly excited bulk GaAs. The cooling behaviour was examined using a picosecond time- and energy-resolved photoluminescence technique, which will be described together with the composition of the samples and the resulting spectra in the next section (4.2). Values of the effective temperature and density of the carriers, which were extracted from the spectra will be discussed in section 4.3, in addition to the lineshape analysis used. It was found that nearly resonant intense photo-excitation of carriers results in a carrier decay time as short as 20 ps, as opposed to 1 ns in case of low intensity excitation. Simultaneously with the rapidly decreasing carrier density, a significantly reduced carrier cooling rate was observed. In section 4.4 an expression will be derived for the total recombination rate for our sample geometry, incorporating both spontaneous and stimulated emission. In section 4.5 a model for the energy relaxation rate including this total recombination and the carrier-phonon interactions will be presented, in order to explain the measured cooling behaviour and the rapid carrier density decay. In section 4.6 it will be shown that both the rapid carrier decay and the resulting reduced cooling can be nicely described by the model, featuring stimulated recombination. The short carrier lifetime will be shown to affect the carrier cooling in two ways; (1) the rapidly decreasing carrier density reduces the cooling rate through recombination heating² and (2) the energy relaxation as a direct result of the loss of energy of the recombining carriers enhances the cooling. The overall effect is a reduction of the cooling. Finally the relevance of the stimulated recombination mechanism for the actual measurements will be discussed in terms of the absolute value of the radiative recombination coefficient and the possible occurrence of competing processes.

4.2 Experimental details and results

The time- and energy-resolved photoluminescence experiments were carried out on two different samples, W285 (MBE-grown) and Aix456 (MOVPE-grown) each consisting of an 0.25 μm thick undoped GaAs layer sandwiched between two (Ga,Al)As layers. These (Ga,Al)As layers, transparent for the incident laser light, avoid both surface recombination and carrier diffusion in the growth direction, to ensure photo-excitation of more or less homogeneous carrier distributions. In sample W285 an extra superlattice buffer layer (50 x 42 \AA GaAs/60 \AA AlAs) was inserted between the Semi-Insulating-GaAs substrate and the lower (Ga,Al)As layer in order to prevent carrier photo-excitation in the substrate which could cause a disturbing photoluminescence background in addition to the signal from the 0.25 μm -thick GaAs layer (see also section 3.2 for more details on the composition of the samples).

Optical excitation was achieved with picosecond light pulses from a mode-locked Ti:sapphire laser at three different energies (1.65, 1.69 and 1.72 eV), which were focused onto the sample surface by a microscope objective to a spot with a diameter of about 20 μm . The laser beam incident on the sample was chopped mechanically to allow for lock-in detection. The laser time-averaged power ranged from $I_0/200$ to I_0 ($I_0 = 1.5 \text{ kW/cm}^2$).

Time- and energy-resolved detection of the emitted luminescence radiation due to electron-hole recombination was performed in a backscattering geometry using the up-conversion technique, where a non linear LiIO_3 crystal was used as a lightgate. The up-converted signal was detected with an EMI 9789/82 QB photomultiplier tube via a 1 m grating monochromator (section 2.5). The sample was mounted in a flow cryostat at a temperature of 10 K.

Figure 4.1 shows typical measured (dotted curves) and calculated (solid curves) photoluminescence spectra for different excitation densities I_0 (a), $I_0/5$ (b), $I_0/20$ (c) and $I_0/200$ (d), at different delay times after excitation of sample Aix456 with laser energy 1.69 eV. The spectra for one excitation intensity are all drawn on the same vertical scale to depict the time-evolution of the luminescence signal. Photo-excitation of sample W285 resulted in very similar spectra (section 3.2). Under the experimental conditions luminescence radiation originates from free carrier recombination and thus contains information about the distributions of carriers in the bands. The carrier distributions are assumed to be thermalized at each stage of the relaxation process, since the thermalization process has been found to be much faster than the processes involved in the phonon cooling^{1, 13, 14}. Consequently the carrier distributions can be characterized by an effective temperature and density. Basically the slope on the high-energy side of the spectra reflects the effective carrier temperature. Obviously the observed enhancement of the high-energy slope with time is directly related to the decreasing carrier temperature due to carrier cooling (figure 4.1). The spectral width corresponds to the band filling, i.e. the carrier density. A higher excitation intensity (figure 4.1 (a)) leads to much broader spectra (higher density) as compared to lower excitation intensities (figure 4.1 (b-d)). It is directly clear from figure 4.1 that after high excitation (I_0) the photoluminescence spectra reduce rapidly in spectral width, in contrast to the spectra for low excitation ($I_0/200$), which exhibit a more or less constant spectral width in the used time interval of 550 ps, in accordance to normal carrier lifetimes of about 1 ns in good quality GaAs. Also the energetic onset of the photoluminescence spectra in figure 4.1(a), which expresses the renormalized band gap, shifts rapidly to higher photon energies with increasing delay time, which agrees with a fast decreasing carrier density (see section 3.4 for the density dependence of the band-gap energy).

4.3 Analysis of the photoluminescence spectra

In order to investigate the carrier cooling in more detail the actual values of the carrier density and temperature are evaluated by fitting the measured spectra to the expression for the band-to-band recombination rate per unit volume with energy $E + E_{\text{gap}}$, neglecting \mathbf{k} -selection, which is given by¹⁵:

$$r_{\text{spont}}(E) = C \int_0^E f_e(E' - E_{F_e}) g_e(E') f_h(E - E' - E_{F_h}) g_h(E - E') dE' \quad (4.1)$$

Herein $f_{e,h}$ are the Fermi-Dirac distribution functions for electrons and holes respectively, determined by the effective carrier temperature T_{eff} and the quasi Fermi levels $E_{F_{e,h}}$, i.e. the

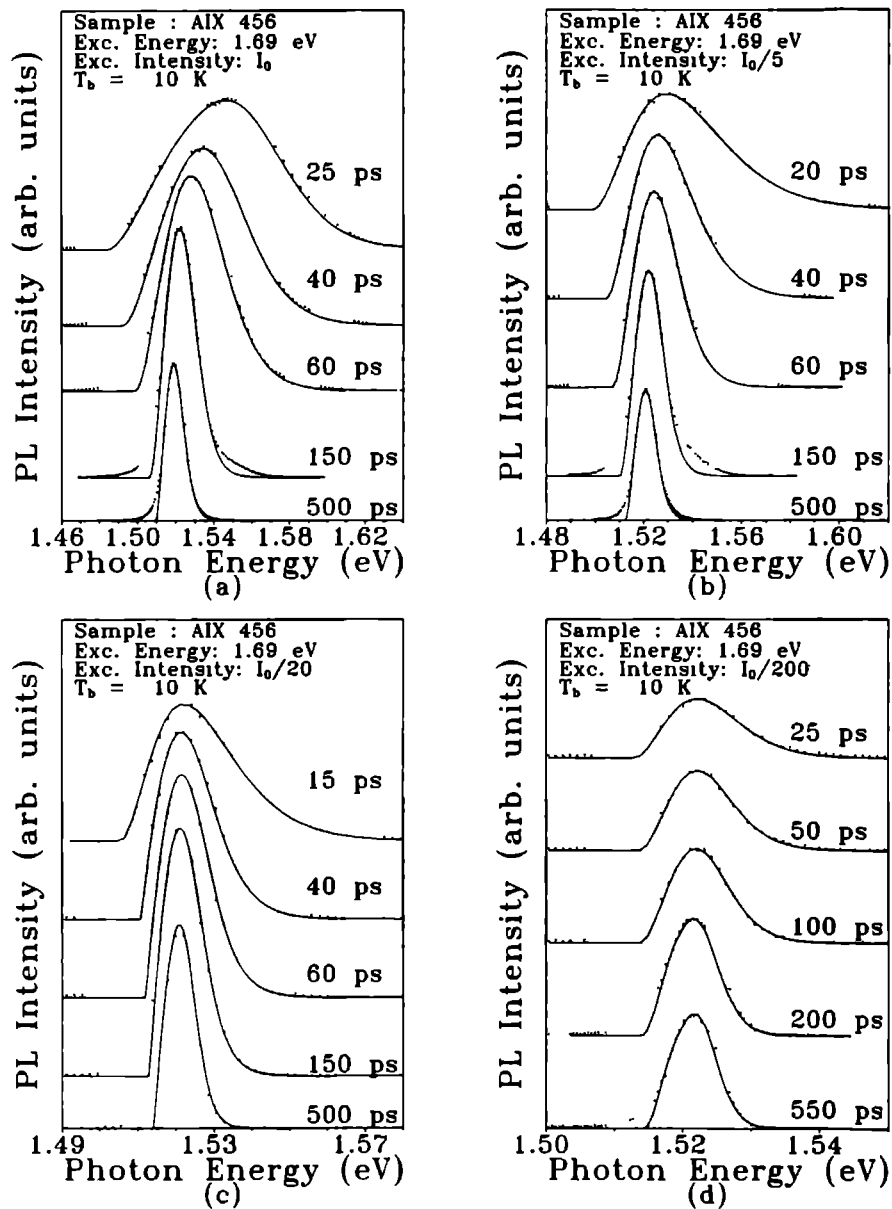


Figure 4.1 Measured (dotted curves) and calculated (solid curves) photoluminescence (PL) spectra at different times after excitation for excitation levels I_0 (a), $I_0/5$ (b), $I_0/20$ (c) and $I_0/200$ (d) for sample AIX456

carrier density $n_{e,h}$, and $g_{e,h}$ are the density of states functions of conduction and valence band respectively (The fitting procedure is described in detail in section 3.3.2).

The coefficient C contains the optical matrix element, which is assumed to be independent of energy and is related to the usual radiative recombination coefficient B_r , according to¹⁵:

$$B_r \equiv \frac{\int \tau_{\text{spont}}(E) dE}{n_{e,h}^2} \quad (4.2)$$

The solid curves in figure 4.1 correspond to the best fits. The values for temperature and density obtained by this relatively simple lineshape analysis turn out to be equal to the values deduced by an analysis using a more elaborate lineshape calculation^{16, 17}, including \mathbf{k} -selection and collision broadening of the single-carrier states (section 3.4). This in contrast to the parameters obtained from fitting the spectra to a lineshape model including \mathbf{k} -selection but without collision broadening, or the determination of merely the effective temperature by fitting the high-energy tail of the spectra to a single exponent. Both fitting models result always in too high carrier temperatures (section 3.4).

From figure 4.1 it is clear that the calculated lineshape cannot describe the measured spectra in every detail. The discrepancy at the low-energy side between the measured and calculated spectra does not influence the resulting values of the carrier density and temperature. Striking however is the appearance of a shoulder at the high-energy side of the spectra. The origin of this feature is discussed in detail in chapter 3. Especially for delay times >20 ps after excitation the deviations of the recorded spectra from the calculated ones are small enough to ensure a unique and reliable determination of the carrier temperature and density.

Figure 4.2 shows the time-evolution of the carrier temperature (a) and density (b) for a various number of excitation intensities (ranging from $I_0/200$ to I_0) for sample Aix456 excited at 1.69 eV. Changing the excitation wavelength to 1.65 or 1.72 eV or replacing the sample by sample W285 did not particularly alter the results. The solid curves in figure 4.2(a) and (b) were calculated from an energy relaxation model which will be discussed in section 4.5. The inset of figure 4.2(b) reports the measured carrier density decay for laser excitation level I_0 on a semi-logarithmic scale (symbols) fitted by a double exponential decay composed out of a rapid and a slow component with time constants 20 ± 5 ps and 200 ± 50 ps respectively (solid line).

Considerable differences are visible between the various excitation levels. The difference in carrier density at 20 ps after excitation is obviously due to the different excitation powers used, whereas the different carrier temperatures shortly after excitation is attributed to the different carrier cooling in the first 20 ps as a function of the carrier density¹. Indeed a rapid decrease of the carrier density with a time constant of about 20 ps (solid line in the inset of figure 4.2(b)) can be seen in the case of the highest excitation level used, which forms a striking contrast to the more gradual density decay for the three lowest excitation levels. Further, significant differences in the respective evolutions of the carrier temperature for excitation levels I_0 and $I_0/5$ are visible. Both temperatures evolve from a comparable value at 20 ps (temperature difference ΔT_{eff} is about 10 K). Subsequently ΔT_{eff} grows, simultaneously with the fast carrier density decay for I_0 excitation, and reaches a maximal value of about 40 K

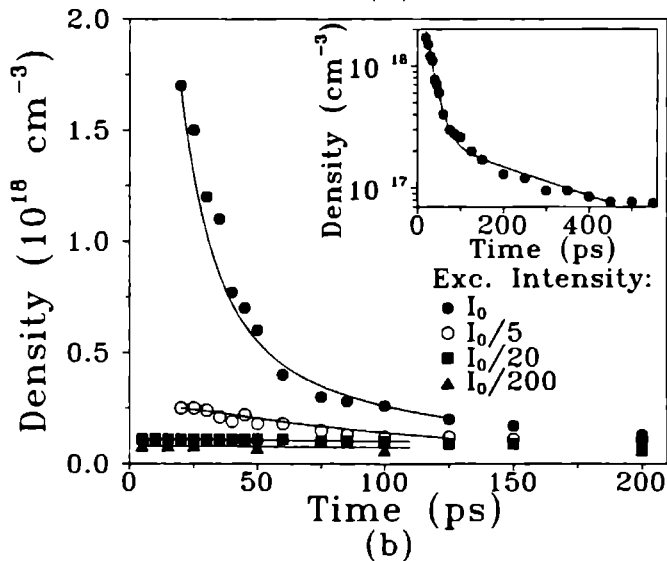
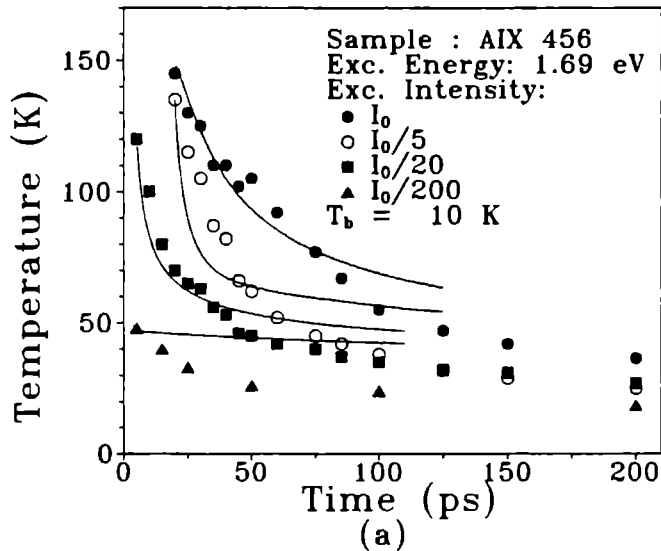


Figure 4.2: Carrier temperature (a) and density (b) as a function of time after excitation (symbols) for excitation levels I_0 (filled dots), $I_0/5$ (open dots), $I_0/20$ (squares), $I_0/200$ (triangles). The solid curves correspond to a model calculation described in section 4.5. The inset in (b) shows the measured carrier density decay on a semi-logarithmic scale (excitation level I_0 , symbols), yielding time constants for the double exponential fit of 20 ± 5 ps and 200 ± 50 ps (solid line).

at 60 ps. Thereafter ΔT_{eff} diminishes slowly. In summary, a remarkably fast carrier density decay rate was measured for the highest excitation level used, coinciding with a conspicuous slower cooling rate with respect to the results for lower excitation levels, where no such rapid density decay was found.

These results can be compared directly with the results of Hollering *et al.*^{18, 19} who performed time-resolved photoluminescence measurements with a very similar experimental set-up on a similar bulk GaAs sample¹⁹. Instead of exciting carriers nearly resonantly as in our case, Hollering *et al.* used laser light with energy 2.03 eV, creating electron and holes much higher in their respective bands, resulting in much higher initial carrier temperatures (typical 250 K), but comparable carrier densities (typical $1 \times 10^{18} \text{ cm}^{-3}$)¹⁹. Although this density is situated in our high excitation regime (I_0), Hollering *et al.* observed no rapid density decay¹⁹, suggesting that the effect is not only critically dependent on the carrier density but also on the carrier temperature.

4.4 Stimulated recombination

It follows that intense nearly resonant photo-excitation results in a rapid decay of the carrier density. In this section stimulated emission will be inserted into the calculation of the total radiative recombination rate, in the attempt to describe the rapid carrier density decay. The eventual stimulated recombination is initiated by spontaneous luminescence travelling through the photo-excited region, as is visualized schematically in figure 4.3. The laser

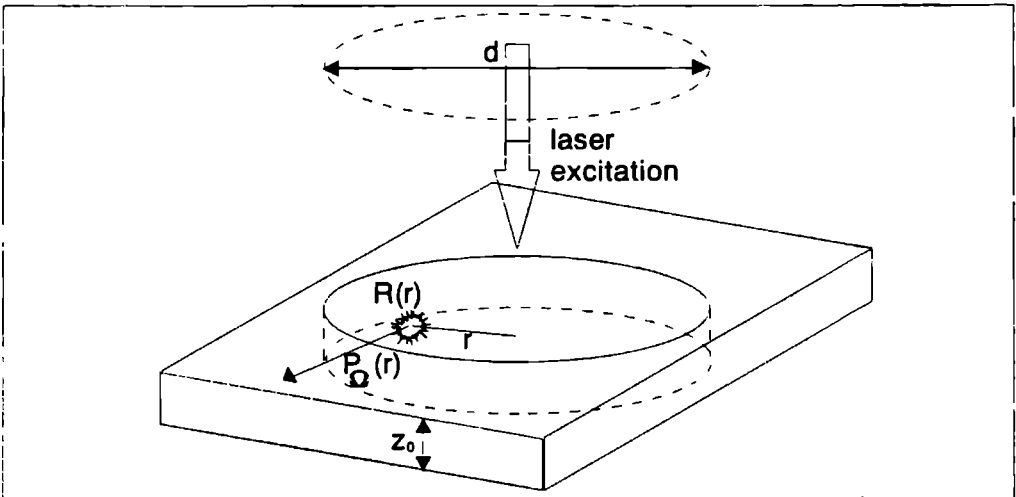


Figure 4.3: Schematic representation of the photo-excited disk in the bulk GaAs sample. d expresses the laser spot diameter and z_0 the thickness of the GaAs-layer. From each position $R(r)$ throughout the disk photoluminescence is emitted in all directions $d\Omega$. The resulting photons leave the disk at position $P_\Omega(r)$.

pulses are assumed to excite a homogeneous electron-hole plasma in a disk with a diameter d approximately equal to the laser spot diameter ($20 \mu\text{m}$) and a thickness z_0 equal to the GaAs layer thickness of $0.25 \mu\text{m}$. Note that figure 4.3 is not drawn on scale and that $z_0 \ll d$.

In order to describe the density decay observed in figure 4.2 the total recombination rate has to be calculated. From every point $\mathbf{R}(\mathbf{r})$ in the photo-excited region photoluminescence is emitted in all directions (figure 4.3). The spontaneous photoluminescence per unit time and volume, with energy $E + E_{\text{gap}}$ emitted at point $\mathbf{R}(\mathbf{r})$ in a solid angle $d\Omega$, is given by $\tau_{\text{spon}}(E) \frac{d\Omega}{4\pi}$, where $\tau_{\text{spon}}(E)$ is given by equation (4.1). Before these photons leave the disk region at point $P_{\Omega}(\mathbf{r})$ (the position of $P_{\Omega}(\mathbf{r})$ depends on the starting point \mathbf{r} of the photon and the direction $(d\Omega)$ in which it is emitted, see figure 4.3), they travel through the photo-excited region over a distance $l(\Omega, \mathbf{r}) = |\mathbf{p}_{\Omega}(\mathbf{r}) - \mathbf{r}|$, during which amplification occurs according to:

$$\tau_{\text{ampl}}(E, \Omega, \mathbf{r}) = \tau_{\text{spon}}(E) \frac{d\Omega}{4\pi} \exp[g(E) \cdot l(\Omega, \mathbf{r})] \quad (4.3)$$

in which $g(E)$ is the gain given by¹⁵:

$$g(E) = \frac{\pi^2 \hbar^3 c^2}{n^2 E^2} \tau_{\text{stim}}(E) \quad (4.4)$$

where n is the index of refraction for GaAs and $\tau_{\text{stim}}(E)$ is the stimulated recombination rate¹⁵:

$$\tau_{\text{stim}}(E) = C \int_0^E dE' g_e(E') g_h(E - E') [f_e(E' - E_{F_e}) + f_h(E - E' - E_{F_h}) - 1] \quad (4.5)$$

Integration over all directions $d\Omega$ and all positions \mathbf{r} and normalisation to the total excited disk volume $V_{\text{disk}} = \frac{1}{4} \pi d^2 z_0$ leads to the average amplification factor for a photon with energy $E + E_{\text{gap}}$:

$$\frac{1}{V_{\text{disk}}} \int_{\text{disk}} d\mathbf{r} \int \frac{d\Omega}{4\pi} \exp[g(E) \cdot l(\Omega, \mathbf{r})] \quad (4.6)$$

resulting in a total emission rate $\tau_{\text{tot}}(E)$ of

$$\tau_{\text{tot}}(E) = \frac{\tau_{\text{spon}}(E)}{V_{\text{disk}}} \int_{\text{disk}} d\mathbf{r} \int \frac{d\Omega}{4\pi} \exp[g(E) \cdot l(\Omega, \mathbf{r})] \quad (4.7)$$

In the case $g(E)$ and/or $l(\Omega, \mathbf{r})$ are small, $\tau_{\text{tot}}(E)$ equals $\tau_{\text{spon}}(E)$ as it should be.

In the calculation of $P_{\Omega}(\mathbf{r})$, i.e. the position where the photon leaves the excited disk, the lateral confinement effect is included by applying the normal Fresnel reflection rules for reflection at the GaAs/(Ga,Al)As interfaces. Basically only the photons which are emitted at an angle larger than the critical one for total internal reflection contribute to the total emission rate.

In this analysis of the stimulated recombination no adjustable parameters enter the calculation other than the coefficient for radiative recombination B_r (equation (4.2)), which determines the coefficient C in equations (4.1) and (4.5), and the laser spot diameter d which

Table 4.1: Values of low-temperature radiative recombination coefficients B_r , reported in the literature.

Material	B_r ($10^{-9} \text{ cm}^3\text{s}^{-1}$)	Reference
GaAs	7.6	(22)
GaAs	5.5	(6)
GaAs	16	(23)
GaAs	50	(24)
GaAs	2.4 ± 1	(25)
$\text{Ga}_{0.81}\text{Al}_{0.19}\text{As}$	4 ± 2	(25)
GaAs	2	(26)

is an experimental parameter. Both values are of vital importance for the total recombination rate since they appear in the exponent of expression (4.7). In the calculations a spot size of $d = 20 \mu\text{m}$ is used. The radiative recombination coefficient B_r is taken to be time-dependent, since B_r depends on the time-dependent temperature and density of the carriers (figure 3.11). The temperature dependence of B_r for non-degenerate carrier systems is well known^{20, 21}. However, for degenerate carrier distributions, the absolute value of B_r and its dependency on carrier density and temperature are not clear exactly. The time-evolution of B_r for the actual high excitation measurements, obtained from the fitting procedure described in the previous chapter (figure 3.11), show a reduced B_r in high density regimes. In the literature the reported low-temperature values of B_r cover a wide range, as can be seen in Table 4.1, which might be the result of the critical dependency of the determination of B_r on the experimental conditions. Consequently the absolute value of B_r is used as an adjustable parameter to obtain the best match between the calculations and observations. Finally the obtained value will be compared to the reported values in Table 4.1.

4.5 Model calculation

Since both the radiative recombination constant and the gain depend on the density and temperature of the carriers, the actual observed carrier density decay and cooling can only be calculated if all relevant energy relaxation processes are taken into account. The time-evolution of both the effective temperature $T_{e,h}$ and the density $n_{e,h}$ of the carriers was computed from the energy relaxation due to carrier-phonon interactions, spontaneous, stimulated and Auger recombination. To carry out these calculations it is assumed that for times after 10 ps both the effective temperature and the density are equal for electrons and holes^{12, 27, 28}. This assumption is justified since the actual carrier densities are situated in the regime where the electron and hole temperatures are not expected to differ much for times $> 10 \text{ ps}$ ¹². Fur-

thermore the redistribution of carriers in energy is assumed to be infinitively fast, that is no spectral hole burning due to stimulated emission is expected to occur⁷, which agrees well with the experimentally deduced thermalization times^{1, 13, 14}.

We start from initial (experimental) values for T_{eff} and $n_{e,h}$ from which the initial average carrier energy $\langle E \rangle$ is determined. After a time interval Δt a new density n' is calculated from the spontaneous, stimulated and Auger recombination, and a new value for the average carrier energy $\langle E' \rangle$ from the energy relaxation rates due to carrier-phonon interactions, and all recombination processes. From n' and $\langle E' \rangle$ a new value for the effective carrier temperature at $t = \Delta t$ is calculated. For the subsequent time intervals this procedure is repeated. The following algorithm describes the calculations in more detail.

From the initial values of T_{eff} and $n_{e,h}$, the reduced Fermi energies for electrons and holes are calculated using the expression:

$$n_{e,h} = \int f_e(E - E_{F_e})g_e(E)dE = \int f_h(E - E_{F_h})g_h(E)dE \quad (4.8)$$

where $f_{e,h}$ are Fermi-Dirac distribution functions with $E_{F_{e,h}}$ the reduced Fermi energy for electrons and holes, and $g_{e,h}$ are the density of states functions. The initial average carrier energy $\langle E \rangle$ then follows from:

$$\langle E \rangle = \frac{1}{n_{e,h}} \int_0^{\infty} dE' E' \times [f_e(E' - E_{F_e})g_e(E') + f_h(E' - E_{F_h})g_h(E')] \quad (4.9)$$

With help of equation (4.7) the reduced carrier density after a time interval Δt is calculated from the expression:

$$n'_{e,h} = n_{e,h} - \Delta t \cdot \left[\int_0^{\infty} dE r_{\text{tot}}(E) - C_p n_{e,h}^3 \right] \quad (4.10)$$

in which the last term on the right hand side denotes the density decay due to Auger recombination with $C_p = 10^{-31 \pm 1} \text{cm}^6/\text{s}$ for undoped GaAs at 77 K²⁹. However, Auger recombination is expected to be of minor importance for the densities involved in our experiment and is only incorporated for the sake of completeness.

To calculate the new average carrier energy $\langle E' \rangle$ after the time interval Δt , we calculate the total energy relaxation rate per unit volume due to carrier-phonon interactions, Auger and radiative recombination of the carriers:

$$\left(\frac{d\mathcal{E}}{dt} \right)_{\text{tot}} = \left(\frac{d\mathcal{E}}{dt} \right)_{\text{c-ph}} + \left(\frac{d\mathcal{E}}{dt} \right)_{\text{Auger}} + \left(\frac{d\mathcal{E}}{dt} \right)_{\text{rec}} \quad (4.11)$$

- The energy relaxation due to carrier-phonon interactions is calculated following Pugnet *et al.*³⁰ including the polar optical (LO), non-polar optical deformation, piezo-acoustic and acoustic deformation (ADP) interactions of both electrons and holes:

$$\left(\frac{d\mathcal{E}}{dt} \right)_{\text{c-ph}} = \left(\frac{d\mathcal{E}}{dt} \right)_{\text{LO}} + \left(\frac{d\mathcal{E}}{dt} \right)_{\text{NPO}} + \left(\frac{d\mathcal{E}}{dt} \right)_{\text{piezo}} + \left(\frac{d\mathcal{E}}{dt} \right)_{\text{ADP}} \quad (4.12)$$

The energy relaxation rates for the different carrier-phonon interactions are computed accounting for static screening in the random phase approximation. For the holes the same expression as for the electrons is used divided by a numerical factor 2, accounting for the reduced overlap of p-like valence band wavefunctions as compared to the s-like conduction band functions³⁰. In front of the electron relaxation rate due to LO-phonon scattering a parameter $\alpha (\leq 1)^3$ is used, instead of solving the coupled Boltzman equations of the carrier and phonon systems, in order to take into account phonon heating^{17, 18, 31, 32}. As a consequence of the relative long lifetime of LO-phonons, a phonon emission bottleneck can arise, resulting in carrier cooling rates which can be 20 times ($\alpha \sim 0.05$) smaller than expected from theory¹. Evidently the use of one single parameter to describe the time-dependent effect of phonon heating is a simplification. However, the strongest transient phonon heating effects occur within the laser pulse and in the first 10 ps thereafter, when a non-equilibrium phonon distribution is formed which ends up in thermal equilibrium with the carriers^{31, 32}. Subsequently both distributions relax in thermal equilibrium on a timescale of tens of picoseconds. As a result phonon heating affects the cooling rate of the hot 3D carriers at all times after excitation whenever the carrier temperature exceeds the threshold for phonon emission³². It is this rather slow phonon heating effect which is accounted for by the parameter α in the calculation. The initial strongly time-dependent phonon heating determines the first carrier temperature measured in figure 4.2 (a) and its variation with excitation intensity.

- In a radiationless Auger recombination event the band-gap energy E_{gap} is added to the plasma, which results in the following energy relaxation rate for Auger recombination:

$$\left(\frac{d\mathcal{E}}{dt}\right)_{\text{Auger}} = -E_{\text{gap}}C_p n_{e,h}^3 \quad (4.13)$$

- The energy relaxation rate due to the recombining carriers is calculated with help of equation (4.7) according to:

$$\left(\frac{d\mathcal{E}}{dt}\right)_{\text{rec}} = \int_0^\infty E r_{\text{tot}}(E) dE \quad (4.14)$$

Finally the average carrier energy after the time interval Δt is given by:

$$\langle E' \rangle = \frac{1}{n'} \left\{ \langle E \rangle \times n - \Delta t \times \left(\frac{d\mathcal{E}}{dt}\right)_{\text{tot}} \right\} \quad (4.15)$$

From this equation the effective carrier temperature and reduced Fermi energies $E'_{F_{a,b}}$ after the time interval Δt are calculated self consistently, using equations (4.8) and (4.9). For the next time interval Δt the algorithm is repeated. In this way the cooling curve and the time-evolution of the carrier density are obtained simultaneously in time steps of width Δt .

The actual size of Δt is not particularly important as long as the variation of the density and temperature within one step is not too large. In practice it appeared that for $\Delta t \leq 100$ fs the computed traces are equal. so in the calculations $\Delta t = 100$ fs is used.

4.6 Discussion

4.6.1 Results model calculation

The results of the complete model calculations are shown by the solid curves in figure 4.2. All curves were calculated with step size $\Delta t = 100$ fs, phonon heating parameter $\alpha = 0.3$, spot size $d = 20 \mu\text{m}$, and radiative recombination constant $B_r = 7 \times 10^{-9} \text{ cm}^3\text{s}^{-1}$. It should be emphasized that in order to match the calculations simultaneously to both the time-evolution of the density and the temperature, the freedom to chose both adjustable parameters (α and B_r) is restricted to a narrow range. The actual values correspond to the only combination which leads to reasonable agreement with the experiment.

The computations starting from the parameters at $t = 20$ ps of the highest excitation intensity (I_0) reveal a drastic decrease of the carrier density within the first 100 ps, which is in the model determined completely by stimulated recombination. Also the much slower decay rates, observed for the lower excitation levels, are nicely described by the computed traces. Regarding the calculation of the time-dependent effective temperature good agreement is obtained for $T_{\text{eff}} > 60$ K. The rather high value of α (0.3) suggests that phonon heating not particularly affects the cooling at times > 20 ps after nearly resonant excitation. It is clear from figure 4.2 (a) that the calculated temperature curves tend towards a final temperature of about 40 K which is the threshold for LO phonon emission. Below this temperature the carriers have to relax by other phonon scattering mechanisms resulting in a smaller energy relaxation rate³⁰, which apparently cannot describe the experimentally observed further decrease below 40 K (figure 4.2 (a)). This deviation could be related to impurity scattering, not included in the present analysis, which recently has been proven to form an extra relaxation channel, dominating the acoustic phonon scattering in relatively pure GaAs (impurity concentration $\sim 10^{14} \text{ cm}^{-3}$), as opposed to ultrapure GaAs (impurity concentration $\sim 10^{12} \text{ cm}^{-3}$)³³. Moreover, a similar discrepancy has been found by Rühle *et al.*¹², who assigned it to the difficulty to analyze low temperature photoluminescence spectra.

It should be noted that although a considerable recombination rate was calculated for the highest excitation level used, the measured spectra in figure 4.1 (which were recorded in a backscattering geometry) can be fitted by using merely the expression for spontaneous recombination. As a direct result of the particular dimensions of the photo-excited region ($d \gg z_0$, figure 4.3) the stimulated recombination rate in the perpendicular direction is orders of magnitude smaller than in the lateral direction. Consequently the density decay is caused completely by stimulated recombination in the lateral direction and it is expected that stimulated emission spectra can be measured in the lateral direction, as was shown by Dubard *et al.*⁹ for a quantum well structure and as commonly is used in measurements following Shaklee *et al.*³⁴, in which the stimulated recombination intensity from the sample edge is detected to determine the gain^{35, 36} or the band-gap renormalization³⁷.

4.6.2 Recombination heating

Let us concentrate on the influence of a short carrier lifetime, on the carrier cooling rate. This influence is visible in figure 4.2 (a) by comparing both the experimental and theoretical results

of excitation intensities I_0 and $I_0/5$. The initial effective temperature difference ΔT_{eff} at $t = 20$ ps is relatively small, i.e. $\Delta T_{\text{eff}} \sim 10$ K, grows significantly at later times to $\Delta T_{\text{eff}} \sim 40$ K at 60 ps, and diminishes subsequently. Thus a reduced cooling rate appears for excitation level I_0 with respect to excitation level $I_0/5$, just at those times after excitation when a considerable density decay rate is present, and which is well described by the model calculation. Hence, the observed reduction of the cooling rate can be attributed completely to the fast density decay rate, without further phonon heating effects.

In order to discuss the bare effect of a short carrier lifetime on the carrier cooling, figure 4.4 illustrates the importance of the contributing mechanisms, that is spontaneous and stimulated recombination and carrier-phonon interactions. The initial carrier temperature and density was taken to be: $T_{\text{eff}} = 145$ K and $n_{e,h} = 1.7 \times 10^{18} \text{ cm}^{-3}$, equal to the experimental results of the highest excitation level used. The solid curves in figure 4.4 represent the results of the complete model calculation and correspond to the solid curves in figure 4.2 for I_0 excitation. The dashed curves correspond to calculations in which the loss of energy of the recombining carriers $(\frac{d\mathcal{E}}{dt})_{\text{rec}}$ was omitted. The dotted curves were calculated by neglecting any recombination to occur. Obviously in the presence of a rapidly decaying density (solid curves) the cooling rate is reduced considerably with respect to the case of no density decay (dotted curves). This reduction is the consequence of two effects:

- (i) due to the rapid decrease of the carrier density, the carrier distribution will be heated, which is known as recombination heating^{2, 3}. The recombination heating originates from the first term on the right hand side of equation (4.15): $\langle E' \rangle = \frac{n}{n'} \langle E \rangle$. Its effect is simulated by the dashed-dotted curve in the inset of figure 4.4 (a), calculated by omitting $(\frac{d\mathcal{E}}{dt})_{\text{tot}}$ for the experimentally observed carrier density decay for excitation level I_0 . In this hypothetical case the mean energy of the system is constant while the density reduces rapidly which results necessarily in a temperature enhancement. For our experimental parameters we deduce an enormous heating from 145 K to 800 K, when the carrier density decreases from $1.7 \times 10^{18} \text{ cm}^{-3}$ to $7 \times 10^{17} \text{ cm}^{-3}$ within 40 ps. These effects are considerably larger than the recombination heating discussed by Bimberg *et al.*² and Leo *et al.*³, because they compare samples with carrier lifetimes between 300 ps and 1.5 ns, whereas in this case lifetimes of about 20 ps are involved. However, for the experimental lifetimes observed by Leo *et al.*³ our model generates comparable results.
- (ii) due to the rapid carrier recombination rate the loss of energy of the recombining carriers $(\frac{d\mathcal{E}}{dt})_{\text{rec}}$ forms an extra energy relaxation channel (expression (4.14)). In order to illustrate the significance of $(\frac{d\mathcal{E}}{dt})_{\text{rec}}$ the time-evolutions of $n_{e,h}$ and T_{eff} are shown by the dashed curves in figure 4.4, calculated without taking $(\frac{d\mathcal{E}}{dt})_{\text{rec}}$ into account. Comparison with the solid curve proves that $(\frac{d\mathcal{E}}{dt})_{\text{rec}}$ enhances the cooling conspicuously and thus definitely cannot be neglected. After comparison of the contributions of the separate energy relaxation processes (expressions (4.12), (4.13), and (4.14)), $(\frac{d\mathcal{E}}{dt})_{\text{rec}}$ appeared one of the major contributions together with $(\frac{d\mathcal{E}}{dt})_{\text{LO}}$.

Thus the experimentally observed extraordinary fast density decay rate reduces the carrier cooling considerably by means of recombination heating, opposed partially by the extra loss

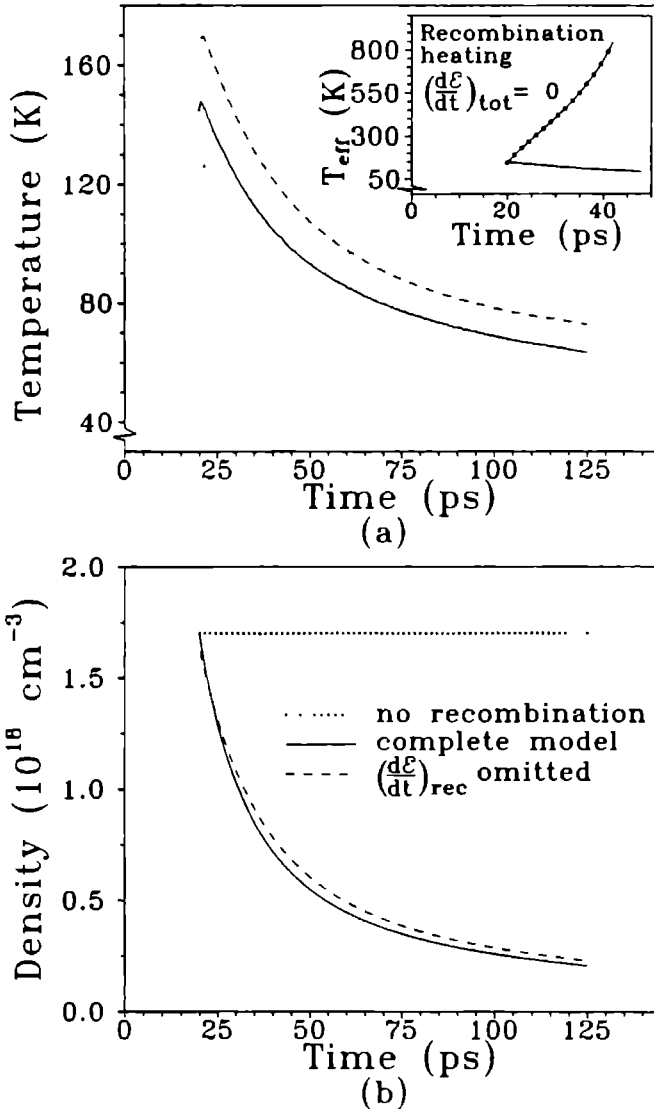


Figure 4.4: Time-evolution of the effective carrier temperature (a) and density (b) calculated with help of the complete model (solid curves), in case recombination is neglected ($\tau_{\text{tot}}(E) = 0$, dotted curves), or in case the loss of energy of the recombining carriers is omitted ($(\frac{d\mathcal{E}}{dt})_{\text{rec}} = 0$, dashed curves). The inset shows the hypothetical case in which no energy relaxation is present ($(\frac{d\mathcal{E}}{dt})_{\text{tot}} = 0$, solid-dotted curve) in comparison with the complete model calculation (solid curve). All calculations start from the initial experimental values for excitation level I_0 .

of energy of the recombining carriers which enhances the cooling. The actual reduction of the cooling is much larger as compared to earlier reports of recombination heating because of the extremely short carrier decay time of about 20 ps. However, no real carrier heating is observed although a huge bare recombination heating effect is present (inset figure 4.4). First, due to a very efficient carrier energy relaxation, basically by LO phonons and recombination, no heating occurs. Second, in case carrier heating would occur the stimulated recombination rate would be diminished drastically due to its strong temperature dependence, which would remove the cause of the heating. The stimulated recombination rate strongly decreases with increasing temperature because the population inversion $[f_e + f_h - 1]$ (equation (4.5))^{15, 38} diminishes with temperature. Consequently, in case carriers are created higher in the bands leading to higher carrier temperatures it is much more difficult to observe stimulated recombination, which could be the reason that Hollering *et al.*¹⁹ did not observe a rapidly decreasing carrier density in their high excitation photoluminescence experiments. We wish to emphasize that the present model calculations nicely reproduce the results of Hollering *et al.*¹⁹, which shows that the mechanism of stimulated recombination indeed exhibits the proper temperature dependence to explain all observations.

The relatively low initial carrier temperature at 20 ps after excitation (145 K, compare with 230 K at 2.03 eV excitation^{18, 19}), is due to the relative resonant creation of electrons in the conduction band. For an excitation energy of 2.03 eV the photo-excited electrons have an excess energy exceeding the energy difference between the Γ and L conduction band minima (290 meV) and the Γ - and X-minima (430 meV). Therefore the electrons will scatter rapidly into the satellite valleys and will return to the Γ -minimum within approximately 10 ps, at an energy of $7 \times$ the LO phonon energy (36.8 meV), heating the carriers already present in the Γ -valley^{15, 16}. Thereupon the electrons will relax to the band edge by LO phonon emission. Excitation with an energy of 1.69 eV results in an excess energy of $5 \times$ the LO phonon energy. Rühle *et al.*⁴¹ discussed the fact that cooling curves obtained from excitation at different energies below the satellite valleys, but with comparable excitation intensities, are very similar. Therefore we conclude that the relatively low carrier temperature shortly after excitation is due to absence of intervalley scattering, which implies that nearly resonant excitation means creation of the electrons at an energy below the satellite valleys.

4.6.3 Radiative recombination coefficient

The absolute value of the radiative recombination coefficient B_r is very important for the density decay, as is illustrated in figure 4.5, which displays the calculated time-evolution of both temperature (a) and density (b) of the carriers for different values of B_r , in addition to the experimental data for excitation intensity I_0 (symbols). Evidently the density decay rate enhances when B_r increases. Furthermore the initial amount of cooling reduction, i.e. recombination heating, increases as the density decay rate becomes faster, in agreement with the calculations of Bimberg *et al.*² For a value of B_r (at 77 K) of $7 \times 10^{-9} \text{ cm}^3\text{s}^{-1}$ the calculated time-evolutions of both the carrier density and temperature nicely describe the experimental results, whilst also the proper density decay curves for the other excitation levels are predicted (figure 4.2). This actual B_r value agrees reasonably with the low temperature values reported in the literature (Table 4.1), although it should be mentioned that these values

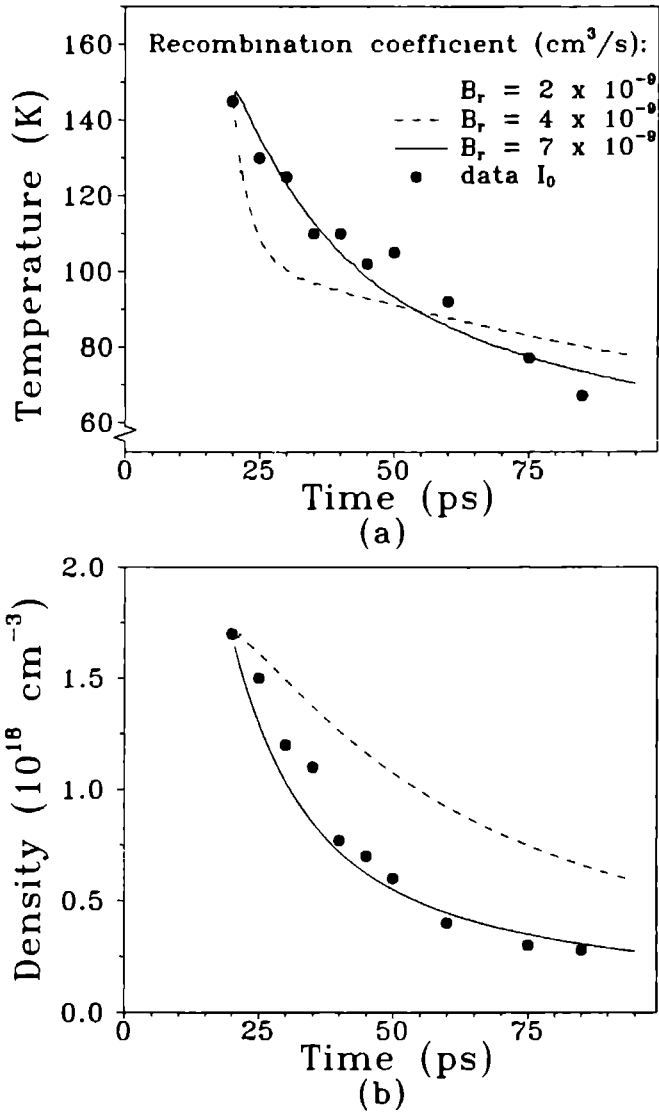


Figure 4.5 Calculated time-evolution of effective carrier temperature (a) and density (b) for a number of values of the radiative recombination coefficients B_r at 77 K. The symbols correspond to the experimental data for excitation intensity I_0 .

cover a remarkable wide range, which is probably due to its sensitivity to the experimental conditions under which the B_r determinations have been performed.

Since the density decay rate depends critically on the absolute B_r value the drastic effect of the stimulated recombination on the carrier decay rate is nearly gone for $B_r = 2 \times 10^{-9} \text{ cm}^3\text{s}^{-1}$ (dotted curves in figure 4.5), a value which still lies within the reported B_r range (Table 4.1). Hence, due to the relative uncertainty in the absolute value of B_r and because the density decay depends dramatically on its absolute value, the occurrence of stimulated recombination in the actual experiment could be questioned. Concerning this point it is important to note that the mechanism of stimulated recombination exhibits the proper dependencies on both the density and the temperature of the carriers. For decreasing excitation levels a decreasing density decay rate was observed, and the result that no such drastic density decay rate has been seen for higher effective temperatures¹⁹, can be well understood in terms of stimulated recombination. Furthermore the stimulated recombination rate might be underestimated in the model calculation due to the relative simplicity of the model, in which a spatial homogeneous electron-hole plasma is assumed and only a very simple confinement effect of the (Ga,Al)As barriers, whereas the latter effect certainly can be of great importance³⁷.

On the other hand it is worthwhile to consider other possible effects which might cause carrier density decay rates as fast as 20 ps for high excitation levels.

- (i) Auger recombination can lead to very short carrier lifetimes (<3 ps) in samples with very high p-doping levels ($9 \times 10^{19} \text{ cm}^{-3}$)²⁶. The nonradiative Auger rate however depends on the density according to $n_{e,h}^3$, which implies that for the densities involved in this study (assuming a value of $10^{-31} \text{ cm}^6/\text{s}$ for the Auger constant of intrinsic GaAs at 77 K²⁹) Auger recombination is of no importance⁴². Also other nonradiative recombination processes, associated with eg. impurities or non-equilibrium phonons, have been reported^{4, 5}, but none of them are expected to dominate the recombination in good quality GaAs.
- (ii) Lateral ambipolar diffusion of the electrons and holes out of the photo-excited region is negligible on a timescale of hundreds of picoseconds, since the purely diffusive drift length in 1 ns is of the order of $3.5 \mu\text{m}$ ³⁷ (assuming a diffusion coefficient equal to $120 \text{ cm}^2/\text{s}$ ⁴⁴). On the other hand the lateral diffusion has been found to be enhanced due to an increased Fermi-pressure, leading to a considerable plasma expansion^{45, 46}. A Fermi-pressure can drive electrons and holes laterally away, which would certainly affect the carrier density on a timescale of hundreds of picoseconds or even faster. This plasma expansion has been proposed originally to explain the measured dependence of the carrier temperature on the laser excess energy in steady state luminescence experiments⁴⁷ and the (Mott-like) linear relation between carrier density and temperature in gain and transmission experiments^{45, 48}. Within its lifetime, an electron-hole plasma can expand laterally, in order to form an equilibrium unbound Boltzman distribution, characterized by a linear dependence between density and temperature. However, the same linear relation has been found for a three dimensional confined plasma, in which no expansion was possible to occur²⁵.

The observed drop of the effective temperature below 40 K, unexplained by the model calculation, including phonon cooling and stimulated recombination, could indicate an expanding plasma, leading to an extra energy relaxation channel. However, the discrepancy could also be related to the neglect of impurity scattering in the energy relaxation model³³, or to the difficulty in fitting low temperature photoluminescence spectra¹². Moreover, it should be noted that any spatial expansion of the plasma tends to increase the actual spot size resulting in a considerable enhancement of the stimulated recombination rate, due to the exponential dependence of the total amplification on the spot size (equation (4.6)). A complete theoretical description of the present experiment, including plasma expansion, is very complicated. These calculations would have to incorporate both time- and spatial-dependent carrier temperatures and densities, yielding a time- and spatial-dependent gain, energy relaxation rate, radiative recombination coefficient, plasma drift and spot size, all very important for the stimulated recombination rate and the plasma expansion. By repeating the experiment for different spot sizes it should be possible to discriminate between both effects, which exhibit an opposite spot size dependence.

4.7 Conclusions

In summary, the cooling of hot carriers in nearly resonantly highly excited GaAs has been investigated. The electrons have been created below the satellite valleys, resulting in relatively low effective carrier temperatures due to the absence of intervalley scattering. It has been found that intense photo-excitation results in a rapidly decreasing carrier density (time constant 20 ps), in contrast to lower excitation levels for which much longer lifetimes have been observed. In addition to the ultrafast density decay rate a significant reduction in the carrier cooling rate has been found.

The short carrier lifetime has been assigned to the occurrence of stimulated recombination due to the high density accompanied by a relative low temperature. The rapidly decreasing carrier density causes a remarkable reduction of the cooling due to recombination heating, opposed partially by the extra cooling due to the loss of energy of the recombining carriers. The resulting reduction of the cooling is well described by a model calculation, which incorporates energy relaxation due to carrier-phonon interactions, the stimulated recombination process, and a time-dependent radiative recombination coefficient. Moreover, the absolute value of the radiative recombination coefficient has been found to be of crucial importance for the occurrence of stimulated recombination and its competition with other ultrafast processes.

It should be noted that the results not only are of interest from the fundamental point of view, but also for the design of direct-gap semiconductor laser structures to improve their operational characteristics⁴⁹. Moreover, the present study subscribes to the discussion of Rühle *et al.*¹² that it is of vital importance in any picosecond carrier cooling experiment to deduce both the carrier density and the effective temperature from the measurements, rather than only the temperature, especially for those excitation conditions which might lead to short carrier lifetimes and thus recombination heating.

References

- [1] J. Shah, *J. Phys. (Paris)* **42**, C-7 445 (1981); J. Shah, *IEEE J. Quantum. Electron.* **QE-22**, 1728 (1986); S.A. Lyon, *J. of Lumin.* **35**, 121 (1986); J. Shah, *Solid-State Electron.* **32**, 1051 (1989).
- [2] D. Bimberg and J. Mycielski, *J. Phys. C: Solid State Phys.* **19**, 2363 (1986).
- [3] K. Leo and W.W. Rühle, *Solid State Commun.* **62**, 659 (1987).
- [4] W.W. Rühle and K. Leo, *Phys. Stat. Sol. (b)* **149**, 215 (1988).
- [5] K. Shum, M.R. Junnarkar, H.S. Chao, R.R. Alfano and H. Morkoç, *Phys. Rev.* **B37**, 8923 (1988).
- [6] P.D. Dapkus, N. Holonyak Jr., R.D. Burnham, D.L. Keune, J.W. Burd, K.L. Lawley and R.E. Walline, *J. Appl. Phys.* **41**, 4149 (1970).
- [7] E.O. Göbel, R. Höger, J. Kuhl, H.J. Polland and K. Ploog, *Appl. Phys. Lett.* **47**, 781 (1985).
- [8] R. Cingolani and K. Ploog, *Advances in Physics* **40**, 535 (1991).
- [9] J. Dubard, J.L. Oudar, F. Alexandre, D. Hulin and A. Orszag, *Appl. Phys. Lett.* **50**, 821 (1987).
- [10] H.A.J.M. Reinen, T.T.J.M. Berendschot, P.C.M. Christianen, H.J.A. Bluysen and H.P. Meier, *Superlattices and Microstructures* **5**, 455 (1989).
- [11] P.C.M. Christianen, H.A.J.M. Reinen, H.J.A. Bluysen and M.R. Leys, *Proc. 20th Int. Conf. on the Physics of Semiconductors (Thessaloniki, Greece)*, edited by E.M. Anastassakis and J.D. Joannopolous (World Scientific, 1990).
- [12] W.W. Rühle, J. Collet, M. Pugno and K. Leo, *Condensed Systems of Low Dimensionality*, edited by J.L. Beeby *et al.* (Plenum Press, New York, 1991).
- [13] D.J. Erskine, A.J. Taylor and C.L. Tang, *Appl. Phys. Lett.* **45**, 54 (1984); A.J. Taylor, D.J. Erskine and C.L. Tang, *J. Opt. Soc. Am.* **B2**, 663 (1985).
- [14] W.H. Knox, C. Hirlimann, D.A.B. Miller, J. Shah, D.S. Chemla and C.V. Shank, *Phys. Rev. Lett* **56**, 1191 (1986); W.H. Knox, D.S. Chemla, G. Livescu, J.E. Cunningham and J.E. Henry, *Phys. Rev. Lett.* **61**, 1290 (1988).
- [15] G. Lasher and F. Stern, *Phys. Rev.* **133**, A553 (1964).
- [16] H. Haug and D.B. Tran Thoai, *Phys. Stat. Sol. (b)* **98**, 581 (1980).
- [17] J.H. Collet, W.W. Rühle, M. Pugno, K. Leo and A. Million, *Phys. Rev.* **B40**, 12296 (1989).
- [18] R.W.J. Hollering, T.T.J.M. Berendschot, H.J.A. Bluysen, H.A.J.M. Reinen, P. Wyder and F. Roozenboom, *Phys. Rev.* **B38**, 13323 (1988).
- [19] R.W.J. Hollering, *Phd. thesis*, University of Nijmegen (1986).
- [20] Y.P. Varshni, *Phys. Stat. Sol. (b)* **19**, 459 (1967).

- [21] G.W. 't Hooft and C. van Opdorp, *Appl. Phys. Lett.* **42**, 813 (1983); G.W. 't Hooft, M.R. Leys and H.J. Talen-v.d. Mheen, *Superlattices and Microstructures* **1**, 307 (1985).
- [22] P.D. Southgate, *J. of Appl. Phys.* **40**, 5333 (1969).
- [23] J. Shah, R.F. Leheny and C. Lin, *Solid State Commun.* **18**, 1035 (1976).
- [24] E.O. Göbel, W. Graudszus and P.H. Liang, *J. of Luminescence.* **24/25**, 573 (1981).
- [25] M. Capizzi, S. Modesti, A. Frova, J.L. Staehli, M. Guzzi and R.A. Logan, *Phys. Rev.* **B29**, 2028 (1984).
- [26] U. Strauss, A.P. Heberle, X.Q. Zhou, W.W. Rühle, T. Lauterbach, K.H. Bachem and N.M. Haegel, preprint
- [27] M. Asche and O.G. Sarbei, *Phys. Stat. Sol. (b)* **141**, 487 (1987).
- [28] W. Pötz, *Phys. Rev.* **B36**, 5016 (1987).
- [29] G. Benz and R. Conradt, *Phys. Rev.* **B16**, 843 (1977).
- [30] M. Pugno, J. Collet and A. Cornet, *Solid State Commun.* **38**, 531 (1981).
- [31] W. Pötz and P. Kocevar, *Phys. Rev.* **B28**, 7040 (1983).
- [32] H.A.J.M. Reinen, *Phd. thesis*, University of Nijmegen (1990).
- [33] J. Aaviksoo, I. Reimand, V.V. Rossin and V.V. Travnikov, *Phys. Rev.* **B45**, 1473 (1992).
- [34] K.L. Shaklee, R.F. Leheny and R.E. Nahory, *Appl. Phys. Lett.* **19**, 302 (1971).
- [35] S. Tanaka, H. Kobayashi and S. Shinoya, *J. Phys. Soc. Jpn.* **49**, 1051 (1980).
- [36] E.O. Göbel, H. Herzog, M.H. Pilkuhn and K.H. Zschauer, *Solid State Commun.* **13**, 719 (1973).
- [37] R. Cingolani, K. Ploog, A. Cingolani, C. Moro and M. Ferrara, *Phys. Rev.* **B42**, 2893 (1990).
- [38] K. Hess, A. Vojak, N. Holonyak, R. Chin and P.D. Dapkus, *Solid-State Electron.* **23**, 585 (1980).
- [39] J. Shah, B. Deveaud, T.C. Damen, W.T. Tsang, A.C. Gossard and P. Lugli, *Phys. Rev. Lett.* **59**, 2222 (1987).
- [40] D.Y. Oberli, J. Shah and T.C. Damen, *Phys. Rev.* **B40**, 1323 (1989).
- [41] W.W. Rühle, K. Leo and E. Bauser, *Phys. Rev.* **B40**, 1756 (1989).
- [42] Also in the case of an enhanced Auger coefficient for strongly p-doped GaAs²⁶ or a calculated value at 300 K⁴³, both approximately equal to 1.5×10^{-29} cm⁶/s, the Auger recombination rate is of minor importance for the density regime in this study.
- [43] A. Haug, *J. Phys. C.* **16**, 4159 (1983).
- [44] K.T. Tsen, O.F. Sankey, G. Halama, Shu-Chen Y. Tsen and H. Morkoc, *Phys. Rev.* **B39**, 6276 (1989).
- [45] K.M. Romanek, H. Nather, J. Fischer and E.O. Göbel, *J. of Luminescence* **24/25**, 585 (1981).

-
- [46] S. Modesti, A. Frova, J.L. Staehli, M. Guzzi and M. Capizzi, *Phys. Stat. Sol. (b)* **108**, 281 (1981).
- [47] E.O. Göbel and O. Hildebrand, *Phys. Stat. Sol. (b)* **88**, 645 (1978).
- [48] K.M. Romanek, E.O. Göbel, O. Hildebrand and H. Weber, *J. of Luminescence* **18/19**, 317 (1979).
- [49] V.I. Tolstikhin, *Sov. Techn. Phys. Lett.* **18**, 50 (1992).

Chapter 5

Ultrafast carrier dynamics at a metal-semiconductor interface

Abstract

The ultrafast carrier dynamics in the high electric field at a Au-GaAs interface has been studied both experimentally, using a subpicosecond photoluminescence correlation technique, and theoretically by a Monte-Carlo simulation. The correlated photoluminescence decay time is directly related to the carrier sweepout from the GaAs depletion region, i.e. to the time needed for electrons and holes to abandon the depletion region travelling in opposite directions. The decay time has been found to increase drastically with input power, ranging from a few picoseconds at low excitation to a considerably higher value (10-20 ps) at high excitation. These results indicate a significant retardation of the sweepout, which can not be explained merely by intervalley scattering and space-charge effects. From the Monte-Carlo calculations it has been found that the applied field collapses totally almost instantaneously after laser excitation, due to the enormous excess of photo-excited charges. The sweepout only recovers after some time needed to recharge the device. Already for a recharging time constant of 1 ps, which corresponds to the estimated device RC-time, a drastic reduction of the carrier sweepout has been found, in good (quantitative) agreement with the experimental findings.

5.1 Introduction

The physics of the ultrafast dynamics of hot carriers in high electric fields is important not only for designing structures for high speed opto-electronics but also for the fundamental understanding of energy relaxation and non linear transient transport in high electric fields. Originally the investigations concerning the ultrafast non-stationary and non-equilibrium carrier transport have been constricted to predictions, due to the lack of experimental techniques¹. However, since the availability of picosecond (and more recently of femtosecond) light sources a large number of time-resolved experimental investigations have been conducted to check the predicted ultrafast behaviour of carriers in semiconductors. Recently, several groups have employed successfully a photoconductivity technique², using (sub)picosecond laser pulses and fast optical switches, to measure the transient transport and have used Monte-Carlo calculations in an attempt to understand the results³⁻⁵. Experimental evidence has been found for a velocity overshoot in GaAs, above the steady state drift velocity, as predicted first by Ruch⁶. The velocity overshoot has been found to occur for electrons photo-excited into the Γ -valley of the conduction band in a biased GaAs photoconductor. The electrons are accelerated in the Γ -valley due to the high electric field. Above a certain field strength the electrons can gain enough energy to be scattered to the satellite L-valley, resulting in a lower drift velocity⁴. Photo-excitation closer to the conduction band-edge results in a larger velocity overshoot, because the electrons spend more time in the Γ -valley, before they can scatter to the satellite valley. These velocity overshoot effects due to the inherent bandstructure and intervalley scattering should not be confused with the transport transients arising from space-charge-separation effects⁵. Since the photo-excited electrons and holes drift in opposite directions the continuously changing electric field can produce a photo-conductive transient as well.

However, the present results cannot be fully interpreted only in terms of intervalley scattering and space-charge effects. As a consequence additional phenomena, such as the influences of the contacts and a time- and spatial-dependent electric field, have to be incorporated.

In this chapter we present an investigation of the ultrafast carrier dynamics in the high intrinsic electric field at a metal-semiconductor interface, in order to study the parameters which determine the transient transport. The carrier sweepout from the depletion region of a modified biased Au-GaAs Schottky barrier was studied both experimentally, by use of a subpicosecond photoluminescence correlation technique⁷ and theoretically by Monte-Carlo simulations. The use of the photoluminescence correlation technique in this kind of experiments, as proposed first by Von Lehmen *et al.*^{8, 9}, offers the possibility to monitor the carrier transport on a subpicosecond timescale. Moreover, in principle this technique can supply us with energy-resolved correlated photoluminescence spectra in order to probe the carrier energy distributions and their energy relaxation.

In the next section (5.2) the composition of the modified Schottky barrier sample will be discussed, which is of major importance for the total photoluminescence yield. Subsequently the experimental results, obtained by the correlation technique, will be presented (section 5.3). The photoluminescence decay time, which is a measure for the carrier sweepout from the 0.3 μm -thick GaAs depletion region, has been found to be increased drastically from

a few picoseconds at low laser intensity (carrier density $< 5 \times 10^{16} \text{ cm}^{-3}$) to a value as high as 10-20 ps after more intense excitation (density $> 5 \times 10^{17} \text{ cm}^{-3}$). These results indicate a significant retardation of the carrier sweepout with increasing laser input power. In order to understand the experimental results a Monte-Carlo simulation was performed. The ingredients and assumptions in this Monte-Carlo simulation will be discussed in section 5.4. In section 5.5 the results of the calculations will be compared with the experimental observations. The experimental carrier sweepout appears to be much too slow to be explained by merely intervalley scattering and space-charge effects. It will be shown that the modelling of the contacts is of crucial importance, and that a contact recharging time has to be introduced, in order to reproduce the drastically retarded sweepout found in the experiment. Finally, the conclusions will be summarized in section 5.6.

5.2 Sample composition

The layer composition of the modified MBE-grown Schottky barrier sample is shown schematically in figure 5.1. The actual barrier is formed by an $0.3 \mu\text{m}$ -thick n-type GaAs (doping

↓			
80 Å	Au		laser excitation
			metal
100 Å	GaAs	undoped	
			caplayer
100 Å	$\text{Al}_{0.4}\text{Ga}_{0.6}\text{As}$	undoped	
$.3 \mu\text{m}$	n-GaAs	10^{17} cm^{-3}	depletion layer
100x	50 Å GaAs/ 50 Å $\text{Al}_{0.33}\text{Ga}_{0.67}\text{As}$ n-type	10^{18} cm^{-3}	superlattice buffer
n ⁺ -GaAs			substrate
Au-Ge-Ni contact			

Figure 5.1: Layer composition of the modified Schottky barrier

concentration: 10^{17} cm^{-3}) layer and a semi-transparent Gold film of 80 Å-thickness, to allow for laser excitation through the metal top contact. To suppress interface recombination and provide for a superior optical quality the sample contains a very thin (100 Å) intermediate undoped $\text{Al}_{0.4}\text{Ga}_{0.6}\text{As}$ -layer between the metal and the depletion layer, capped by a 100 Å-thick undoped GaAs-layer, as well as a heavily doped n-type (doping concentration: 10^{18} cm^{-3}) superlattice buffer layer (100 x 50 Å GaAs/ 50 Å $\text{Al}_{0.33}\text{Ga}_{0.67}\text{As}$) between the depletion layer and the n^+ -GaAs substrate. The superlattice has been inserted to prevent carrier creation in the substrate which could cause a disturbing background signal in addition to the depletion layer photoluminescence. Since the superlattice luminescence wavelength differs from that from GaAs this signal can be easily filtered out by a monochromator. The actual size of the sample equals 4 x 4 mm. A voltage bias can be applied across the sample between an AuGeNi backside-contact and the top contact. The insertion of the intermediate (Ga,Al)As-layer and the superlattice was found to leave the current-voltage characteristics unchanged for reverse biases. Capacitance-voltage measurements indicate a value for the Schottky barrier height of 0.90 V and a total capacitance of 8.3 nF for a reverse bias of 3 V, yielding a capacitance per area of $5.2 \times 10^{-4} \text{ F m}^{-2}$.

5.3 Experimental details and results

Subpicosecond time-resolved photoluminescence measurements were performed with help of a correlation technique, of which more details are given in section 2.5. The sample was excited by two laser pulse trains (generated by a CPM dye laser, pulse width 60 fs, energy 2.03 eV, repetition rate 100 Mhz) of equal amplitude, with a variable time delay δt in between. The two beams were chopped separately at frequencies ω_1 and ω_2 and were focused to a 20 μm diameter spot onto the sample surface. The time-integrated photoluminescence signal of the depletion layer was guided through a 1 m monochromator (Monospek) and detected by a cooled GaAs photomultiplier with use of a lock-in amplifier tuned to frequency $\omega_1 - \omega_2$. The resulting photoluminescence signal can be expressed as the crosscorrelation of the electron (n_i) and hole (p_i) populations, photo-excited by the first ($i = 1$) and second ($i = 2$) laser pulses (section 2.5):

$$I(\delta t) = \int [n_1(t)p_2(t + \delta t) + n_2(t + \delta t)p_1(t)] dt \quad (5.1)$$

As a consequence the correlated photoluminescence intensity is determined by the overlap in both real space and \mathbf{k} -space, of the photo-injected electron and hole distributions inside the GaAs depletion region. The dependence of the signal on the time delay δt between the two pulses is a measure for the carrier sweepout from the depletion region. The correlated photoluminescence intensity was measured at an energy close to the band-edge, as a function of the reverse bias across the sample ($0 \leq V_{\text{bias}} \leq 4.0 \text{ V}$), i.e. the backside-contact is positively charged with respect to the top contact (figure 2.3 (b)). Also the laser excitation power was varied from 0.1 mW to 2.0 mW. that is the concentration of created carriers ranged from about 1×10^{16} to $5 \times 10^{17} \text{ cm}^{-3}$.

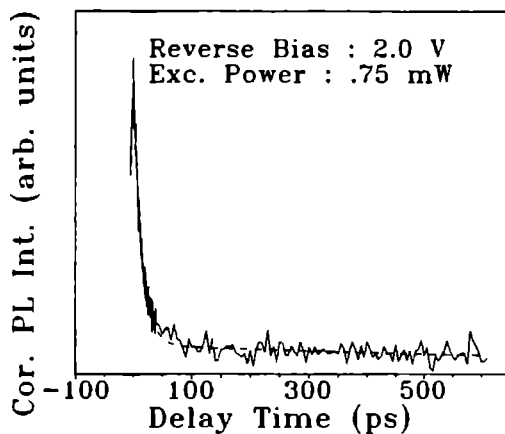


Figure 5.2: Typical correlated photoluminescence (PL) intensity as a function of the time delay between the pulses. The dashed curve corresponds to a fit according to equation (5.2).

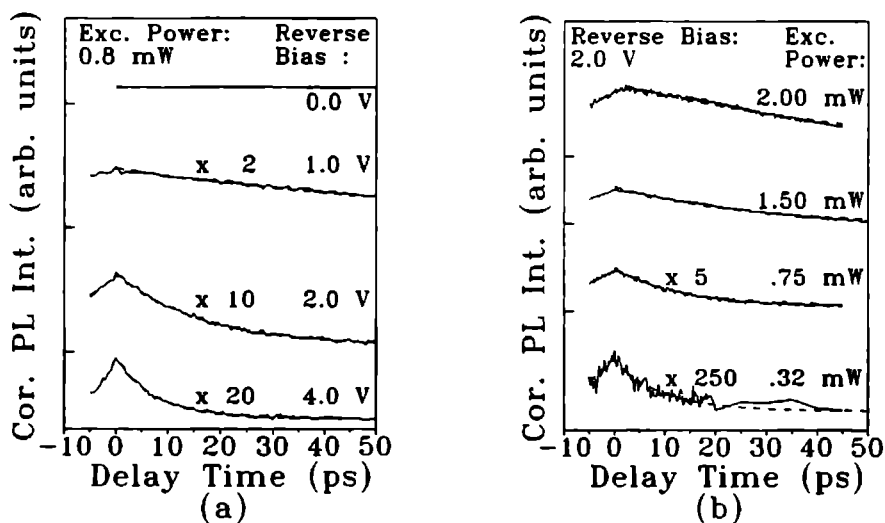


Figure 5.3: Correlated photoluminescence (PL) intensity as a function of time delay between the pulses for different reverse bias voltages (a) and excitation powers (b). The dashed curves correspond to the best fits to the data. Some of the traces are vertically shifted and multiplied by the given numbers for clarity.

A typical correlation trace for the entire time interval used ($\delta t \leq 600$ ps) is depicted in figure 5.2 for a reverse bias of 2.0 V and an excitation power of 0.75 mW. It is clear that the photoluminescence decay is composed out of a rapidly and a slowly decaying component. As a consequence the experimental data were fitted to the sum of two exponential functions, according to:

$$I(\delta t) = A_{\text{short}} \cdot \exp\left[-\frac{\delta t}{\tau_{\text{short}}}\right] + A_{\text{long}} \cdot \exp\left[-\frac{\delta t}{\tau_{\text{long}}}\right] \quad (5.2)$$

The dashed curve in figure 5.2 represents the best fit. The contribution to the signal with the long time constant hardly decays within the time interval used. But the short decay time, which we attribute to the carrier sweepout from the GaAs depletion layer, strongly depends on reverse bias and excitation power, as follows from figure 5.3, which shows typical measured correlation curves for different applied reverse bias voltages (figure 5.3 (a)) and excitation powers (figure 5.3 (b)). The dashed curves correspond to the best fits according to equation (5.2).

The measured correlated photoluminescence decay curves are well described by the double exponential decay. For no applied bias and an excitation power of 0.8 mW the recorded curve is completely flat on the displayed time interval. With increasing reverse bias voltage the decay time becomes considerably shorter. Apparently the amplitude of the correlated signal decreases with the decay time as follows from figure 5.3 (a), in which the input power is constant. From figure 5.3 (b) it is clear that reducing the excitation power also causes the correlated photoluminescence decay times to be shortened significantly. Concerning the fast decay times τ_{short} , figures 5.4 and 5.5 overview the results of fitting the experimental curves to equation (5.2), for a variety of reverse bias voltages and input powers respectively.

The main features to be noted are the following. With increasing reverse bias voltage (figure 5.4) the photoluminescence decay time reduces drastically over three orders of magnitude, from several nanoseconds at zero bias voltage to a few picoseconds at 4.0 V reverse bias voltage. For the lowest reverse bias voltages (< 0.2 V) the depletion width of the Schottky barrier was estimated to be considerably thinner ($\sim 0.1 \mu\text{m}$, expression (2.5)) than the total active GaAs layer thickness ($0.3 \mu\text{m}$). Therefore the decay time approaches the spontaneous carrier lifetime, since the photoluminescence decay is determined mainly by carriers in the flat band region. With increasing reverse bias both the depletion width as well as the internal electric field increase, leading to a considerably faster carrier sweepout, which results in photoluminescence decay times as fast as 3 ps under favourable conditions. This time constant agrees with the results of Von Lehmen *et al.*⁹, who assigned it to electrons traversing the depletion region at their saturation velocities. In addition, the correlated photoluminescence decay time increases with increasing excitation power. For instance for 3.0 V and 4.0 V reverse bias voltage the correlated photoluminescence decay time grows from a few picoseconds at 0.1 mW to a significantly higher value of about 10-20 ps at 2.0 mW excitation power (figure 5.5).

Figure 5.6 shows the dependence on the excitation power of the fitted coefficients A_{short} , normalised to the input power, for various applied reverse bias voltages. Since the *time-integrated* correlated photoluminescence was measured (equation (5.1)) the amplitude of the

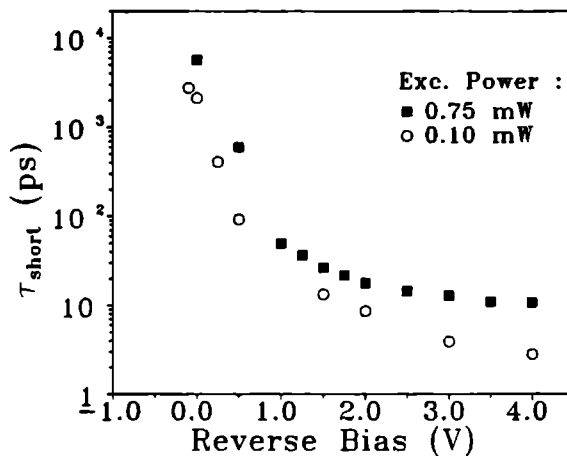


Figure 5.4: Short correlated photoluminescence (PL) decay times as a function of reverse bias voltage for input powers 0.1 mW (open dots) and 0.75 mW (squares). The values are obtained by fitting the experimental correlation curves to expression (5.2).

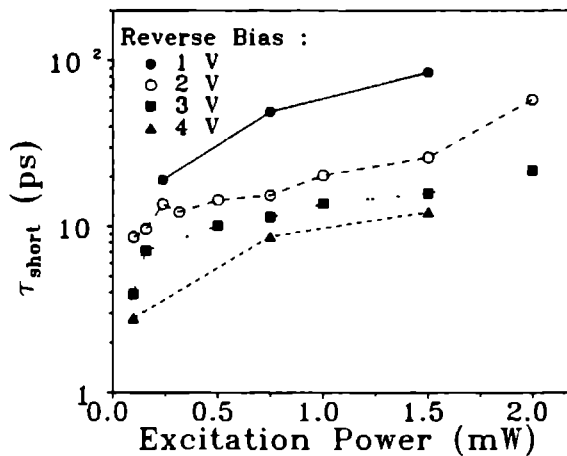


Figure 5.5: Short correlated photoluminescence (PL) decay time as a function of excitation power for a number of reverse bias voltages. The values were obtained by fitting the experimental correlation curves to expression (5.2).

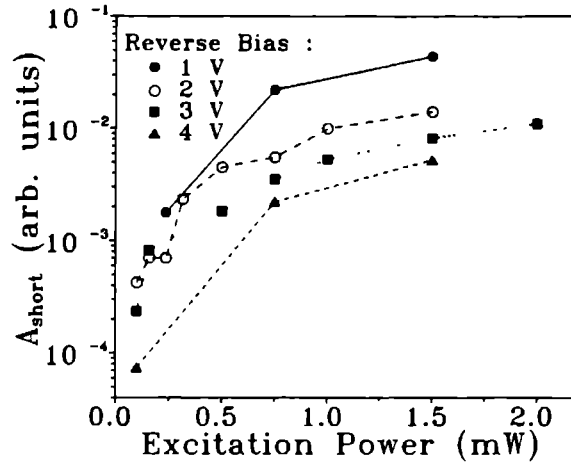


Figure 5.6: Fitted correlated photoluminescence (PL) amplitudes for the rapid component as a function of the input power for a number of reverse bias voltages. The amplitudes were normalised to the excitation power.

signal is connected to the photoluminescence decay time, resulting in a similar dependence on the excitation level for A_{short} (figure 5.6) as compared to τ_{short} (figure 5.5).

In addition to the rapidly decaying correlated photoluminescence contribution also a background-like signal is present (figure 5.2). Since this component hardly decays within the time interval used, a reliable determination of its time constant τ_{long} would require an extension of the measurements towards longer delay times. From the present experimental results τ_{long} was estimated to amount to several nanoseconds, within the experimental error independent of the parameters varied (input power and reverse bias voltage). Moreover, also the normalised coefficient A_{long} of this slowly decaying component does not vary strongly with bias voltage or input power. For the origin of this component a few explanations are possible:

- (i) despite the precaution taken by growing the superlattice buffer, carriers are created in the substrate causing a disturbing luminescence background.
- (ii) carriers created in the 100Å-thick GaAs caplayer cause the background.
- (iii) the background is due to carriers which are left behind in the depletion layer after the first carrier sweepout because of the built-in potential barriers, i.e. the intermediate AlGaAs layer and the superlattice buffer layer for low-energetic holes or electrons respectively.

To our opinion the lack of a distinct dependence on the experimental parameters, suggests the background to originate from the region which is the least affected by the bias voltage, that is the substrate.

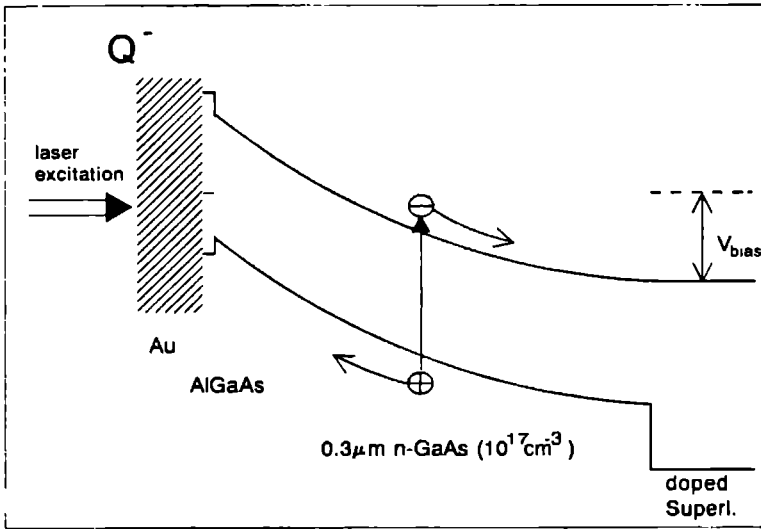


Figure 5.7: Schematic representation of the band bending at the metal-semiconductor interface, as it is used in the Monte-Carlo simulations.

5.4 The Monte Carlo simulations

In order to find an interpretation of the presented experimental results Monte-Carlo simulations were performed. Special attention was given to the striking retardation of the carrier sweepout in the case of an increasing laser input power.

In these simulations the device is modelled schematically assuming a band bending at the metal-semiconductor interface as is indicated in figure 5.7. The $0.3 \mu\text{m}$ -thick GaAs layer is separated from the Au by a barrier formed by the intermediate AlGaAs layer and the Schottky barrier. Due to its heavy doping the superlattice is assumed to form no barrier for the electrons and a large one for the holes. The applied bias voltage creates an interface charge at the Au film which is compensated for by a constant intrinsic space-charge throughout the whole depletion layer giving rise to a linear decreasing electric field and a parabolic potential (figure 5.7). This means that in this model the depletion width is constant and equal to the GaAs layer thickness, whereas the doping concentration is varied with the applied bias voltage. In an actual Schottky device the doping level is constant and the depletion width changes with bias voltage (section 2.2). Although this model is rather schematic we believe it nevertheless contains the basic physics needed for describing semi-quantitatively the experimental results for the high reverse bias voltages ($> 2.0 \text{ V}$), when the depletion region approaches the GaAs layer thickness.

The carriers are created in the depletion layer according to the absorption coefficient of GaAs for the laser light. The subsequent transport and energy relaxation of both electrons and holes in the GaAs layer are computed in a Monte-Carlo simulation¹¹, accounting for the various scattering mechanisms such as optical and acoustic phonon-, ionised impurity-

intervalley-, and carrier-carrier scattering^{12 13} Both electron-heavy- and -light-hole pairs are considered, including hole inter-band transitions¹⁴ Standard 10^4 electron-hole pairs were used In some cases the statistical accuracy of the results was checked with simulations using 10^5 electron-hole pairs

The correlated photoluminescence signal is calculated according to equation (5.1), making two simplifying assumptions in order to keep the problem manageable

- (i) the carrier distributions excited by both pulses are the same, but shifted in time Thus the effect of the second pulse arriving at the sample whose features (eg absorption, local electric field) may be changed by the carriers of the first pulse, is neglected
- (ii) the distribution in k -space is taken to be independent of the real space position inside the device A scaling factor, which represents the integral over k -space, counts the number of carriers at each position

Evidently photo-excitation of charged particles may give rise to a space-charge field Directly after excitation, when the electrons and holes are still close to each other this field is zero However, as soon as the electrons and holes start to separate as a result of the applied field, a counteracting electric field will build up To account for this space-charge effect, which can be especially large for the highest intensities used, the Poisson equation is solved in one dimension every 10 fs of the calculation, resulting in a time-dependent local driving field in addition to the applied field

5.5 Theoretical results and discussion

5.5.1 Results of the Monte-Carlo simulations

The calculations were performed for reverse bias voltages of 1.5 V and 3.0 V, viz average fields of 50 kV/cm and 100 kV/cm respectively and input powers ranging from 0.1 to 2.5 mW Figure 5.8 shows the calculated correlated photoluminescence signal arising from recombination of electrons with heavy-holes, as a function of the delay time between the pulses for a number of input powers The photoluminescence intensity due to electron-light-hole recombination appeared to be one order of magnitude smaller It is directly clear from this figure that for all excitation powers and both bias voltages the computed photoluminescence correlation signal decays within 3 ps, in sharp contrast to the experimental results (figure 5.3) On the other hand, as in the experiment, an enhancement of the photoluminescence decay time is found with increasing input power This result indicates the significance of the building of a space-charge field for the sweepout Furthermore, in some cases the calculated correlation signal exhibits irregularities, especially visible at 3.0 V reverse bias voltage (1.0 and 1.5 mW input power), where at about 400 fs delay time a kind of plateau in the intensity decay is formed and some scattering can be seen in the respective data points It should be noted here that the actual time steps used in the calculation (10 fs) are much smaller than the horizontal space in between the points in figure 5.8

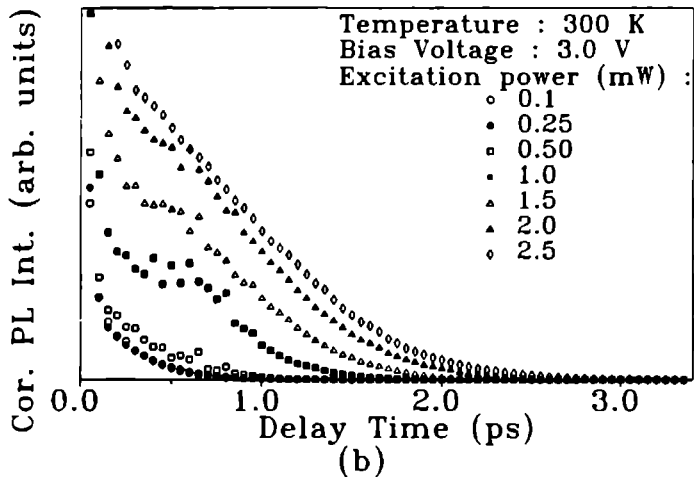
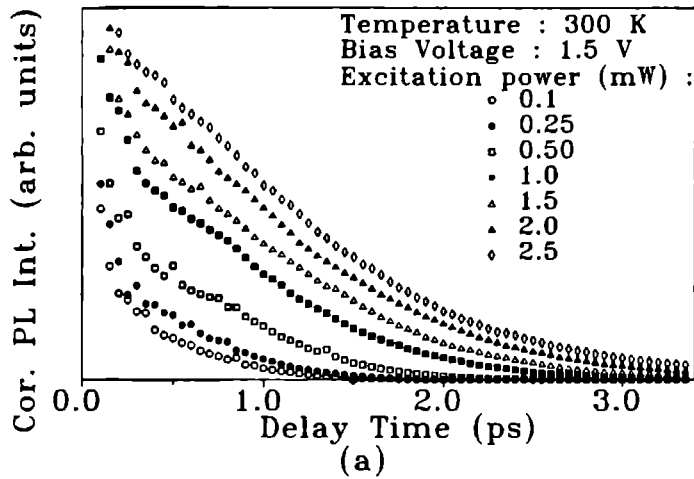


Figure 5.8: Calculated correlated photoluminescence (PL) decay curves for 1.5 V (a) and 3.0 V (b) bias voltage, for different excitation powers ranging from 0.1 mW to 2.5 mW.

In order to gain insight in the physical behaviour of the easy to measure but difficult to interpret photoluminescence correlation signal, figure 5.9 reports the time-evolution of the electron-heavy-hole photoluminescence in real time, as would be measured with the up-conversion technique. All luminescence traces start from the same value of 0.67 at zero time after excitation. This value corresponds to the fraction of heavy holes in the simulation. In the time-evolution of the photoluminescence signal roughly two regimes can be distinguished. Within the first 300 fs the photoluminescence intensity rapidly decreases, followed by a more slowly decay on a picosecond timescale.

- (i) The initial rapid decay is predominantly the result of intervalley scattering. The electrons are created by a 2.03 eV laser pulse and possess an excess energy larger than the energy of the L- and X-satellite valleys in the conduction band. As a result of the large effective mass of the satellite valleys the photo-excited electrons are very efficiently scattered into these valleys^{15, 16}, where they do not contribute to the photoluminescence intensity. As a matter of fact most of the electrons leave the depletion region travelling in the satellite valleys. It should be emphasized that these electrons keep contributing to the space-charge field and the electrical current, and are probed in photo-conductivity measurements, but are not seen in photoluminescence experiments.
- (ii) The electrons which remain in the Γ -valley give rise to a more slowly decaying photoluminescence signal. because of their sweepout from the depletion region on a picosecond timescale (figure 5.9). This carrier sweepout apparently strongly slows down with increasing laser input power. When the total number of carriers increases, the field strength of the counteracting field, as opposed to the applied electric field, gets stronger leading to a somewhat retarded carrier sweepout.
- (iii) But the actual situation is more complicated, since the effects discussed in (i) and (ii) cannot be regarded as completely independent. Due to the separation of electrons and holes, the local electric field varies both in real space and time. Electrons scattering back from the L- and X-satellite valleys into the Γ -valley can gain enough energy by the electric field to be rescattered to the satellite valleys. However, in the regions of low electric field the electrons remain in the Γ -valley giving rise to an enhanced photoluminescence signal, i.e. an extra shoulder, at about 400 fs after excitation. Obviously the number of rescattered electrons that remain in the Γ -valley grows with increasing importance of the space-charge field, i.e. with increasing input power. This is the origin of the increase of the correlation signal with increasing laser power (figure 5.8).

Basically it is the slow contribution of the direct photoluminescence signal which corresponds to the calculated correlated photoluminescence decay in figure 5.8 and its power dependence. Apparently the shoulder in the direct photoluminescence starting at about 300 fs for high input powers corresponds to the faint feature at similar delay times in the correlated signal. The physical behaviour of both computed luminescence signals can be well understood in terms of intervalley scattering and charge-separation effects. but it appears that they can by no means explain the anomalous long correlated photoluminescence decay times measured (figure 5.5). which are probably the result of an other mechanism. neglected so far.

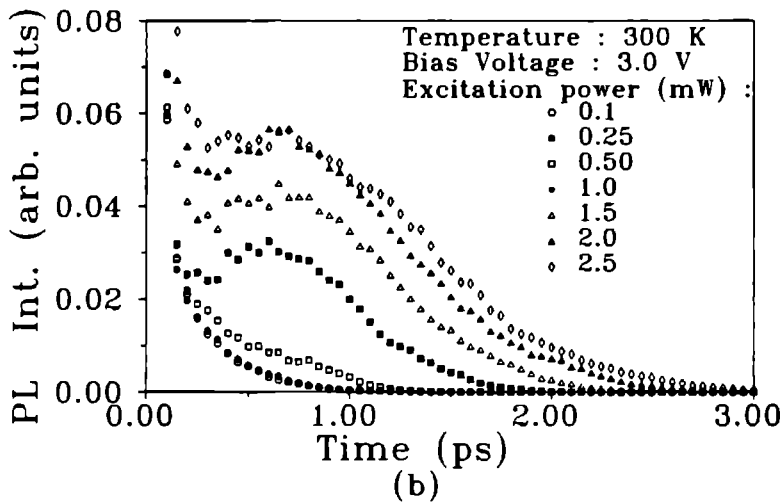
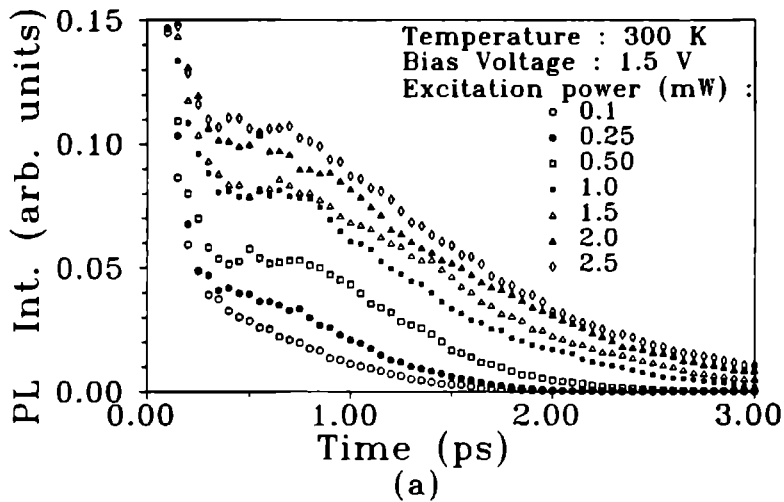


Figure 5.9: Calculated time-dependent photoluminescence (PL) intensity for 1.5 V (a) and 3.0 V (b) bias voltages, for different input powers. The results correspond to the calculations leading to the correlation traces in figure 5.8.

5.5.2 Calculations including a contact regeneration time

The pronounced input power dependence and the tendency to instabilities present in the computed photoluminescence curves suggest that the photo-excited charge is dominating the charge initially present in the biased device. It is therefore worthwhile to consider the situation in more detail. In the case of the highest input power the photo-injected charge is still four orders of magnitude lower than the total charge on the device. However, it is the charge density, i.e. the charge on the illuminated part, that is important and not the total charge present on the device. For example the photo-excited charge density can exceed the intrinsic one by a factor of 20, inevitably leading to serious consequences for the carrier sweepout, as will be shown in the following.

Very shortly after excitation a number of holes will reach the top contact, where these holes neutralize the metal surface charge, leading to a reduced field strength. In the case that the photo-excited charge density exceeds significantly the intrinsic one, the applied field may be destroyed totally by only a small part of the excited holes. It will take some time before the field will be restored, that is the time needed to recharge that part of the device which is discharged, i.e. the illuminated part. Obviously this recharging time is connected to the RC-time constant of the device studied, which is basically the illuminated part incorporated in the total device on which a surplus of charge is present. From C-V measurements the capacitance of the illuminated part was estimated to be about 0.2 pF. The resistance is believed to be determined by the very thin semi-transparent top Au-contact which has a square resistance of a few Ohms, rather than the low Ohmic highly doped backside-contact. As a result the RC-time is expected to be about 1.0 ps. In order to investigate the consequences for the carrier sweepout of such a recharging time, we introduced a so-called regeneration time constant τ_{reg} by which charge is transferred to the illuminated part of the top contact tending to keep the total voltage across the depletion layer constant. In practice the positive charge reaching the top contact is compensated for by adding negative charge with a time constant τ_{reg} in order to keep the effective bias constant. However, it should be noted that also in the case holes are stuck in the band bending region, eg. at the built-in barrier due to the intermediate AlGaAs layer (figure 5.7), an extra amount of charge has to be transferred to the top contact.

The correlation traces were recalculated for a number of regeneration times ranging from 0.25 to 1.0 ps. The results for excitation powers 0.1 mW (a), 1.0 mW (b) and 2.0 mW (c), and a bias voltage of 3.0 V are shown in figure 5.10. In the calculations with $\tau_{\text{reg}} = 0$, which are equivalent to the calculations described in the previous section (figure 5.8), the recharging is given infinite speed to keep the voltage across the depletion layer constant. The curves for a bias voltage of 1.5 V show a similar behaviour as a function of the regeneration time and the input power. When a finite value for the regeneration time is used the correlated photoluminescence decay times become much longer. Even for the lowest excitation power (0.1 mW) already a noticeable reduction of the correlated photoluminescence decay rate is visible. For the intermediate (1.0 mW) and high (2.0 mW) input powers the reduction in the photoluminescence decay rate becomes enormous. It is striking that the introduction of a regeneration time which is still considerably small ($\tau_{\text{reg}} \leq 1.0$ ps), already can retard the

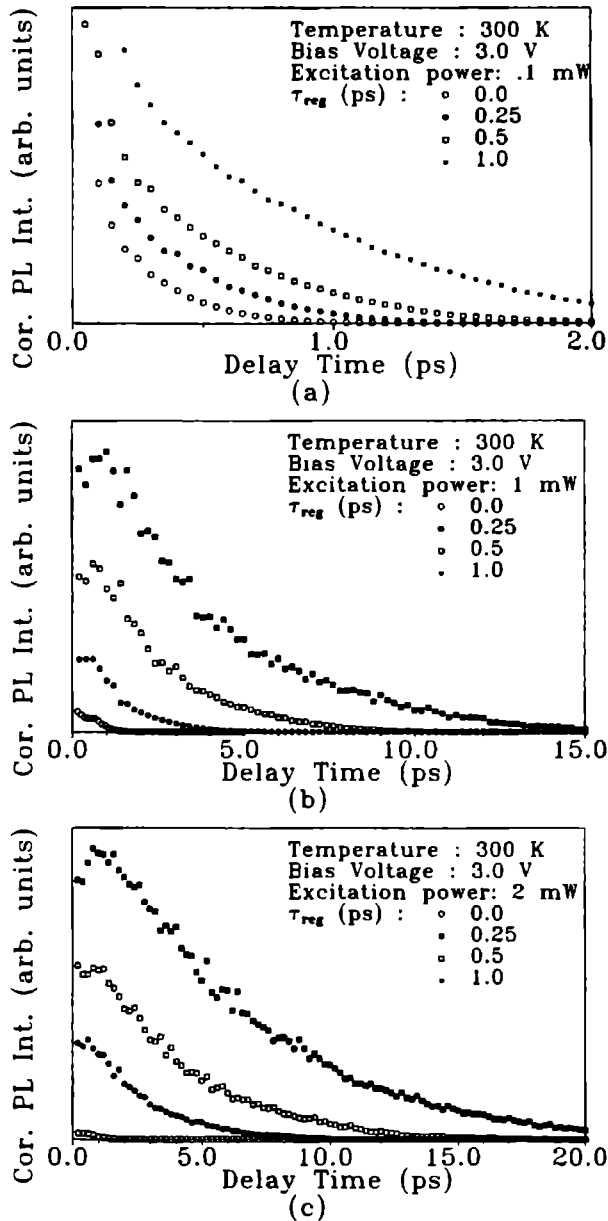


Figure 5.10: Calculated correlated Photoluminescence (PL) decay curves for a bias voltage of 3.0 V and the input powers 0.1 mW (a), 1.0 mW (b) and 2.0 mW (c) for a number of values for the regeneration time τ_{reg} .

carrier sweepout up to timescales of ten picoseconds, in case of the highest input powers. This can be traced back directly to the enormous excess of photo-excited charge density. Ultimately, the measured carrier sweepout depends not only on the regeneration time but also on the photo-excited charge density.

Figure 5.11 summarizes the calculated photoluminescence correlation decay time as a function of input power, for a number of bias voltages and regeneration times. The results for an infinitely fast regeneration time ($\tau_{\text{reg}} = 0$) indicate some retardation of the carrier sweepout with input power, determined completely by space-charge effects. Obviously for this case the calculated decay times appear much too small with respect to the experimental observations. The discrepancy between the experiment and these first calculations can be solved by the introduction of one single time constant τ_{reg} , which represents a device recharging time. For all input powers the decay times get considerably longer with increasing τ_{reg} . Note that the calculated decay times for a regeneration time of 1.0 ps are in reasonable quantitative agreement with the experimental results (figure 5.5). Furthermore the calculated decay times for the higher bias voltage (3.0 V) are shorter than for the lower bias voltage (1.5 V) in agreement with the results of figure 5.4. However, the assumption in the model of a homogenous space-charge for all bias voltages, rather than a bias dependent depletion region width, makes a detailed comparison not possible. Concerning the measured coefficient A_{short} of the correlated signal as a function of the laser input power (figure 5.6), the model also produces comparable dependencies, which is not surprisingly because in the photoluminescence correlation technique the decay times and amplitudes are closely related.

Evidently the amount of photo-excited charge is of crucial importance for the actual sweepout. It is therefore interesting to see what happens to the effective bias across the depletion region after intense laser excitation. Figure 5.12 depicts the time-evolution of the effective bias for an initial bias voltage of 3.0 V, 1.0 mW input power and for different values of the regeneration time τ_{reg} . It is clear that directly after excitation the effective bias is destroyed completely due to the neutralization of the metal surface charge by the photo-excited holes that reach the top contact. Note that the effective bias may even be inverted for some time, which is caused by the inertia of the carriers moving to the contacts. Obviously the speed of the recharging process depends on the value of the regeneration time, that is the longer the regeneration time the longer the effective bias remains destroyed. In the absence of the electric field, a large number of electrons is returning from the satellite valleys to the Γ -valley, while in addition the carrier sweepout from the depletion region is delayed. Both effects give rise to a considerable enhancement of the photoluminescence decay time.

The effect of the photo-excited charge density on the electric field gains definitely in importance with increasing input power as follows from figure 5.13, which shows the time-evolution of the effective bias for a number of input powers calculated with a regeneration time of 1.0 ps and an initial bias voltage of 3.0 V. For the lowest input power the amount of photo-excited charge is too low to destroy the applied field completely, however already a significant retardation of the carrier sweepout is present (figure 5.11 (b)). With increasing power the voltage drop increases and exists longer. Apparently for the highest input powers

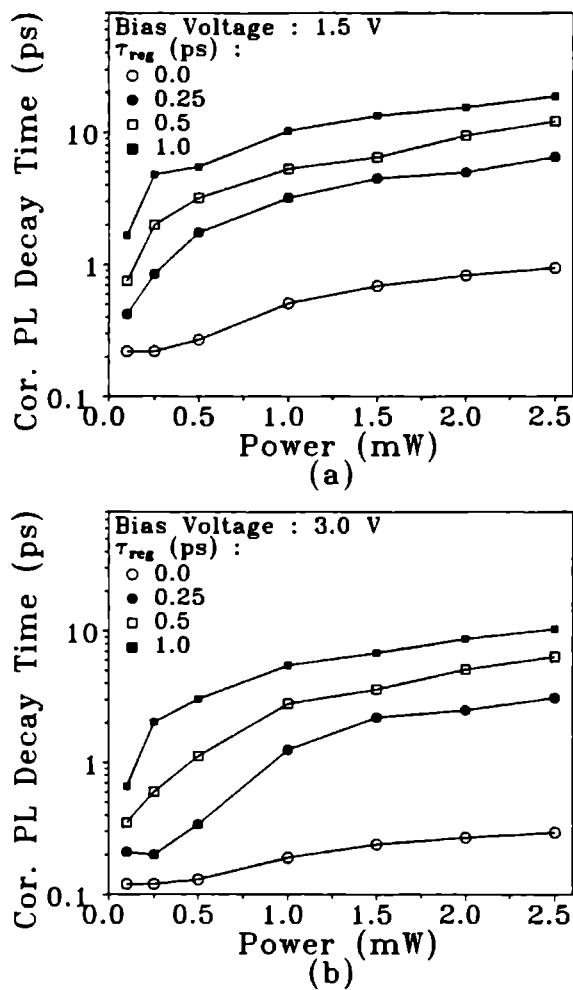


Figure 5.11: Calculated Photoluminescence (PL) correlation decay times for 1.5 (a) and 3.0 V (b) bias voltage, as a function of the input power and various regeneration times.

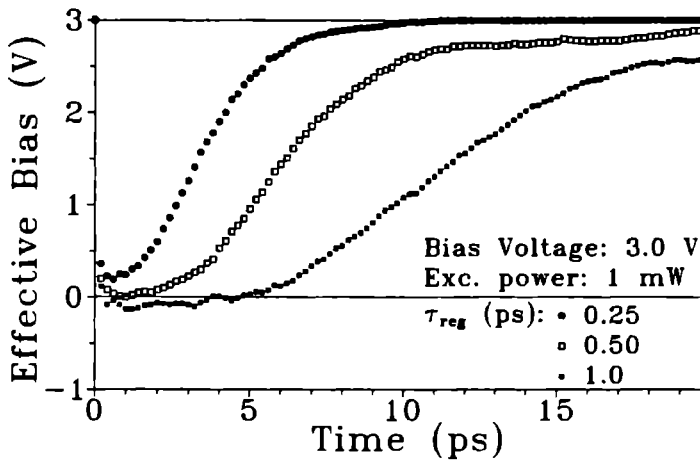


Figure 5.12: Time-evolution of the effective bias voltage calculated for an initial bias voltage of 3.0 V and an input power of 1.0 mW for a number of values of the regeneration time constant.

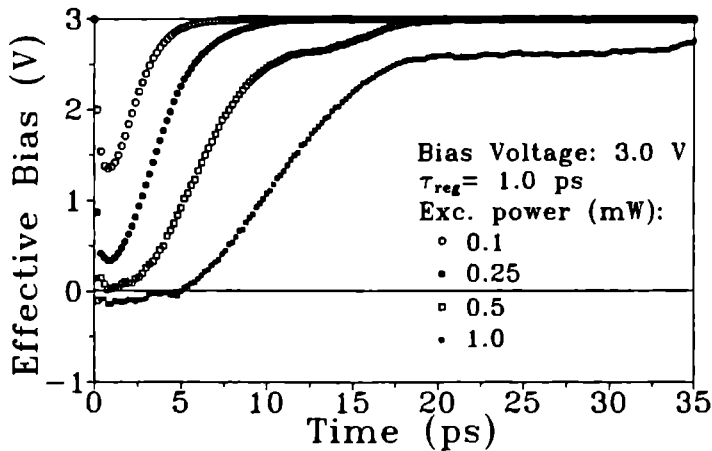


Figure 5.13: Time-evolution of the effective bias voltage, calculated for an initial bias voltage of 3.0 V and a regeneration time of 1.0 ps for a number of input powers.

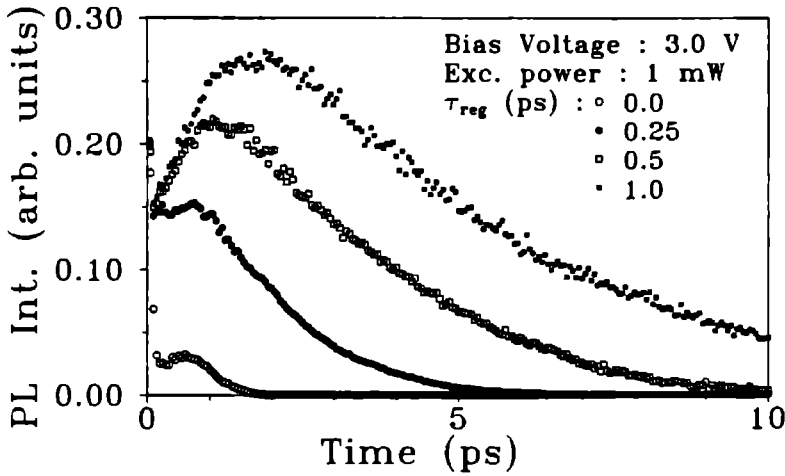


Figure 5.14: Calculated time-evolution of the photoluminescence (PL) intensity for a bias voltage of 3.0 V and an input power of 1.0 mW for a number of values of the regeneration time constant.

the bias voltage can be inverted due to the inertia of the carriers moving to the contacts. For excitation powers > 1 mW the effective bias may even show chaotic oscillations on a timescale of more than ten picoseconds¹⁷. The enormous amount of excess charge can lead to peculiar highly non linear transport transients. The precise nature of the chaotic behaviour is subject of a further study¹⁷.

The consequences of the total collapse of the electric field are enormous for the photoluminescence decay, which is depicted in figure 5.14 for a bias voltage of 3.0 V, an input power of 1.0 mW and for several values of the regeneration time constant. For each regeneration time constant used the photoluminescence intensity still decays very fast within the first hundreds of femtoseconds, due to the intervalley scattering. But the appearance of the extra intensity peak starting at about 500 fs becomes more and more distinct. Without an electric field the electrons return relatively rapidly to the Γ -minimum^{15, 16}, where they contribute again to the photoluminescence signal, resulting in a conspicuous rise in the photoluminescence intensity after the first fast decay. Moreover, as long as the effective bias is not restored, the electrons and holes are not separated in real space and the carrier sweepout is retarded, leading to a drastic reduction of the photoluminescence decay rate, in accordance with the measured photoluminescence correlation decay times (figure 5.10).

5.6 Conclusions

In summary, the ultrafast carrier sweepout from the depletion region of a Au-GaAs Schottky barrier has been found to be strongly affected by the contacts, which might act as an extra

limit for operating a device at its maximum frequency or which might lead to peculiar highly non linear transport transients. Since even at moderate laser input powers the injected charge density is dominating the one initially present, the applied field collapses almost instantaneously after laser excitation, while its reconstruction takes the time needed to recharge the device. A contact recharging time constant had to be invoked in the Monte-Carlo analysis to explain the experimental observations. The use of a recharging time of 1 ps, which corresponds to the estimated device RC-time, leads to the nice quantitative reproduction of the experimentally observed carrier sweepout. Ultimately the actual carrier sweepout is determined by both the contact regeneration time and the photo-created carrier concentration. In view of the common values of the electric fields involved and the laser input levels used, it should be noted that the concept of a finite time for the restoration of the internal electric field should be applicable to other opto-electronic devices as well, for example fast opto-electronic switches¹⁸.

References

- [1] D.K. Ferry, H.L. Grubin and G.J. Iafrate, in *Semiconductors Probed by Ultrafast Laser Spectroscopy*, edited by R.R. Alfano (Academic Press, New York, 1984).
- [2] D.H. Austin, *Appl. Phys. Lett.* **26**, 101 (1975).
- [3] R.B. Hammond, *Physica* **134B**, 475 (1985).
- [4] K. Meyer, M. Pessot, G. Mourou, R. Grondin and S. Chamoun, *Appl. Phys. Lett.* **53**, 2254 (1988).
- [5] A. Evan Iverson, G.M. Wysin, D.L. Smith and A. Redondo, *Appl. Phys. Lett.* **52**, 2148 (1988).
- [6] J.G. Ruch, *IEEE Trans. Electron. Devices* **ED-19**, 652 (1972).
- [7] D. Rosen, A.G. Doukas, Y. Budanski, A. Katz and R.R. Alfano, *Appl. Phys. Lett.* **39**, 935 (1981); D. Rosen, A.G. Doukas, A. Katz, Y. Budanski and R.R. Alfano in *Semiconductors Probed by Ultrafast Laser Spectroscopy*, edited by R.R. Alfano (Academic Press, New York, 1984).
- [8] A. Von Lehmen and J.M. Ballantyne, *Appl. Phys. Lett.* **44**, 87 (1984).
- [9] A. Von Lehmen and J.M. Ballantyne, *Appl. Phys. Lett.* **45**, 767 (1984).
- [10] S.M. Sze, *Physics of Semiconductor Devices*, 2nd edition, (Wiley & Sons, New York, 1981).
- [11] C. Jacoboni and L. Reggiani, *Reviews of Modern Physics* **55**, 645 (1983).
- [12] C. Jacoboni and P. Lugli, in *The Monte Carlo Method for semiconductor device simulation* (Springer-Verlag, New York, 1989).
- [13] *Hot electron transport in semiconductors*, edited by L. Reggiani (Springer-Verlag, New York, 1985).
- [14] M. Costato and L. Reggiani, *Phys. Stat. Sol. (b)* **58**, 461 (1973).

-
- [15] J. Shah, B. Deveaud, T.C. Damen, W.T. Tsang, A.C. Gossard and P. Lugli, *Phys. Rev. Lett.* **59**, 2222 (1987).
 - [16] D.Y. Oberli, J. Shah and T.C. Damen, *Phys. Rev.* **B40**, 1323 (1989).
 - [17] P.J. van Hall, private communication.
 - [18] P.J. van Hall and V. Brücker, *Proc. of the 8th Vilnius Symposium on Ultrafast Phenomena in Semiconductors* (Vilnius, Lithuania, 1992).

Chapter 6

Energy Relaxation of hot 2D carriers in high magnetic fields due to optical and acoustic phonons

Abstract

The energy relaxation rate of hot carriers in a GaAs/(Ga,Al)As quantum well structure has been studied for different laser excitation intensities in magnetic fields up to 17 T using c.w. photoluminescence spectroscopy. In the regime where LO-phonon scattering dominates the hot carrier cooling a magnetic field reduces the energy relaxation rate. For the lowest excitation power used, an enhancement of the cooling with magnetic field has been found due to acoustic phonon scattering. These results are supported by model calculations. Furthermore the results are discussed with respect to previously reported time-resolved photoluminescence measurements on GaAs/(Ga,Al)As quantum well structures and bulk GaAs. The present c.w. photoluminescence measurements provide a better quantitative understanding of the time-resolved data.

6.1 Introduction

Study of hot carrier energy relaxation rates in quasi zero-dimensional carrier systems simulated by a GaAs/(Ga,Al)As quantum well structure in high magnetic fields, has been carried out mainly by time- and energy-resolved photoluminescence (PL) spectroscopy¹. It has been found that the carrier cooling in highly excited bulk GaAs is reduced considerably in high magnetic fields². In a GaAs/(Ga,Al)As quantum well system however, an enhancement of the carrier cooling with magnetic field has been observed after an initial reduction up to $B \simeq 9 \text{ T}^2$.³ Although these time- and energy-resolved experiments have provided valuable information on the carrier dynamics in these systems, a full comprehension of the results is difficult due to the variation in time of all the relevant parameters like the effective temperature and density of the carriers and the Landau level linewidths.

In this chapter we present the results of a study on the energy relaxation rate of two dimensional carriers in magnetic fields up to 17 T using c.w. photoluminescence spectroscopy. Under these steady state conditions, hot carrier phenomena are governed by the balance between power input into the carrier system due to photo-excitation and the power loss due to the interaction with optical and acoustic phonons. The influence of the magnetic field on the energy relaxation rate has been investigated for different excitation intensities, by determination of the effective temperature from photoluminescence spectra.

In the next section (6.2) the used quantum well sample will be described, followed by a brief description of the experimental set-up. Section 6.3 will present the experimental results, which will be analyzed with the use of an energy relaxation model, including optical and acoustic phonon scattering in the presence of a magnetic field. It has been found that for low excitation intensities, in the regime where acoustic deformation potential scattering dominates the cooling process, the effective carrier temperature reduces with increasing magnetic field, which expresses the enhanced energy relaxation rate due to acoustic phonon scattering with magnetic field strength. For higher laser excitation levels, when optical phonon scattering is most important, the magnetic field has been found to reduce the carrier cooling rate, leading to an increase of the carrier temperature with increasing magnetic field. In section 6.4 these results will be compared with time-resolved photoluminescence measurements, which leads to a better quantitative understanding of the time-resolved data. Finally section 6.5 will summarize the main conclusions.

6.2 Experimental details

The photoluminescence measurements were performed on a MBE-grown modulation doped quantum well sample⁴ consisting of 10 GaAs layers of 9 nm width, separated by 31 nm thick (Ga,Al)As barriers ([Al]=0.34). Each barrier consists of two 9 nm undoped layers which surround a 13 nm thick Si-doped layer.

A Krypton ion laser operating at 647.2 nm was used to excite carriers optically. The laser beam was mechanically chopped to allow for lock-in detection. The emitted photoluminescence signal was guided through a 1 m grating monochromator (Monospek) and detected by a GaAs photomultiplier tube using a lock-in amplifier. The sample was

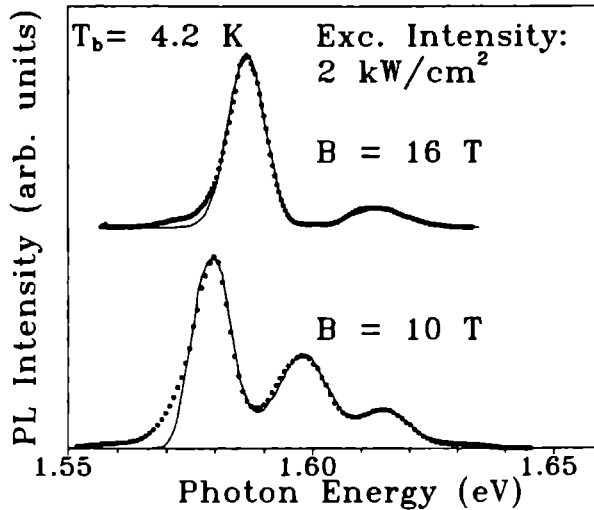


Figure 6.1: Typical photoluminescence (PL) spectra for magnetic fields of 10 and 16 T, for a laser excitation intensity of 2 kW/cm^2 (dotted curves). The solid curves correspond to the best lineshape fits of the spectra, according to expression (6.1).

cooled down to a temperature of 4.2 K in a He bath cryostat, mounted in one of the hybrid magnet systems (25 T) of the High Field Magnet Laboratory of the University of Nijmegen.

6.3 Experimental results and model calculation

Photoluminescence spectra were measured as a function of magnetic fields up to 17 T, oriented parallel to the sample growth direction, for a number of laser excitation intensities. Figure 6.1 shows typical photoluminescence spectra at magnetic fields of 10 and 16 T, for the lowest laser excitation intensity used (2 kW/cm^2). The low excitation spectrum at $B=10 \text{ T}$ shows one full and two partially filled Landau levels. For higher laser excitation levels more Landau levels are filled, i.e. a different Landau level occupation is present, as can be seen in figure 6.2, which displays a typical spectrum at a magnetic field of 9 T for 20 kW/cm^2 laser intensity. The inset shows the high energy tail of some spectra on a semi-logarithmic scale in addition to the corresponding values of the effective carrier temperatures T_{eff} (dashed lines), as obtained from the high-energy slopes. In both figures 6.1 and 6.2 the solid curves correspond to the best lineshape fits to the spectra, according to an expression for the band-to-band photoluminescence radiation given by^{5, 6}:

$$I(\hbar\omega) \sim \int_0^{\hbar\omega - E_{\text{gap}}} g_e(E) g_h(\hbar\omega - E_{\text{gap}} - E) f_e(E) f_h(\hbar\omega - E_{\text{gap}} - E) dE \quad (6.1)$$

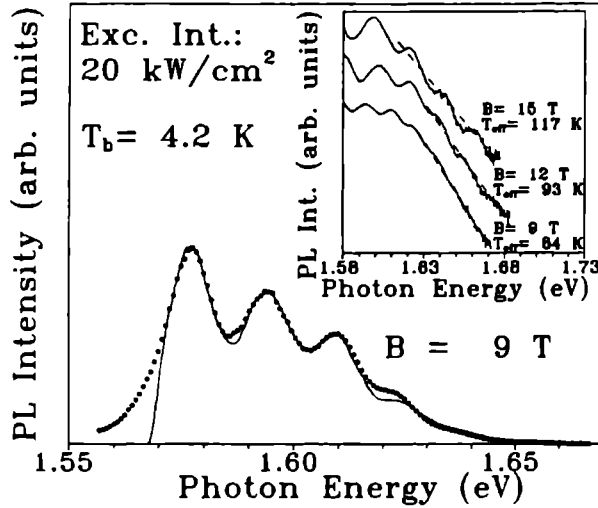


Figure 6.2: Typical photoluminescence (PL) spectrum at a magnetic field of 9 T, for a laser excitation intensity of 20 kW/cm^2 (dotted curve). The solid curve corresponds to the best lineshape fit of the spectrum, according to equation (6.1). The inset shows the high energy tails of some photoluminescence spectra on a semi-logarithmic scale with the straight lines representing the deduced effective carrier temperatures.

containing the Fermi-Dirac distribution functions $f_{e,h}$ for electrons and holes, and the two dimensional Landau level density of states functions $g_{e,h}$ given by^{5, 6}:

$$g_{e,h}(E) = \frac{1}{\pi l^2} \left(\frac{\pi}{2}\right)^{-\frac{1}{2}} \sum_{i=0}^{\infty} \frac{1}{\Gamma_i} \exp\left\{-\frac{2[E - (i + \frac{1}{2})\hbar\omega_c]^2}{\Gamma_i^2}\right\} \quad (6.2)$$

where $l = \sqrt{\frac{\hbar}{eB}}$ is the magnetic length, i runs over the Gaussian broadened Landau levels with linewidths Γ_i , and $\omega_c = \frac{eB}{m^*}$ is the cyclotron frequency with $m_e^* = m_e^*(E)$ due to the nonparabolicity of the conduction band^{7, 8}. From the lineshape analysis, the density n_c and the effective temperature T_{eff} of the carrier distributions were obtained, as well as the values for the Landau level linewidths Γ_i .

Figure 6.3 shows the values for the effective temperature, as obtained from the lineshape analysis, as a function of the magnetic field for an excitation intensity of 2 kW/cm^2 . The effective temperature increases from 65 K at $B=7 \text{ T}$ up to 80 K at $B=11 \text{ T}$, and decreases subsequently to 40 K at $B=17 \text{ T}$, while at 15 T a shoulder is visible. The increased cooling for $B > 11 \text{ T}$, resulting in a lower effective temperature, is attributed to acoustic deformation potential (ADP) scattering of the carriers.

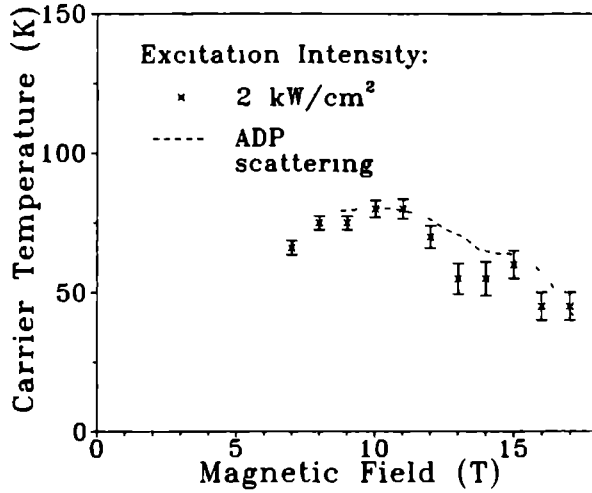


Figure 6.3 The effective carrier temperature as a function of the magnetic field for an excitation intensity of 2 kW/cm^2 . The dashed curve is the result of a model calculation for ADP scattering where experimentally obtained values for n_c and Γ_1 were used. $B_0 = 10 \text{ T}$.

In order to support this assertion, we calculated $T_{\text{eff}} = T_{\text{eff}}(B)$ from the equilibrium condition

$$\langle dE/dt \rangle_{\text{in}} = \langle dE/dt \rangle_{\text{phonons}} \quad (6.3)$$

where $\langle dE/dt \rangle_{\text{in}}$ is the average power input per carrier into the two dimensional carrier gas by laser photo-excitation, which was kept constant for all values of the magnetic field, and $\langle dE/dt \rangle_{\text{phonons}}$ is the average energy relaxation rate per carrier due to carrier-phonon interactions, which depends on the temperature and concentration of the carriers, the Landau level linewidths and the magnetic field strength⁹. Since it is difficult to determine $\langle dE/dt \rangle_{\text{in}}$ directly from the laser excitation power, its value was calculated from the equilibrium condition (6.3) using the expressions for $\langle dE/dt \rangle_{\text{phonons}}$ as given by Reinen *et al.*⁹ for one value of the magnetic field $B = B_0$ (10 T in figure 6.3) and with the values for T_{eff} , n_c and Γ_1 which were determined from the photoluminescence spectrum at $B = B_0$. For all other values of the magnetic field this $\langle dE/dt \rangle_{\text{in}}$ was assumed to be constant and T_{eff} was chosen such that the equilibrium condition (6.3) was fulfilled, using the experimental values for n_c and Γ_1 . Thus in the analysis no adjustable parameters were used. The resulting dashed curve in figure 6.3, calculated using only $\langle dE/dt \rangle_{\text{ADP}}$, does not follow the experimental points exactly, however the main features for $B > 9 \text{ T}$ are well described by the model. The initial increase of the effective temperature up to a magnetic field of $B \approx 9 \text{ T}$ is due to a reduction of carrier-LO phonon interactions dominating the carrier cooling in this field range. The observed decrease of T_{eff} for $B > 9 \text{ T}$ is a direct result of the increase of $\langle dE/dt \rangle_{\text{ADP}}$ with B . This is due to the increasing Landau Level degeneracy with magnetic

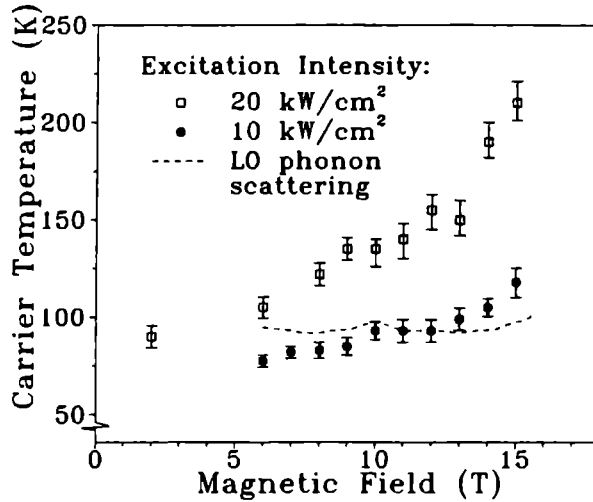


Figure 6.4. The effective carrier temperature as function of the magnetic field strength for two excitation intensities; The dashed curve corresponds to a model calculation for LO phonon scattering with experimental values for n_c and Γ_1 and $B_0=11$ T.

field ($1/\pi l^2 = eB/\pi\hbar$) and a resulting increase of the density of states. As a consequence intra Landau level transitions, which dominate the ADP scattering in this field range, are enhanced⁹. The variation of the effective temperature for higher fields, i.e. around 15 T, is due to the oscillating density of states when the Fermi energy moves in between the first and zeroth Landau level⁹. The strong dependence of $\langle dE/dt \rangle_{ADP}$ on the density of states at the Fermi energy was previously observed in the width of a partially filled Landau Level as a function of its occupation, which is under these conditions mainly determined by ADP scattering⁶.

With increasing excitation intensity up to 10 kW/cm² a transition is visible from a decrease of the effective temperature with the magnetic field strength to a monotonic increase. This is shown in figure 6.4 where the effective temperature increases from 70 K at $B=6$ T up to 110 K at $B=15$ T, whilst at $B=8$ T and $B=13$ T shallow minima are present due to hot electron magneto-phonon resonances, which have been discussed in detail by Reinen *et al.*^{10, 11}. For even higher excitation intensities, i.e. 20 kW/cm², the effective temperature increases more drastically with magnetic field. The dashed curve in figure 6.4 shows the results for the energy relaxation rate due to LO-phonon scattering $\langle dE/dt \rangle_{LO}$ using the model mentioned above. Reasonable agreement is obtained showing that LO-phonon scattering dominates the cooling. However, the slight monotonic increase of the temperature with magnetic field strength is not explained by the model, indicating an additional reduction of the carrier cooling due to the magnetic field. The effective temperature in the high excitation regime, considerably enhances with B in this field range, and can eventually show

a pronounced maximum beyond 17 T due to magneto-phonon resonances^{10, 11}. The present results for $B \leq 15$ T indicate clearly the reduced carrier cooling with field in this regime where the energy relaxation is dominated by LO phonon scattering.

6.4 Discussion

Time- and energy-resolved photoluminescence measurements on GaAs/(Ga,Al)As quantum well systems in high magnetic fields have shown a reduction of the carrier cooling up to $B \simeq 9$ T, followed by an enhancement up to 20 T. The reduction due to LO-phonon interactions up to $B \simeq 9$ T with respect to the zero field cooling rates, has been assigned to the formation of quasi zero-dimensional carrier states, i.e. well separated Landau levels, and a resulting enhancement of non-equilibrium phonon effects². The enhancement observed for $B > 9$ T in these quantum well systems has been assigned to an increased hole-phonon coupling^{3, 12} and an increase of ADP scattering with the magnetic field strength². The measurements in figure 6.3 show a similar enhancement of the carrier cooling rate, and a corresponding decreasing effective temperature, with increasing magnetic field strength. Also the Landau Level occupation observed in the experiments of figure 6.3 are comparable to those observed in the time-resolved experiments on the quantum well systems. A direct comparison of Landau level occupation is difficult due to the variation in time of both the temperature and density of the carriers in the time-resolved photoluminescence measurements. However, the photoluminescence spectra reported by Hollering *et al.*² and Ryan *et al.*³ show roughly one full and two partially filled Landau levels at field values above 9 T, which is similar to the occupation observed in our low excitation c.w. photoluminescence measurements (figure 6.1). Therefore our measurements and theoretical analysis confirm the conclusions by Hollering *et al.*² that the enhancement of the carrier cooling for $B > 9$ T is due to ADP scattering which dominates the cooling in this field range and these carrier densities ($n_c \sim 1 \times 10^{17} \text{ cm}^{-3}$) and effective temperatures ($T_{\text{eff}} \leq 60 \text{ K}$), i.e. observed Landau Level occupation.

However, with increasing excitation intensity the decrease of the effective temperature with increasing magnetic field strength changes into a monotonic increase, that becomes even stronger at higher excitation intensities. Our calculations show that in this regime LO phonon scattering dominates the carrier cooling. This behaviour of the effective temperature with field resembles very much the results from time-resolved PL measurements on bulk GaAs², where LO phonon scattering has been found to dominate the energy relaxation up to the highest magnetic fields used, and where a monotonic reduction of the carrier cooling with increasing magnetic field has been found.

6.5 Conclusions

We conclude from the present measurements and the time-resolved photoluminescence data that in the regime where LO phonon scattering dominates the carrier cooling, a magnetic field reduces the energy relaxation. For lower excitation levels, i.e. lower Landau Level occupation, where acoustic phonon scattering dominates the carrier cooling, an increase of the carrier cooling rate with magnetic field has been found, which is related directly to the

increase of intra Landau Level scattering due to an increasing Landau Level degeneracy with field. Finally it should be noted that a transition from LO-phonon scattering to ADP scattering dominating the hot carrier cooling should be observed both in bulk and lower dimensional structures. The magnetic field value at which this transition will occur depends on the excitation conditions. This conclusion is confirmed by the recent experiments of Rossin and coworkers^{13, 14} who found an enhanced exciton photoluminescence intensity and a corresponding exciton cooling in ultrapure bulk GaAs samples, related directly to an enhanced free electron-acoustic phonon energy relaxation rate with increasing magnetic field strength.

References

- [1] J. Shah, *IEEE J. of Quantum Electron.* **QE-22**, 1728 (1986).
- [2] R.W.J. Hollering, T.T.J.M. Berendschot, H.J.A. Bluysen, H.A.J.M. Reinen, P. Wyder and F. Roozeboom, *Phys. Rev.* **B38**, 13323 (1988).
- [3] J.F. Ryan, R.A. Taylor, A.J. Turberfield and J.M. Worlock, *Surf. Sci.* **170**, 511 (1986).
- [4] K. Leo, W.W. Rühle, H.J. Queisser and K. Ploog, *Appl. Phys.* **A45**, 35 (1988).
- [5] T.T.J.M. Berendschot, *Phd. thesis*, University of Nijmegen (1989).
- [6] T.T.J.M. Berendschot, H.A.J.M. Reinen and H.J.A. Bluysen, *Solid State Commun.* **63**, 873 (1987).
- [7] D.C. Rogers, J. Singleton, R.J. Nicholas, C.T. Foxon and K. Woodbridge, *Phys. Rev.* **B34**, 4002 (1986).
- [8] U. Ekenberg, *Proc. 19th Int. Conf. on the Physics of Semiconductors* (Warsaw, Poland, 1988) p. 287; U. Ekenberg, *Phys. Rev.* **B36**, 6152 (1987).
- [9] H.A.J.M. Reinen, T.T.J.M. Berendschot, R.J.H. Kappert and H.J.A. Bluysen, *Solid State Commun.* **65**, 1495 (1988).
- [10] H.A.J.M. Reinen, T.T.J.M. Berendschot, P.C.M. Christianen, H.J.A. Bluysen, K. Ploog and M.R. Leys, *Solid-State Electron.* **32**, 1315 (1989).
- [11] H.A.J.M. Reinen, *Phd. thesis*, University of Nijmegen (1990).
- [12] A.J. Turberfield, *Solid-State Electron.* **31**, 387 (1988).
- [13] Yu.V. Zhilyaev, V.V. Rossin, T.V. Rossina and V.V. Travnikov, *Sov. Phys. JETP* **72**, 692 (1991).
- [14] V.V. Rossin, P.C.M. Christianen and V.V. Travnikov, to be published.

Chapter 7

Vertical transport in a GaAs/(Ga,Al)As superlattice containing an enlarged quantum well in high in-plane magnetic fields

Abstract

Vertical transport in a GaAs/(Ga,Al)As superlattice has been studied using photoluminescence and magnetophotoluminescence measurements with in-plane fields of up to 25 T at temperatures in the range 4-80 K. Vertical transport at 4 K (which is determined by exciton transport) has been found to be less efficient than free-carrier like transport at high temperatures (47 K and 80 K). Application of a high in-plane magnetic field tends to reduce the hole transport considerably. In addition a drastic enhancement of the total photoluminescence yield with in-plane field has been observed.

7.1 Introduction

With the improvement of crystal growth techniques such as molecular beam epitaxy (MBE) it has become possible to grow superlattice (SL) structures, as were first envisaged by Esaki and Tsu¹, with abrupt interfaces. Consequently, the study of transport in the SL growth direction (vertical transport) has attracted considerable research interest^{2,3}. Most studies have used GaAs/(Ga,Al)As SLs because of the more mature state of the growth technology for this system. The use of Enlarged Quantum Wells (EQWs), which act as a carrier sink when embedded in a SL structure, has allowed the dynamics of carriers through the SL minibands to be examined using time-resolved photoluminescence⁴⁻⁷. The application of a magnetic field oriented parallel to the plane of the SL has provided insight in some fundamental vertical transport properties in SLs⁸⁻¹³. From the observation of Landau Levels in inter-band absorption experiments with in-plane field Belle *et al.*^{8,9} were able to deduce the combined electron and hole miniband width, since the Landau Levels disappeared when the cyclotron energy just exceeded the miniband width (in agreement with cyclotron-resonance experiments performed by Duffield *et al.*¹²). More recently, an investigation of the SL photoluminescence (PL) intensity in parallel magnetic fields up to 8 T has been performed¹⁴. In the present study we have further exploited vertical transport in GaAs/(Ga,Al)As SLs containing an EQW in high in-plane magnetic fields up to 25 T by means of magnetophotoluminescence (MPL). We have also examined the variation of PL intensity with laser excitation power at three different temperatures (4 K, 47 K and 80 K).

We have found the vertical transport at 4 K (which is due to exciton transport) to be less efficient than the free-carrier like transport at higher temperatures (47 K and 80 K). The application of an in-plane magnetic field has been found to reduce the vertical transport considerably due to magnetic field-induced suppression of hole transport. A drastic additional increase of the total PL intensity has been observed with increasing field which is suggested to originate from the decreased influence of nonradiative recombination.

7.2 Experimental details

Two superlattice samples, NU374 and NU443, were grown by MBE with nominally the same layer composition during different growth runs. A relatively wide GaAs EQW of 8.5 nm was grown on top of a 0.15 μm thick (Ga,Al)As layer ([Al] = 0.33), with a 0.6 μm SL structure consisting of 1.3 nm (Ga,Al)As ([Al] = 0.33) barriers and 3.4 nm GaAs QWs being grown above the 8.5 nm EQW. A 50 nm (Ga,Al)As ([Al] = 0.33) and 20 nm GaAs capping layer completed the structure. The laser light entered the structure from the capping layer and not the GaAs substrate. The superlattice samples were excited at energies above the (Ga,Al)As bandgap using picosecond pulses generated by a Rh6G dye laser synchronously pumped by a mode-locked Krypton ion laser (Excitation wavelength: 600 nm, Repetition rate: 82 MHz). The laser light was focused to a 15 μm spot on the sample surface. Magnetic fields of up to 25 T were provided by one of the hybrid magnet systems¹⁵ of the High Field Magnet Laboratory at the University of Nijmegen. The samples were mounted with the planes of the SL and the EQW parallel to the magnetic field direction. Measurements were made at

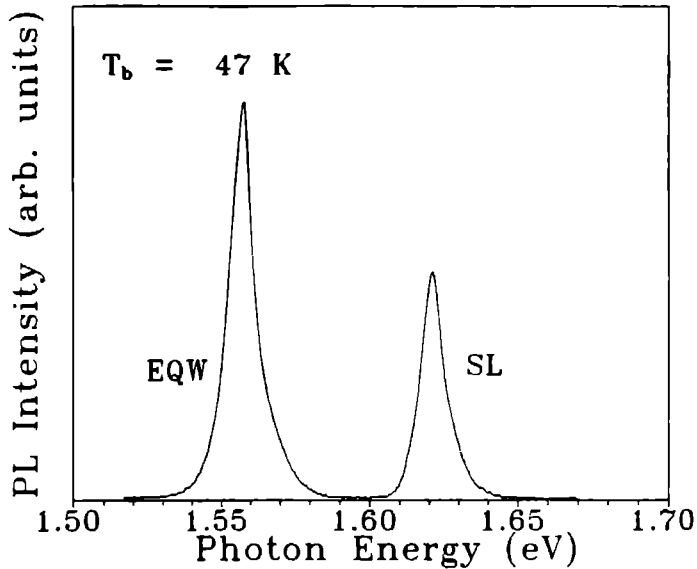


Figure 7.1: Typical photoluminescence (PL) spectrum for sample NU443. The two peaks originate from the superlattice (SL) and the enlarged quantum well (EQW).

different temperatures in the range 4-80 K.

7.3 Results

Figure 7.1 shows a typical time-integrated PL spectrum for sample NU443 at 47 K recorded without a magnetic field. Sample NU374 displayed a similar spectrum. Two clearly resolved peaks are observed at approximately 1.62 eV and 1.56 eV and the energies are in agreement with those expected for the SL and EQW¹³⁻¹⁷. The effect of increasing excitation intensity on the EQW and SL spectrally-integrated PL intensities is displayed in figure 7.2 for the sample temperatures of 4 K (a), 47 K (b) and 80 K (c). We should emphasise that the results of figure 7.2 are obtained by a spectral integration of the time-integrated PL spectra, rather than a simple determination of the PL peak height. The latter method would give a significant underestimate for the emitted PL at the higher powers, since it does not account for the broadening of the PL peaks with increasing excitation power. It can be seen that the slope of the PL intensity (indicated between brackets in figure 7.2) versus excitation intensity remains essentially linear (slope 0.9-1.0) with increasing temperature for the EQW, whereas the slope for the SL luminescence changes from linear at 4 K to (sub)quadratic (slope 1.5-1.6) at 47 K and 80 K. Note that the vertical transport in the present SL samples is rather efficient; this follows from the minimum ratio of EQW and SL integrated PL intensity ($\sim .2$) in comparison with the volume ratio of the EQW and the whole SL (0.014).

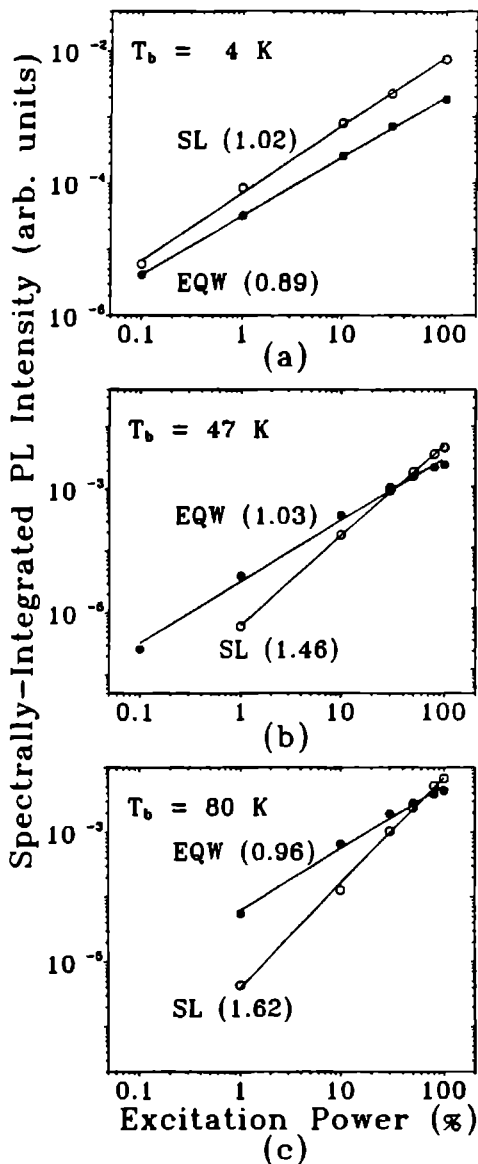


Figure 7.2: Spectrally-integrated intensity of the SL (open symbols) and EQW (filled symbols) photoluminescence (PL) as a function of excitation power at three temperatures for sample NU443. 100% excitation power corresponds to 15 mW dye laser excitation. The solid lines reflect the best linear fit through the points. The resulting slopes are displayed between brackets.

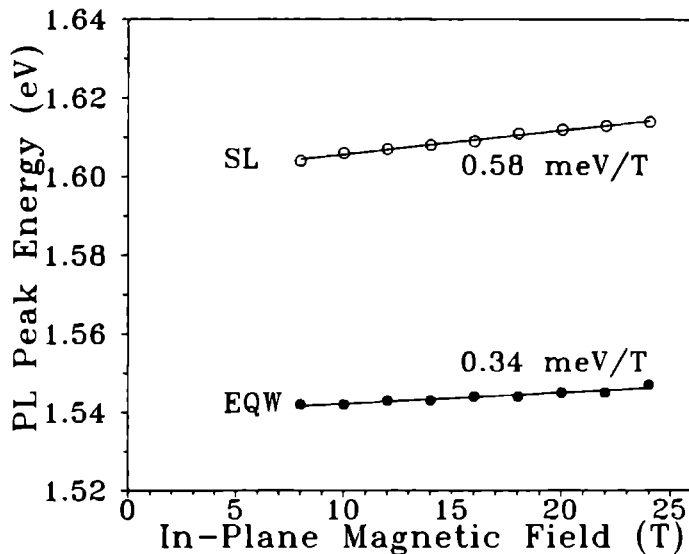


Figure 7.3: The shift of the PL peak energy versus in-plane magnetic field for the SL (open symbols) and the EQW (filled symbols) for sample NU374.

Magnetophotoluminescence measurements in sample NU374 have been performed at 77 K with in-plane magnetic fields of up to 25 T. Figure 7.3 shows the shifts in the peak positions of the lowest Landau level for increasing magnetic field. Over the whole range of magnetic field values used both the SL and the EQW peak energies shift linearly with field, i.e. 0.58 meV/T and 0.34 meV/T respectively for the SL and EQW. The SL shift agrees well with the experimental and theoretical values of Belle *et al.*⁸ and Maan¹³. The shift of the EQW peak is smaller than for the SL as would be expected for a two-dimensional system¹⁸ and compares favourably with the lower field results of previous reports^{16, 17, 19} for a similar well width.

The filled symbols in figure 7.4 show the in-plane magnetic field dependence of spectrally-integrated PL intensities for the SL (squares) and EQW (circles), together with their sum (triangles) for excitation powers of 5 mW and 15 mW. The open symbols correspond to the SL (squares) and EQW (circles) spectrally-integrated PL intensities when normalised to their values at 8 T. Again, it is important to note that in figure 7.4 the spectrally-integrated PL intensities are displayed and not the PL peak heights; any broadening effect on the PL lineshape, (e.g. such as power broadening) will exclude the use of the simple peak height determination. In the case of a changing magnetic field the simultaneously changing Landau Level degeneracy accounts for a varying PL linewidth which implies that the spectrally-integrated PL intensity must be used. In figure 7.4 the SL PL increases in an approximately linear fashion with increasing magnetic field. For high excitation power only,

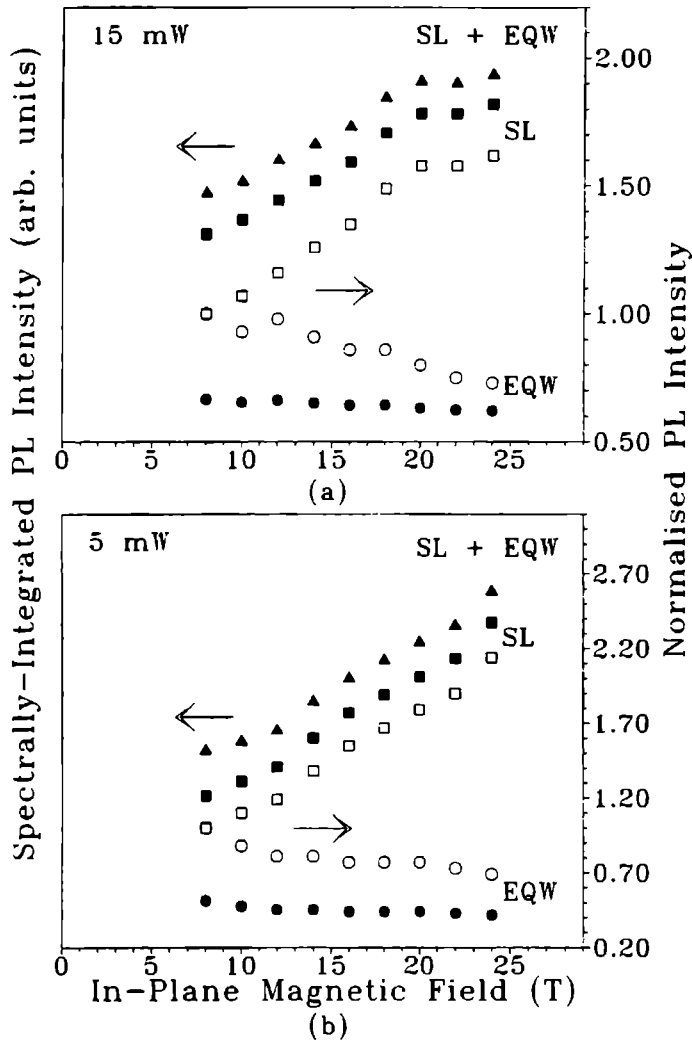


Figure 7.4: The spectrally-integrated PL intensity (filled symbols) of the SL (squares), EQW (dots) and SL + EQW (triangles) as a function of in-plane field for two excitation powers. The open symbols reflect the PL intensity of the SL (squares) and EQW (dots) normalised to their values at 8 T.

the SL PL intensity tends to saturate beyond approximately 20 T. The EQW PL decreases with increasing field for both excitation powers. From the normalised PL data in figure 7.4 (b) it follows directly that this decrease of the EQW PL with in-plane field can be as large as 30% at 25 T. However, as shown by the filled triangles, the sum of the EQW and SL PL increases considerably with field, in contrast to similar previous in-plane MPL measurements in which a 5% decrease of the EQW PL intensity at 8 T has been observed, but without an increase in total PL intensity¹⁴.

7.4 Discussion

The increased exciton binding energy in two-dimensional systems^{16, 17} means that for temperatures up to 80 K the EQW PL is mainly excitonic, as is evidenced by the narrow symmetric PL lineshape for the range of sample temperatures investigated. Following the reasoning of Block *et al.*⁷ all vertical transport parameters are assumed to be linear with excitation power, so the number of carriers arriving in the EQW is also expected to be linear with excitation power. In the case when the time of exciton formation is short enough, the exciton PL intensity will be proportional to the number of excitons present, i.e. linear with excitation power. This is shown in the present measurements (figure 7.2). The 3-dimensional properties of a SL mean that excitons are ionised^{20, 21} at a temperature of 80 K creating free electrons and holes in SL minibands. For this reason many of the PL studies of vertical transport in SL structures have been conducted at 77 K to ensure free carriers are indeed present^{5, 7, 21}. The radiative processes in a SL are therefore expected to involve both free electrons and holes at 80 K. The slope of the PL intensity versus excitation power graph would therefore be expected to be approximately quadratic⁷, as is observed at 80 K. Moreover, the slope of PL intensity versus power graph at 47 K (figure 7.2 (b)) is also found to be (sub)quadratic, revealing that a considerable amount of excitons are ionised at this temperature, resulting in a free-carrier like recombination mechanism. At 4 K the linear slope in figure 7.2(a) for the SL shows that luminescence is excitonic, as might be expected. At lower excitation powers (<10%), the ratio of the PL intensities from the SL and EQW strongly depends on the sample temperature, reflecting the different efficiencies of the vertical transport at the various temperatures. Apparently, the vertical transport through the SL at 4 K, which is governed by excitons (figure 7.2(a)) is less efficient than the free carrier transport at 47 K and 80 K, resulting in a relatively weaker PL signal at 4 K originating from the EQW as compared with the SL. The more efficient tunnelling mechanism at the higher temperatures raises the EQW PL intensity above that emitted by the SL for excitation powers smaller than 10%, as is observed in figures 7.2 (b) and (c). Similar trends of the vertical transport behaviour with temperature have been found by others^{6, 22}. The growing relative intensity of the SL PL with respect to the EQW with increasing excitation power for the higher temperatures is not due to a reduction in vertical transport, but is the direct consequence of the different radiative recombination mechanisms, i.e. excitonic (linear with power) for the EQW and free-carrier like (quadratic with power) for the SL. Consequently at 47 K and 80 K a cross-over appears where the SL PL intensity starts to exceed the EQW PL intensity. Obviously this cross-over is absent at 4 K since at this temperature the respective slopes of the SL and EQW PL

intensity versus excitation powers are more or less equal.

The present measurements are the highest magnetic field (25 T) photoluminescence measurements in SL structures in the in-plane orientation. The sample temperature was 77 K, which means that the vertical transport is dominated by free carriers; this is confirmed by a determination of the PL intensity as a function of the excitation power at a constant magnetic field of 8 T which yielded a slope of approximately 1.5 for the SL. Obviously the ratio between the SL and EQW PL intensities in the presence of an in-plane field (figure 7.4) is much larger than without field (figure 7.2(c)). The excitation powers used, 5 mW and 15 mW, correspond to respectively the 30% and 100% laser power levels in figure 7.2(c), which is the region where the SL and EQW PL intensities are of the same order of magnitude. Moreover, as will be discussed subsequently, the parallel magnetic field affects the carrier recombination in such a way²³ that the ratio between SL and EQW PL intensity indeed reaches much higher values than without a magnetic field.

Previous MPL measurements with in-plane fields up to 8 T reported in-plane field induced shrinkage of the hole wavefunction, which localises the holes in a single well of the SL, whenever the cyclotron energy exceeds the miniband width, leading to a reduction of the vertical transport¹⁴. Although in the present experiments this condition is not yet reached^{13, 24} the decrease of the EQW PL intensity with parallel field (figure 7.4) strongly suggests a reduction in vertical transport, which might be due to a less-efficient hole tunnelling. Certainly the present excitation powers are such that the photo-excited electron and hole concentrations (10^{16} cm^{-3} - 10^{18} cm^{-3}) are larger than the residual doping levels; as reported in previous studies without a magnetic field^{6, 25, 26} the vertical transport in this so-called high density regime is completely determined by the hole dynamics which controls the ambipolar motion. This argument will also hold, it is believed, in the presence of a magnetic field. Therefore, the diminishing EQW PL intensity with increasing in-plane field (figure 7.4) is most probably due to reduced hole vertical transport, in agreement with the results obtained by Uraltsev *et al.*¹⁴, so less holes will reach the EQW before recombination. As a result the observed enhancement of the SL PL intensity with growing parallel field can be also expected (figure 7.4). However, this mechanism of reducing the hole vertical transport will not affect the total PL yield, i.e. the sum of the EQW and SL PL intensity should remain constant with changing magnetic field¹⁴. Consequently, to explain the drastic enhancement of the total PL intensity with field (triangles in figure 7.4) an additional effect must be incorporated. A similar increase of the PL intensity with in-plane field has been observed by Stanaway *et al.*²³ in the MPL of a relatively wide quantum well (300 Å), which could be qualitatively described by a reduced efficiency of nonradiative traps with in-plane field. A reduction in the influence of nonradiative traps with parallel field implies that more carriers recombine radiatively when the field increases, giving rise to a larger total PL signal. It should be noted that this mechanism also affects the EQW PL signal from our sample. However, this second mechanism affecting the PL yield (in competition with the magnetic field-induced suppression of the hole vertical transport) has a greater effect on the SL PL than on the EQW PL. This follows from the fact that the nonradiative traps are mostly located at the interfaces²³

and there are many more interfaces in the SL region (approximately 440) than in the EQW region. The effect of the field is thus much greater for the SL PL.

In the case of 15 mW laser excitation (figure 7.4(a)) the SL as well as the total PL intensity tends to saturate beyond 20 T, in contrast to 5 mW excitation where no saturation appears. This saturation can be described in terms of the suppression of the nonradiative recombination be described as follows: for moderate magnetic field strengths in figure 7.4(a) (8-20 T) the radiative recombination rate is strongly affected by the field-induced reduction in nonradiative recombination efficiency; but beyond a certain threshold field value (in this case approximately 20 T) the influence of the nonradiative traps is reduced to such an extent that they can be neglected. Consequently no further enhancement of the PL signal with field is observed (figure 7.4(a)) for fields larger than 20 T. In the case of lower laser power (figure 7.4(b)) the threshold field value is not yet reached and no saturation is observed.

We wish to emphasise that although we are able to explain the drastic enhancement of the total PL yield in figure 7.4 qualitatively in terms of nonradiative traps in an in-plane field and their influence on the PL intensity, the actual mechanism which takes place is by no means clear at the moment. More theoretical and experimental work is needed to clarify this point.

7.5 Conclusions

Photoluminescence in a 3.4/1.3 nm GaAs/(Ga,Al)As SL structure containing an enlarged quantum well (EQW) has been investigated. The PL intensity for the SL and EQW is seen to depend strongly on the excitation power. From this dependence the nature of the recombination mechanism could be deduced. Variation of the sample temperature from 4 K to 80 K shows that the EQW PL is mainly excitonic in this temperature range, while the SL PL changes from mainly excitonic at 4 K to mainly free carrier-like at 47 K and 80 K. The vertical transport through the SL at 4 K (determined by excitons) is found to be less efficient than the free carrier-like transport at higher temperatures (47 K and 80 K).

Magnetophotoluminescence measurements in in-plane fields of up to 25 T reveal a diminishing EQW PL signal with growing field due to a suppression of the hole vertical transport. Moreover, a strong enhancement of the total PL intensity with in-plane field has been found, which can be qualitatively described by a reduced influence of nonradiative traps. However, more experimental and theoretical work is needed to gain insight into the actual mechanisms which provide for this behaviour.

References

- [1] L. Esaki and R. Tsu, *IBM Res. Note RC-2418* (1969).
- [2] L. Esaki, *IEEE J. Quantum Electronics QE-22*, 1611 (1986).
- [3] B. Deveaud, J. Shah, T.C. Damen, B. Lambert, A. Chomette and A. Regreny, *IEEE J. Quantum Electronics QE-24*, 1641 (1988).

- [4] B. Deveaud, A. Chomette, B. Lambert, R. Romestain and P. Edel and A. Regreny, *Solid State Comm.* **57**, 885 (1986).
- [5] A. Nakamura, K. Fujiwara, Y. Tokuda, T. Nakayama and M. Hirai, *Phys. Rev.* **B34**, 9019 (1986).
- [6] B. Deveaud, J. Shah, T.C. Damen, B. Lambert and A. Regreny, *Phys. Rev. Lett.* **58**, 2582 (1987).
- [7] D. Block, B. Boulanger, P. Edel, R. Romestain, B. Deveaud, B. Lambert and A. Regreny, *Superlattices and Microstructures* **5**, 427 (1989).
- [8] G. Belle, J.C. Maan and G. Weimann, *Solid State Comm.* **56**, 65 (1985).
- [9] G. Belle, J.C. Maan and G. Weimann, *Surface Science* **170**, 611 (1986).
- [10] T. Duffield, R. Bhat, M. Koza, F. DeRosa, D.M. Hwang, P. Grabbe and S.J. Allen Jr., *Phys. Rev. Lett.* **56**, 2724 (1986).
- [11] T. Duffield, R. Bhat, M. Koza, F. DeRosa, K.M. Rush and S.J. Allen Jr., *Phys. Rev. Lett.* **59**, 2693 (1987).
- [12] T. Duffield, R. Bhat, M. Koza, D.M. Hwang, F. DeRosa, P. Grabbe and S.J. Allen Jr., *Solid State Commun.* **65**, 1483 (1988).
- [13] J.C. Maan *Festkörperprobleme (Advances in Solid State Physics)* **27**, edited by P. Grosse, (Vieweg, Braunschweig, 1987) p 137-167.
- [14] I.N. Uraltsev, E.L. Ivchenko, V.P. Kochereshko, P.S. Kop'ev, R.A. Suris, A.M. Vasiliev and D.R. Yakovlev, *Proc. 20th Int. Conf. on the Physics of Semiconductors, Thessaloniki*, edited by E. M. Anastassakis and J. D. Joannopoulos (World Scientific, 1990).
- [15] K. Van Hulst, H. von Luong, J.A.A.J. Perenboom, J. Rook and J. Singleton, *Proc. 11th Int. Conf. on Magnet Technology, Tsukuba*, edited by T. Sekiguchi and S. Shimamoto (London: Elsevier) p 668 (1990).
- [16] J.C. Maan, G. Belle, A. Fasolino, M. Altarelli and K. Ploog, *Phys. Rev.* **B30**, 2253 (1984).
- [17] J.C. Maan, A. Fasolino, G. Belle, M. Altarelli and K. Ploog, *Physica* **127B**, 426 (1984).
- [18] F. Ancilloto, A. Fasolino and J.C. Maan, *Superlattices and Microstructures* **3**, 187 (1987).
- [19] N.J. Pulsford, J. Singleton, R.J. Nicholas and C.T. Foxon, *Journal de Physique* **C5**, 231 (1987).
- [20] A. Chomette, B. Lambert, B. Deveaud, F. Clerot, A. Regreny and G. Bastard, *Europhys. Lett.* **4**, 461 (1987).
- [21] B. Lambert, A. Chomette, F. Clerot, B. Deveaud, A. Regreny and G. Bastard, *Journal de Physique* **C5**, 533 (1987).
- [22] K. Fujiwara, N. Tsukada, T. Nakayama and A. Nakamura, *Phys. Rev.* **B40**, 1096 (1989).
- [23] M.B. Stanaway, J.M. Chamberlain, M. Henini, O.H. Hughes, H.A.J.M. Reinen, P.C.M. Christianen and J. Singleton, *Superlattices and Microstructures* **9**, 319 (1991).

-
- [24] A. Fasolino, *Proc. 19th Int. Conf. on the Physics of Semiconductors, Warsaw*, edited by W. Zawadzki (Warsaw: Institute of Physics, Polish Academy of Sciences) (1988).
- [25] B. Lambert, F. Clerot, B. Deveaud, A. Chomette, G. Talalaeff and A. Regreny, *J. of Luminescence* **44**, 277 (1989).
- [26] B. Lambert, F. Clerot, A. Chomette, A. Regreny and B. Sermage, *Superlattices and Microstructures* **5**, 565 (1989).

Summary

The fundamental physics of hot carriers in semiconductors is of great importance for the understanding of carrier behaviour in high electric fields. The basic properties of hot carriers in pure material are related to their mutual interactions and their coupling to the lattice. Consequently the investigation of hot carrier energy relaxation rates delivers valuable information about the carrier-carrier and carrier-phonon interactions, which are important topics in solid state research. Since the relevant scattering mechanisms take place on a very short timescale, the use of laser systems capable of generating light pulses of (sub)picosecond duration offers the possibility to monitor the carrier dynamics in real time. Direct band-gap semiconductors, such as GaAs are ideally suited for this purpose using (time-resolved) optical spectroscopy. Moreover, the development of sophisticated growth techniques for GaAs and related compounds has made it possible to produce layered structures in which carriers behave in a two dimensional way or in which new bandstructures are formed arising from quantum confinement or macroscopic (super)lattice periodicities. The consequences for carrier energy relaxation and transport have been studied extensively, leading to a growing fundamental insight. Furthermore, the application of a magnetic field can be used to quantize the carrier motion perpendicular to the field giving rise to Landau Levels. For high fields this results in an effective dimensionality reduction of two and thus, in measuring two dimensional systems, it is possible to study carrier systems with a zero-dimensional density of states.

This thesis describes experiments using ((sub)picosecond time-resolved) photoluminescence spectroscopy on GaAs (hetero)structures in order to investigate the ultrafast hot carrier dynamics, under varying experimental conditions. Both the effect of electric and magnetic fields on the carrier energy relaxation, recombination and transport is studied. In Chapter 1 a brief introduction is given to the important aspects of fundamental hot carrier research, followed by a brief description of the different experiments presented in this thesis. Chapter 2 deals with the basic properties of the GaAs (hetero)structures, with specific emphasis to the ultrafast carrier scattering mechanisms relevant on a short timescale. Furthermore, the different time-resolved photoluminescence techniques, i.e. photoluminescence up-conversion and photoluminescence correlation, are introduced. In chapter 3 different photoluminescence lineshape models are discussed, which are used to extract values for the time-dependent effective temperature and density of the photo-excited carrier distributions, in order to monitor the ultrafast carrier cooling. From a careful comparison of the carrier densities and temperatures, as deduced from different many- and single-particle recombination models, it becomes clear that the results obtained with a single-particle model including \mathbf{k} -conservation leads to deviating carrier cooling curves. The effective temperature determined using this model is slightly higher than those using a many-body theory or a single-particle model neglecting \mathbf{k} -conservation in the recombination process. Further, the high excitation photoluminescence spectra exhibit shoulders on their high-energy tail, which cannot be explained by single-

particle recombination models, and are specifically pronounced for degenerate carrier distributions. The spectral position of the shoulder seems to be related to the electron-hole plasma density. These results suggest the shoulder to be caused by many-particle interactions, however it appears that it can not be explained by a many-particle recombination model, incorporating plasmon-assisted transitions.

In chapter 4 the cooling of hot carriers in highly excited GaAs has been investigated. The electrons have been created below the satellite valleys in the conduction band, resulting in relatively low effective carrier temperatures due to the absence of intervalley scattering. It has been found that intense photo-excitation results in a rapidly decreasing carrier density (time constant 20 ps), in contrast to lower excitation levels for which much longer lifetimes have been observed. In addition to the ultrafast density decay rate a significant reduction in the carrier cooling rate has been found. The short carrier lifetime has been assigned to the occurrence of stimulated recombination due to the high density accompanied by a relative low temperature. The rapidly decreasing carrier density causes a remarkable reduction of the cooling due to recombination heating, opposed partially by the extra cooling due to the loss of energy of the recombining carriers. The resulting reduction of the cooling is well described by a model calculation, which incorporates energy relaxation due to carrier-phonon interactions, the stimulated recombination process, and a time-dependent radiative recombination coefficient. Moreover, the absolute value of the radiative recombination coefficient has been found to be of crucial importance for the occurrence of stimulated recombination and its competition with other ultrafast processes. These results not only are of interest from the fundamental point of view, but also for the design of direct-gap semiconductor laser structures to improve their operational characteristics. Moreover, the present study stresses that it is of vital importance in any picosecond carrier cooling experiment to deduce both the carrier density and the effective temperature from the measurements, rather than only the temperature, especially for those excitation conditions which might lead to short carrier lifetimes and thus recombination heating.

In chapter 5 the ultrafast carrier dynamics in the high electric field at a Au-GaAs interface has been studied both experimentally, using a subpicosecond photoluminescence correlation technique, and theoretically by a Monte-Carlo simulation. The ultrafast carrier sweepout from the depletion region of the Au-GaAs Schottky barrier, has been found to be strongly affected by the contacts, which might act as an extra limit for operating a device at its maximum frequency or which might lead to peculiar highly non linear transport transients. Since even at moderate laser input powers the injected charge density is dominating the one initially present, the applied field collapses almost instantaneously after laser excitation, while its reconstruction takes the time needed to recharge the device. A contact recharging time constant had to be invoked in the Monte-Carlo analysis to explain the experimental observations. The use of a recharging time of 1 ps, which corresponds to the estimated device RC-time, leads to the nice quantitative reproduction of the experimentally observed carrier sweepout. Ultimately the actual carrier sweepout is determined by both the contact regeneration time and the photo-created carrier concentration. In view of the common values of the electric fields involved and the laser input levels used, it should be noted that the concept of a finite time for the restoration of the internal electric field should be applicable

to other opto-electronic devices as well, for example fast opto-electronic switches.

Chapter 6 presents a study on the energy relaxation rate of hot carriers in a GaAs/(Ga,Al)As quantum well structure for different laser excitation intensities in magnetic fields up to 17 T using continuous wave photoluminescence spectroscopy. In the regime where LO-phonon scattering dominates the hot carrier cooling a magnetic field reduces the energy relaxation rate. For the lowest excitation power used, an enhancement of the cooling with magnetic field has been found due to acoustic phonon scattering. These results are supported by model calculations. Furthermore, the results are discussed with respect to previously reported time-resolved photoluminescence measurements on GaAs/(Ga,Al)As quantum well structures and bulk GaAs. The present continuous wave photoluminescence measurements provide a better quantitative understanding of the time-resolved data.

Finally chapter 7 deals with experiments on vertical transport in a GaAs/(Ga,Al)As superlattice containing an enlarged quantum well, using photoluminescence and magnetophotoluminescence measurements with in-plane fields of up to 25 T at temperatures in the range 4-80 K. Variation of the sample temperature from 4 K to 80 K shows that the enlarged quantum well photoluminescence is mainly excitonic in this temperature range, while the superlattice photoluminescence changes from mainly excitonic at 4 K to mainly free carrier-like at 47 and 80 K. The vertical transport through the superlattice at 4 K (determined by excitons) is found to be less efficient than the free carrier-like transport at higher temperatures (47 and 80 K). Magnetophotoluminescence measurements in in-plane fields reveal a diminishing enlarged quantum well photoluminescence signal with growing field due to a suppression of the hole vertical transport. Moreover a strong enhancement of the total photoluminescence intensity with in-plane field has been found, which can be qualitatively described by a reduced influence of nonradiative traps.

Samenvatting

Studie van de fundamentele fysica van hete elektronen in halfgeleiders is van groot belang voor het doorgronden van hun gedrag in hoge elektrische velden. In voldoende zuiver materiaal worden de primaire eigenschappen van hete ladingsdragers bepaald door hun onderlinge interacties en hun wisselwerking met het rooster. Als gevolg levert onderzoek naar de energie-relaxatie processen van hete ladingsdragers belangrijke informatie op, wat betreft de interacties tussen ladingsdragers onderling en de koppeling tussen ladingsdragers en fononen. Gezien het feit dat de relevante verstrooiings mechanismen plaatsvinden op een zeer korte tijdschaal, biedt het gebruik van lasersystemen die lichtpulsen kunnen genereren met een (sub)picoseconde pulsbreedte, de mogelijkheid om de dynamica van de ladingsdragers nauwgezet te volgen. Het halfgeleidermateriaal GaAs, wat een directe bandafstand bezit, is uitermate geschikt voor het doen van (tijdsopgeloste) optische metingen. Bovendien is het de laatste jaren mogelijk geworden om, met behulp van geavanceerde kristalgroei methoden voor GaAs, gelaagde structuren te fabriceren waarin de ladingsdragers zich in feite tweedimensionaal gedragen, of waarin een nieuwe bandstructuur is gevormd door quantumopsluiting of een macroscopische roosterperiodiciteit. Dit heeft grote gevolgen voor zowel de energie relaxatie als het transport van hete ladingsdragers, welke uitvoerig bestudeerd zijn. Bij dit onderzoek is o.a. gebruik gemaakt van een hoog magneetveld, die de ladingsdragers een beweging loodrecht op het veld oplegt, waarbij de mogelijke energietoestanden gequantiseerd zijn in Landau niveaus. Voor hoge magneetvelden resulteert dit in een reductie van de dimensie met twee. Het aanleggen van een voldoende sterk magneetveld op een tweedimensionale structuur geeft als zodanig de mogelijkheid om systemen van ladingsdragers te onderzoeken waarvan de toestands-dichtheidsfunctie nul dimensionaal is.

In dit proefschrift zijn ((sub)picoseconde tijdsopgeloste) fotoluminescentie experimenten beschreven, aan GaAs (hetero)structuren uitgevoerd, teneinde de ultrasnelle dynamica van hete ladingsdragers te bestuderen onder verschillende experimentele omstandigheden. Zowel het effect van een elektrisch veld, als een magneetveld op de energie-relaxatie, recombinatie en het transport van ladingsdragers is onderzocht. In hoofdstuk 1 is een korte inleiding gegeven wat betreft het belang van fundamenteel onderzoek aan de dynamica van hete ladingsdragers, gevolgd door een korte beschrijving van de experimenten die gepresenteerd worden in dit proefschrift. In hoofdstuk 2 zijn enige belangrijke eigenschappen van de gebruikte halfgeleider preparaten beschreven, waarbij speciale aandacht is besteed aan de verstrooiings processen die van belang zijn op (sub)picoseconde tijdschaal. Aansluitend zijn de gebruikte tijdsopgeloste fotoluminescentie technieken, te weten de op-conversie en correlatie technieken, geïntroduceerd.

Hoofdstuk 3 beschrijft de verschillende methoden die gebruikt zijn om de lijnvorm van fotoluminescentie spectra te berekenen. Uit de lijnvorm worden namelijk de dichtheid en de temperatuur van de hete ladingsdragers bepaald, zodat het koelproces gevolgd kan wor-

den. Zorgvuldige vergelijking van de dichtheden en temperaturen, bepaald met behulp van verschillende recombinatie modellen met of zonder veel-deeltjes interacties, leert ons dat de resultaten verkregen met een één-deeltje model inclusief k -selectie een afwijkend koelgedrag te zien geven. De temperatuur bepaald met behulp van dit model is namelijk hoger dan wordt bepaald met behulp van een geavanceerd veel-deeltjes model of een één-deeltje model zonder k -selectie. Verder vertonen de fotoluminescentie spectra, gemeten met intensieve laserexcitatie, een intensiteits schouder aan de hoge energie kant van de spectra. Deze schouder kan niet verklaard worden met behulp van één-deeltje recombinatie modellen, en is juist geprononceerd in het geval van gedegenerende ladingsdragers distributies. De spectrale positie van de schouder is ogenschijnlijk gerelateerd aan de dichtheid van de ladingsdragers. Deze resultaten suggereren dat de schouder veroorzaakt wordt door veel-deeltjes interacties. Het blijkt echter dat ze niet verklaard kan worden met behulp van het gebruikte veel-deeltjes recombinatie model.

In hoofdstuk 4 is het koelgedrag van hete ladingsdragers in GaAs onder intense laserexcitatie bestudeerd. In dit experiment worden elektronen geïnjecteerd beneden de satelliet minima in de geleidingsband, wat resulteert in relatief lage temperaturen van ladingsdragers. Dit heeft een opvallend snelle afname van de dichtheid van de ladingsdragers tot gevolg, met een tijdconstante van 20 picoseconden. Dit staat in sterk contrast tot metingen met een lage laserintensiteit, die een veel langzamer afname van de dichtheid tot gevolg hadden. Bovendien wordt tegelijkertijd met de snelle afname van de dichtheid ook een sterke reductie in de koelsnelheid van de ladingsdragers waargenomen. De korte levensduur van de ladingsdragers is toegeschreven aan het optreden van gestimuleerde emissie, als gevolg van een hoge dichtheid samen met een relatief lage temperatuur. De snelle afname van de dichtheid leidt tot een reductie van de koeling ten gevolge van het zogenaamde recombinatie opwarmingsmechanisme. Dit resultaat wordt ondersteund door een modelberekening, met als ingrediënten de gebruikelijke energie-relaxatie t.g.v. fonon-wisselwerkingen, gestimuleerde emissie en een tijdsafhankelijke constante voor stralende recombinatie. De absolute waarde voor deze constante blijkt van essentieel belang voor het optreden van gestimuleerde emissie, en de competitie met andere processen op picoseconde tijdschaal. De gepresenteerde resultaten zijn van belang voor het verbeteren van de specificaties van halfgeleider laserstructuren. Tevens blijkt dat het van wezenlijk belang is om zowel de dichtheid als de temperatuur van de ladingsdragers te bepalen in een picoseconde experiment naar het koelgedrag van ladingsdragers, omdat een snelle dichtheidsafname een reducerend effect op de koelsnelheid van de ladingsdragers heeft.

In hoofdstuk 5 wordt de ultrasnelle dynamica van ladingsdragers onderzocht in het sterke elektrische veld aan een metaal-halfgeleider overgang. Het betreft een experimentele studie met behulp van subpicoseconde fotoluminescentie correlatie metingen, ondersteund door theoretische berekeningen m.b.v. een Monte-Carlo simulatie. Het blijkt dat het ultrasnelle transport van geïnjecteerde elektronen en gaten uit het depletiegebied van een Au-GaAs Schottky barrière sterk afhangt van de contacten, wat kan leiden tot sterk niet-lineaire transport verschijnselen. Omdat zelfs voor gemiddelde laserintensiteiten de geïnjecteerde ladingsdichtheid de intrinsieke dichtheid geheel domineert, stort het aangelegde veld bijna meteen na de laserexcitatie geheel in. Het herstel van het intrinsieke veld duurt een poosje, nl. die

tijd die nodig is om het device weer op te laden. In de Monte-Carlo simulatie is daarom een zogenaamde regeneratietijd geïntroduceerd om de waarnemingen te kunnen verklaren. Een tijdconstante van 1 picoseconde, die overeenkomt met de geschatte RC-tijd van het preparaat, leidt tot een goede kwantitatieve overeenkomst met de experimentele resultaten. Uiteindelijk wordt het snelle transport van de ladingsdragers bepaald door de regeneratie tijdconstante en de geïnjecteerde dichtheid van ladingsdragers. Gezien de normale waarden van de elektrische velden en laserintensiteiten in het experiment, is het te verwachten dat het concept van een herstelperiode voor het interne veld ook van toepassing is op andere opto-elektronische devices, zoals bijvoorbeeld snelle optische schakelaars.

Hoofdstuk 6 beschrijft een fotoluminescentie studie naar de snelle energie-relaxatie van hete ladingsdragers in een GaAs/(Ga,Al)As quantum put structuur, voor verschillende laser-excitatie intensiteiten, in magneetvelden tot 17 T. In het regime waar LO-fonon verstrooiing de energie-relaxatie domineert, wordt deze vertraagd in een magneetveld. Voor de laagste laserintensiteiten die gebruikt zijn, wordt echter het koelgedrag gedomineerd door akoestische fonon verstrooiing, wat leidt tot een betere koeling van de ladingsdragers in een magneetveld. Deze resultaten zijn ondersteund door model berekeningen. Tevens is een vergelijk gemaakt met eerder gepubliceerde tijdsopgeloste fotoluminescentie metingen aan bulk GaAs en quantum put structuren. De huidige continue metingen leiden tot een beter kwantitatief begrip van de tijdsopgeloste metingen.

Tenslotte presenteert hoofdstuk 7 experimenten wat betreft het verticaal transport van ladingsdragers in een GaAs/(Ga,Al)As superrooster. Aan het einde van het superrooster is een enigszins verbrede quantum put ingebouwd om het verticaal transport zichtbaar te maken. De studie is uitgevoerd m.b.v. fotoluminescentie en magneto-fotoluminescentie metingen in magneetvelden tot 25 Tesla, en voor temperaturen tussen 4 en 80 Kelvin. Het verticaal transport bij 4 Kelvin, wat bepaald wordt door excitonen, blijkt minder efficiënt te zijn dan het transport van vrije ladingsdragers voor hogere temperaturen (47 en 80 Kelvin). Magneto-fotoluminescentie metingen, met het magneetveld loodrecht op de superrooster groei-richting, tonen een verminderde fotoluminescentie van de verbrede quantum put met een groeiend magneetveld, wat terug te voeren is op een verminderd verticaal transport van gaten. Bovendien wordt een sterke toename van de fotoluminescentie intensiteit van het superrooster waargenomen in een magneetveld, wat kwalitatief beschreven kan worden door een verminderde invloed van niet-stralende recombinatie.

List of publications

- “Temperature and magnetic field dependence of the lifetime of resonantly excited 2D carriers in magnetic fields up to 25 T studied using picosecond time-resolved photoluminescence”
T.T.J.M. Berendschot, H.A.J.M. Reinen, P.C.M. Christianen, H.J.A. Bluysen and H.P. Meier, *Springer Series in Solid-State Sciences* vol. **87**, 309 (1989).
- “Cooling and radiative recombination of resonantly excited 2D carriers in magnetic fields up to 25 T studied using picosecond time-resolved photoluminescence”
H.A.J.M. Reinen, T.T.J.M. Berendschot, P.C.M. Christianen, H.J.A. Bluysen and H.P. Meier, *Superlattices and Microstructures* **5**, 455 (1989).
- “Hot-electron magnetophonon resonances in doped and undoped GaAs/(Ga,Al)As quantum wells studied using photoluminescence”
H.A.J.M. Reinen, T.T.J.M. Berendschot, P.C.M. Christianen, H.J.A. Bluysen, K. Ploog and M.R. Leys, *Solid-State Electronics* **32**, 1315 (1989).
- “Carrier heating due to stimulated recombination”
P.C.M. Christianen, H.A.J.M. Reinen, H.J.A. Bluysen and M.R. Leys, *Proc. 20th International Conference on the Physics of Semiconductors (Thessaloniki, Greece)*, edited by E.M. Anastassakis and J.D. Joannopolous, (World Scientific, 1990), page 2526.
- “Magnetic field-induced charge transfer to a GaAs/(Ga,Al)As quantum well interface studied by $C(e, A_0^+)$ photoluminescence”
M.B. Stanaway, J.M. Chamberlain, M. Henini, O.H. Hughes, H.A.J.M. Reinen, P.C.M. Christianen and J. Singleton, *Superlattices and Microstructures* **9**, 319 (1991).
- “Energy relaxation of hot 2D carriers in strong magnetic fields due to optical and acoustic phonons”
P.C.M. Christianen, H.A.J.M. Reinen, T.T.J.M. Berendschot, H.J.A. Bluysen and K. Ploog, *Superlattices and Microstructures* **9**, 323 (1991).
- “Vertical transport in a GaAs/(Ga,Al)As superlattice containing an enlarged quantum well studied by photoluminescence in high in-plane magnetic fields”
P.C.M. Christianen, M.B. Stanaway, J.M. Chamberlain, H.A.J.M. Reinen, G.M.H. Knippels, J. Singleton and M. Henini, *Semiconductor Science & Technology* **7**, 676 (1992).
- “Ultrafast carrier dynamics at a metal-semiconductor interface studied by femtosecond luminescence spectroscopy”
P.J. van Hall, P.C.M. Christianen, H.J.A. Bluysen, M.R. Leys and J.H. Wolter, *Proc. 8th Vilnius Symposium on Ultrafast Phenomena in Semiconductors* (Vilnius, Lithuania, 1992)

- *“Effect of hot electrons on magnetic enhancement of exciton luminescence in GaAs”*
V.V. Rossin, P.C.M. Christianen and V.V. Travnikov, submitted to Solid State Communications.
- *“Cooling reduction due to a rapid density decay of hot carriers in GaAs”*
P.C.M. Christianen, E.J.A. de Bekker, H.J.A. Bluyssen, P.R. Hageman and M.R. Leys, to be published.
- *“Ultrafast carrier dynamics at a metal-semiconductor interface studied by femtosecond luminescence spectroscopy”*
P.C.M. Christianen, P.J. van Hall, H.J.A. Bluyssen and J.H. Wolter, to be published.

Curriculum Vitae

Peter C M Christianen

Geboren 6 juli 1966 te Hoeven

- 1978-1984 ongedeeld VWO
Katholieke Scholengemeenschap Etten-Leur e o
- 1984-1989 Studie Natuurkunde, Katholieke Universiteit Nijmegen
30 augustus 1985: Propaedeutisch examen
12 januari 1989: doctoraal examen
Afstudeerrichting: Experimentele Vaste stoffysica
Afstudeerthema: Ultrasnelle dynamica van ladingsdragers in halfgeleiders
- 1989-1993 Promotie onderzoek in dienst van de
Stichting voor Fundamenteel Onderzoek der Materie
aan de Katholieke Universiteit Nijmegen
op de afdeling Experimentele Vaste Stoffysica 2
o.l.v Dr. H.J A. Bluysen en Prof. Dr. H van Kempen
Onderzoeksthema: Ultrasnelle dynamica van hete ladingsdragers in
GaAs (hetero)structuren
- Februari 1993 In dienst van het Laboratorium voor Hoge Magneetvelden
aan de Katholieke Universiteit Nijmegen

ISBN 90-9006185-1